2013

Regulation of mechanics and dynamics of actin filaments and networks by actin-binding proteins

BOSTON UNIVERSITY

GRADUATE SCHOOL OF ARTS AND SCIENCES

Dissertation

REGULATION OF MECHANICS AND DYNAMICS OF ACTIN FILAMENTS AND NETWORKS BY ACTIN-BINDING PROTEINS

by

MIKKEL HERHOLDT JENSEN

B.Sc., University of Southern Denmark, 2005
M.A., Boston University, 2009

Submitted in partial fulfillment of the

requirements for the degree of

Doctor of Philosophy

2013

Approved by

First Reader

Jeffrey R. Moore, Ph.D.
Associate Professor of Physiology and Biophysics

Second Reader

Rama Bansil, Ph.D.
Professor of Physics

ACKNOWLEDGEMENTS

There are many people who deserve great thanks for their help and support during my years as a graduate student. Of course, many thanks to my advisor, Jeffrey R. Moore, with whom I've had the pleasure of working for the majority of my years in graduate school. Jeff has always encouraged and supported me in pursuing projects that I find exciting, and has exposed me to a range of exciting techniques and biological problems. Jeff has the wonderful ability to get excited about a wide range of topics and is always willing to reach outside his comfort zone to learn something new and tackle interesting scientific problems, an attitude towards doing science I find inspiring.

Furthermore, I would like to thank the people I have gotten to know at Boston University over the years. My classmates and fellow graduate students, particularly Christopher Sanborn, Christopher Serino, Jacob Davis, Eitan Anzenberg, Andrew Strikwerda, and Erica Raber, who helped make classes all the more enjoyable and were great friends both in and out of school. Also a great thanks to my fellow labmates in the Moore lab, Michael Greenberg, William Schmidt, James Watt, Anastasia Karabina, and Gerrie Farman.

I have also had the pleasure of working with several faculty members through my semesters of teaching. In particular, I would like to thank Robert Carey, Claudio Rebbi, Ed Kearns, and Manher Jariwala, with whom teaching has been a real pleasure. I am also thankful for having gotten to work with so many

within the undergraduate community at Boston University through my teaching, the names of whom are far too many to list here. I've very much enjoyed getting to know all of you!

I would also like to extend my gratitude towards David A. Weitz at Harvard University, whose lab has often been a home away from home for me, as well as the several students and post docs I've had the pleasure of working with in his lab. I would particularly like to thank Allen Ehrlicher, Ming Guo, and Helen Wu, with whom I've not only gotten to collaborate and do great science, but have also gotten to know as good friends. Through working with Dave, I have also had the pleasure of getting to know and work with Fred MacKintosh, whose insights I have enjoyed and benefited from on more than one occasion.

Finally, I give no greater thanks than to my wife, colleague, and best friend Eliza Morris. It is truly fantastic in all aspects having you in my life.

REGULATION OF MECHANICS AND DYNAMICS OF ACTIN FILAMENTS AND NETWORKS BY ACTIN-BINDING PROTEINS

(Order No.)

MIKKEL HERHOLDT JENSEN

Boston University Graduate School of Arts and Sciences, 2013

Major Professor: Jeffrey R. Moore, Associate Professor of Physiology and Biophysics

ABSTRACT

Actin is a highly ubiquitous and evolutionarily conserved protein capable of polymerizing and forming filamentous polymers which play a central role in cell mechanics and motility. Here, we study the *in vitro* regulation of actin mechanics and dynamics by calponin and caldesmon, two actin-binding proteins believed to be involved in regulating cytoskeletal mechanics and structure through mechanisms not currently well understood.

Chapters 1 and 2 introduce the reader to actin and its roles in the cell, as well as to the methods and theoretical foundations used in this work.

In Chapter 3, we use total internal reflection and confocal fluorescence microscopy to investigate the polymerization dynamics of actin in the presence of a caldesmon C-terminal fragment, H32K. We show that H32K stabilizes a nascent structural state of actin without altering the polymerization dynamics of the filament. We also show that H32K-stabilized nascent actin has increased

affinity for the actin branching protein complex Arp2/3 involved in driving membrane protrusions during cell motility, and propose the nascent state of actin as a possible transient differentiator targeting certain actin-binding proteins to actin *in vivo*. This is to our knowledge the first reported direct functional effect of nascent actin.

In Chapter 4, we use fluorescence microscopy to quantify actin bending mechanics in the presence of the binding protein calponin and show that calponin reduces the persistence length of actin. We compare our results to the literature and compare the mechanical change to electron microscopy reconstructions, which suggest that calponin affects actin intermonomer contacts through interactions with actin subdomain 2.

In Chapter 5, we expand on the results from Chapter 4 using bulk rheology and show that calponin increases the tensile strength of reconstituted actin networks, similar to the effect seen in whole cells and tissues. We discuss these data within an affine network model and show that the results can be entirely explained in terms of the reduced actin persistence length. We use this to propose a novel physical mechanism for calponin function *in vivo*.

This work elucidates the physical mechanisms of calponin and caldesmon function and their role in regulating the cellular cytoskeleton.

TABLE OF CONTENTS

LIST OF TABLES

LIST OF FIGURES

LIST OF ABBREVIATIONS

ADF: actin depolymerizing factor

ADP: adenosine di-phosphate

Arp2/ 3 complex: actin-related protein 2/ 3 complex

ATP: adenosine tri-phosphate

ATPase: adenosine tri-phosphatase enzyme

BSA: bovine serum albumin

ccf: cosine correlation function

DNA: deoxyribonucleic acid

DNase: deoxyribonuclease enzyme

DTT: dithiothreitol

EDTA: ethylene diamine tetraacetic acid

EGTA: ethylene glycol tetraacetic acid

EM: electron microscopy

F-actin: filamentous (polymeric) actin

FRET: Förster resonance energy transfer

G-actin: globular (monomeric) actin

h1CaP: basic calponin (calponin 1); the smooth muscle-specific calponin isoform

h2CaP: neutral calponin (calponin 2)

H32K: 32 kDa C-terminal fragment of caldesmon

h3CaP: acidic calponin (calponin 3)

HP: human platelet

mv: mode variance

NA: numerical aperture

pH32K: phosphorylated H32K

Pi: inorganic phosphate

RS: rabbit skeletal muscle

TIRF: total internal reflection fluorescence

Tm6: α-smooth muscle tropomyosin

Tris: tris(hydroxymethyl)aminomethane

WASP: Wiskott-Aldrich Syndrome Protein

WCA: C-terminal region of WASP protein

1 Introduction and Overview

1.1 Actin

Actin is a 43 kDa protein 375-377 amino acids long. First discovered as part of the actomyosin protein complex responsible for producing the contractile force in skeletal muscle [Straub, 1942], actin is a highly ubiquitous protein abundant in nearly all eukaryotic cells. In addition to its role as the binding partner of myosin motors, actin is an important dynamic mechanical component of both muscle and non-muscle cells.

Actin is extraordinarily well conserved across species as diverse as primitive unicellular organisms to plants and animals [Sheterline & Sparrow, 1994]. A total of six different actin isoforms are expressed in human, each isoform differing in sequence from the others by less 8% (and even less if silent mutations, i.e., mutations between functionally similar residues, are excluded from the count) [Elzinga et al., 1973; Vandekerckhove & Weber, 1978a; Vandekerckhove & Weber, 1978b; Vandekerckhove & Weber, 1979; Herman, 1993]. Each one of these isoforms is completely identical across a wide range of mammals, such as human, cow, rat, mouse, chicken, and pig. The number of isoform differences between the six isoforms is summarized in Table 1.1. Despite the high degree of sequence similarities, actin isoform expression levels differ greatly between different tissues. For example, skeletal muscle actin is virtually all α-skeletal muscle actin, whereas actin from human platelets is a mixture of β

and γ cytoplasmic actin. Even within individual cells, different actin isoforms are found in different regions, suggesting possible functional differences between isoforms [Gordon et al., 1977; Pardo et al., 1983; Otey et al., 1986; Rubenstein, 1990; Herman, 1993; North et al., 1994; Khaitlina, 2001]. In most cases, different actin isoforms are also unable to functionally substitute for each other [Chaponnier et al., 1995; Kumar et al., 1997].

	α skel.	α card.	α vasc.	β cytopl.	γ cytopl.	γ smooth
α skel.	-	4	8	27	24	9
α card.	4	-	6	25	24	7
α vasc.	8	6	-	25	26	6
β cytopl.	27	25	25	-	4	26
γ cytopl.	26	24	24	4	-	23
γ smooth	9	7	6	26	23	-

Table 1.1: Residue differences between actin isoforms.
Listed are the six actin isoforms expressed in human subdivided into two classes: striated muscle (α skeletal, cardiac, and vascular muscle) and non-muscle actin (β and γ cytoplasmic, and γ smooth muscle). Comparisons between different classes (α striated muscle actin and non-muscle actin isoforms) are highlighted in grey. Sequences of these actin isoforms from different organisms can be found online at www.uniprot.org.

In the presence of monovalent and divalent salts and ATP, monomeric actin (G-actin) will polymerize into filamentous actin (F-actin) [Tobacman & Korn, 1983], a semiflexible biopolymer. *In vitro*, these polymers can form filaments tens of microns long; *in vivo*, the assembly and disassembly of actin is tightly regulated by actin-binding proteins [Ayscough, 1998; McGough, 1998; Pollard & Borisy, 2003; Dominguez, 2004, Paavilainen et al., 2004]. The

polymerization process involves two steps; first, actin monomers come together and form an actin tetramer in a slow diffusive-limited nucleation process, after which the filament elongates off of this seed in a process limited by the second-order binding constant of monomers to the filament ends [Oosawa & Kasai, 1962; Wegner & Engel, 1975; Tobacman & Korn, 1983]. The F-actin polymer is double-helical with a half helical repeat of about 36 nm and a diameter of about 7 nm (Figure 1.1). The polymer is dynamic and polar, with constant polymerization and depolymerization occurring *in vitro* at both the plus (or barbed) end and the minus (or pointed) end, which have different critical concentrations of dynamic equilibrium. Upon polymerization, actin hydrolyzes its ATP nucleotide, and the phosphate group is released on the order of minutes in a random fashion [Murakami et al., 2010; Jégou et al., 2011]. These resulting ADP-actin filaments are known to be more dynamic and susceptible to turnover in the cell [Pollard & Borisy, 2003], and also have different polymerization dynamics *in vitro* [Carlier & Pantaloni, 1988; Kuhn & Pollard, 2005; Jégou et al., 2011; Niedermayer et al., 2012].

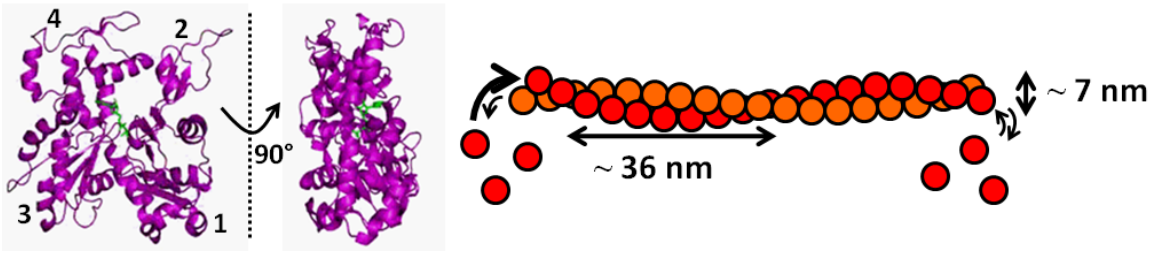

Figure 1.1: Structure of G- and F-actin.
Left: Ribbon model of the actin monomer (purple). The monomer is roughly globular but flattened, as evident from the side view. The monomer can be divided into two subdomains, separated vertically on the figure by a nucleotide binding cleft (nucleotide shown in green). Each of these can be further subdivided into upper and lower subdomains, for four domains total; these are labeled on the figure. Right: Cartoon representation of F-actin. When polymerized, actin forms a double-helical polymer with a long-pitch half helical repeat of about 36 nm and a diameter of about 7 nm. The filament is dynamic at both ends and polar, with a plus (barbed) end exhibiting fast elongation and a minus (pointed) end, which has a higher critical concentration. In vivo, actin assembly and disassembly is highly regulated by actin-binding proteins; in vitro, the differing dynamics results in treadmilling, in which the filament grows at the barbed end and shrinks at the pointed end. In the filament, all monomers are oriented with the nucleotide binding cleft (subdomains 2 and 4) facing towards the pointed end.

Structures of both G-actin and F-actin have been obtained [Suck et al., 1981; Egelman, 1985; Holmes et al., 1990; Kabsch et al., 1990; Bremer & Uebi, 1992; Oda et al., 2009]. These have revealed G-actin as a flattened globular protein with two major domains separated by a cleft in which one ATP or ADP binds. Each of these two sides of actin is further subdivided into two subdomains each, or four subdomains per G-actin monomer. The most recent studies have elucidated the structural changes occurring in the filament upon the G to F transition, which involves the rotation of two subdomains to cause each monomer to form contacts with several of its neighbors. These multiple contacts

and the double-helical nature of the polymer makes for a very stable filament which, as opposed to an Einstein polymer, does not readily exchange monomers or break in the middle of the filament in the absence of severing proteins.

Differences in *in vitro* polymerization dynamics between actin isoforms have been reported; whereas α-actin from striated muscle has a barbed end critical concentration of about 100 nM [Kuhn & Pollard, 2005], the barbed end of non-muscle F-actin has an equilibrium concentration of 500 nM or higher [Gordon et al., 1977; Rubenstein, 1990; Herman, 1993].

Actin function in the cell is tightly regulated by upwards of 60 known actin-binding proteins [Ayscough, 1998; McGough, 1998; Pollard & Borisy, 2003; Dominguez, 2004, Paavilainen et al., 2004]. For example, in the striated muscle sarcomere, the actin-binding protein tropomyosin lies along the long pitch of the actin double helix and blocks myosin binding sites. Activation of muscle contraction involves calcium binding to a second actin-binding protein, troponin, which then allows tropomyosin to move and frees up myosin binding sites on actin [Huxley, 1969; Gordon et al., 2000; Geeves & Holmes, 2005]. In non-muscle cells, actin-binding proteins exist to sequester actin monomers and control polymerization, nucleate new filaments, sever or buttress existing filaments, and form bundled and branched cytoskeletal actin networks through highly regulated cellular processes. This makes the actin cytoskeleton a highly dynamic mechanical component of the cell essential in many processes, such as cell

adhesion, mechanosensing and mechanotransduction, cell motility, and the determination of cell shape and stiffness [Cooper, 1991; Janmey, 1998; Katsumi et al., 2004; Small & Resch, 2005]. However, it also makes for a highly complex system of several levels of emergent behavior in which it is challenging to extract physical information about the workings and mechanisms of individual proteins. This is the underlying motivation for the approach taken in this work, in which reconstituted model systems are used to study actin and two of its binding partners, calponin and caldesmon.

1.2 Smooth muscle, calponin, and caldesmon

Calponin and caldesmon were both discovered in smooth muscle, although both proteins have both smooth muscle and non-muscle isoforms. Smooth muscle tissue lacks the highly ordered and strictly aligned sarcomeric organization of striated muscle, and smooth muscle cells can best be thought of as ordinary cells that have the machinery to substantially contract in a non-directional fashion. Examples of smooth muscle tissue are found in the vasculature, in which smooth muscle needs to modulate its mechanical properties to respond to the pulsatile pressure of the flowing blood while also contracting or relaxing in response to other mechanical or chemical stimuli [Hahn & Schwartz, 2009]. Smooth muscle contractile regulation differs from the troponin-tropomyosin regulation model that so well describes striated muscle types. At the time of the discovery of calponin and caldesmon in the mid-1980s,

the regulation of actomyosin contraction in smooth muscle was poorly understood, and while smooth muscle was known to contain tropomyosin, no troponin was found. Upon its discovery in smooth muscle [Lehman & Kaminer, 1984; Takahashi et al., 1986], calponin was proposed to be a calcium-binding troponin-analogous protein in smooth muscle that could play the role of troponin in actomyosin regulation, hence the name calponin [Winder & Walsh, 1990; Shirinsky et al., 1992; Winder et al., 1998; Takahashi et al., 1988a; Takahashi et al., 1988b]. Although calponin was found to affect actomyosin ATPase activity and actin sliding velocities in *in vitro* myosin motility assays, the notion that calponin functions analogously to troponin has since been proven wrong. Indeed, its role and importance in actomyosin contractile regulation in smooth muscle remains somewhat unclear, as other mechanisms, e.g., myosin light chain phosphorylation [Chalovich, 1988; Trybus, 1991], later have become apparent mechanisms of actomyosin contractile regulation in smooth muscle, and as the absence of calponin does not abolish smooth muscle contractility [Nigam et al., 1998]. This has left calponin as somewhat of a mystery protein in the cell.

Similarly to calponin, caldesmon was initially studied as a possible actomyosin regulator in smooth muscle. Caldesmon was found to inhibit the sliding velocity of actin in *in vitro* actomyosin motility assays [Shirinsky et al., 1992] and actomyosin ATPase activity [Chalovich, 1987] in a phosphorylation-dependent manner, but as was the case for calponin, it was unclear whether this

or other mechanisms, such as myosin regulatory light chain phosphorylation, was the primary regulatory mechanism of smooth muscle contraction. Electron micrograph reconstructions placed caldesmon near weak myosin-binding sites on actin, and showed that caldesmon was well situated to compete sterically with other actin-binding proteins, but also made it clear that caldesmon did not fit with the established troponin-tropomyosin framework of regulation in striated muscle [Lehman et al., 1997]. Like calponin, this left the primary role and mechanism of caldesmon unclear and also left unexplained the role of the non-muscle caldesmon isoform nearly ubiquitous in vertebrates.

1.3 Calponin and caldesmon as cytoskeletal regulators

In recent years, studies of both basic calponin (the smooth muscle-specific isoform of calponin) and the two non-muscle calponin isoforms (neutral and acidic calponin, all named after their respective isoelectric points) have revealed a significant involvement of calponin in cellular mechanotransduction and cytoskeletal regulation, both as an end product and as an intermediary part of mechanosensory regulatory pathways. (For a recent review of our understanding of the biological role of calponin as a cytoskeletal regulator, see [Rozenblum & Gimona, 2008].) Basic calponin, or h1CaP, has been shown to respond to agonist-induced smooth muscle contraction by relocating to the cortical actin, away from contractile actin filaments [Parker et al., 1994]. This translocation was later found to accompany changes in cytoskeletal remodeling,

resulting in larger amounts of F-actin in the cortical regions of the cell [Kim et al., 2008]. A recent study demonstrated the importance of acidic calponin in the rearrangement and regulation of the actin cytoskeleton to facilitate cell fusion [Shibukawa et al., 2010]. As acidic calponin was knocked down, actin cytoskeletal rearrangements and subsequent cell fusion was promoted, suggesting that acidic calponin is an actin cytoskeleton stabilizer which negatively regulates cell fusion. The neutral calponin isoform has also been shown to regulate cytoskeletal actin and is itself regulated by mechanical cellular stimuli [Hossain et al., 2005], and influences cell migration and vascular development [Tang et al., 2006] and cytokinesis through regulation of cytoskeletal actin networks [Hossain et al., 2003]. Basic calponin expression upregulated by vitamin C in smooth muscle tissue was recently found to alter smooth muscle mechanical properties by increasing the tensile strength of the tissue but reducing its stiffness [Arrigoni et al., 2006], an effect potentially important for proper function of smooth muscle tissue under strain. Basic calponin has also been found to stabilize actin in cultured smooth muscle cells and reduce the actin turnover induced by exogenously added chemical stimuli.

Caldesmon is also emerging as a possible regulator of actin, rather than actomyosin contraction, in the cell. Recently, caldesmon has been suggested to stabilize a structural state of actin filaments, termed the “nascent” state [Huang et al., 2010], preventing actin from irreversibly transitioning to a separate

"mature" state after polymerization. The notion that actin exists in multiple structural states is not a new one [Oda & Maéda, 2010]; indeed, some studies have proposed that filamentous actin can exhibit as many as six distinct structures, each of which can coexist within a filament [Galkin et al., 2010]. The concept of transient structural actin maturation from an initial nascent state following polymerization has also been previously proposed [Steinmetz et al., 1997; Bryan & Rubenstein, 2005; Kueh et al., 2008; Galińska-Rakoczy et al., 2009], but because this nascent state is relatively short-lived, it has been poorly characterized, and its significance remains controversial. Caldesmon stabilization of nascent actin opens the door to more detailed studies of this actin structure. The distribution of caldesmon in the cell also offers clues about its function. When cells are stimulated to migrate, caldesmon is phosphorylated and translocated from the cytosol to the cell periphery [Kordowska et al., 2006], including regions of membrane ruffling at the leading edge [Bretcher & Lynch, 1985]. This region is characterized by a high degree of actin filament turnover and polymerization, which drives membrane protrusions and in turn cell motility [Lai et al., 2008]. A key protein complex in this process is the actin-related protein complex Arp2/ 3, which binds to the side of actin filaments in this region and nucleates new filaments which drive the membrane protrusions and cell motility (Figure 1.2). While the state of the actin nucleotide has been shown to be change the affinity of actin for Arp2/ 3 complex

[Ichetovkin, 2002], any role played by caldesmon in this process is unclear, as is the functional importance of the nascent actin state.

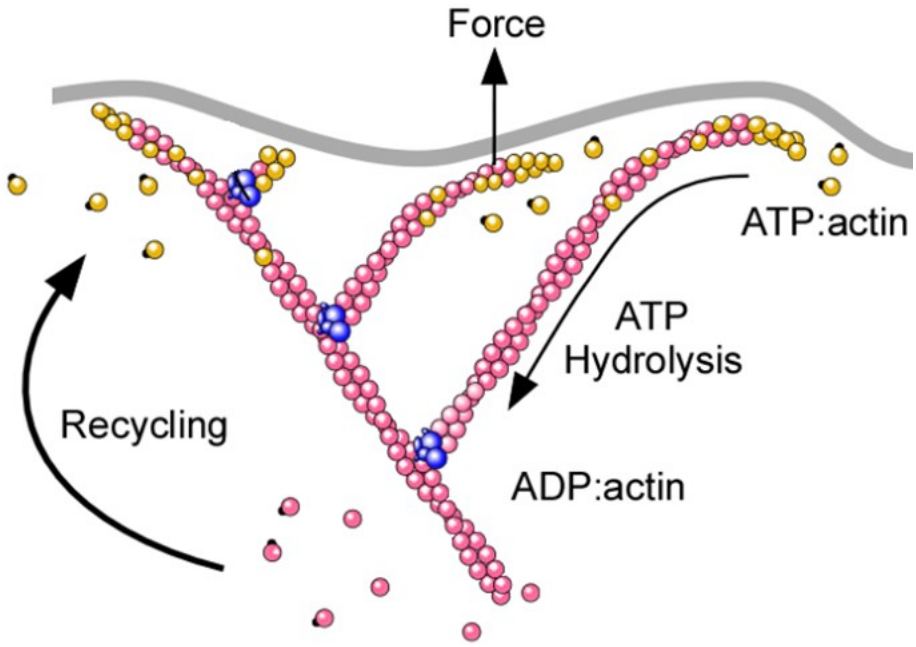

Figure 1.2: Cartoon of Arp2/3-facilitated membrane protrusions.
Arp2/3 complex (blue) binds to the sides of actin near the leading edge of a cell and nucleates new actin filaments. ATP-actin (yellow) is added to the barbed end of new filaments, while ADP-actin (pink) is eventually severed and recycled by actin-binding proteins away from the leading edge. This highly directional process generates actin filaments which polymerize against the cell membrane and drives cell motility.

1.4 Overview of this thesis

The goal of the work presented here is twofold. We aim to shed light on the proposed functions of caldesmon and calponin in regulating the actin cytoskeleton by gaining a better understanding of what role these proteins can play in the cell. We also wish to gain insight into the mechanistic details of how each protein works. Our approach uses *in vitro* reconstituted actin systems

consisting of either single actin filaments or ensembles of filaments, which allow a greater insight into the physical mechanisms and properties of the proteins involved.

In Chapter 2, we describe the methods used in this work, including protein preparation protocols, fluorescence microscopy and bulk rheology techniques, and also introduce the necessary theoretical framework needed to understand the mechanics of single actin filaments and actin networks.

In Chapter 3, we study the role of caldesmon in regulating actin polymerization and maturation, and investigate a novel biological mechanism of caldesmon in cell motility. A C-terminal fragment of caldesmon, H32K, when added before initiation of polymerization, attenuates the pyrene fluorescence intensity of polymerizing actin, which is usually used as a measure of actin polymerization [Huang et al., 2010; Collins et al., 2011]. However, we show using TIRF microscopy that H32K does not affect the polymerization rate of actin, suggesting that the changes in pyrene fluorescence reflects a different structural maturation transition in the filament, which is inhibited by the early addition of H32K [Collins et al., 2011]. The notion that H32K delays a maturation transition in actin and prolongs its nascent state is consistent with electron micrographs, showing a change in the staining of actin that evolves over time into the smooth-looking canonical electron micrograph actin appearance, and that this transition is delayed upon addition of H32K to G-actin prior to

polymerization. To investigate the possible biological role of such a prolonged nascent structural state stabilized by H32K, we compare the ability of nascent actin filaments stabilized by phosphorylated H32K and mature actin in binding Arp2/ 3 complex and forming actin branches. We find that H32K-decorated actin more readily binds Arp2/ 3 complex and forms branches, but only when H32K is present during initial actin polymerization [Jensen et al., 2012a]. These data are consistent with a delay of an irreversible maturation process of actin independent of other transient markers of actin polymerization, such as ATP hydrolysis in the filament. This suggests a novel regulatory mechanism by which the state of actin determines the interactions with Arp2/ 3 complex, and is to our knowledge the first reported direct functional importance of nascent actin filaments.

In Chapter 4, we study single actin filaments with and without calponin and quantify the flexural rigidity as a first step in understanding how calponin alters the mechanics of actin. We measure the flexural rigidity of two actin isoforms (α-skeletal muscle actin and non-muscle β-actin) and compare our measurements to published values. We then show that basic calponin reduces the flexural rigidity of both α-skeletal muscle actin and non-muscle β-actin, suggesting that the slight differences between the actin isoforms does not affect the gross mechanical changes induced by calponin and suggests that either actin isoform can be used as a basis for a more intricate model system. Actin filaments

decorated with calponin are found to be more susceptible to shear during sample preparation. We compare these results to reconstructions of calponin-decorated actin from cryo-electron microscopy images and argue that changes around actin subdomain 2 could account for the mechanical changes observed on the filament level [Jensen et al., 2012b]. These results show that calponin alters the mechanics of F-actin without other cellular constituents present and points to regulation of filament rigidity as a possible parameter of importance in understanding calponin's effects on actin in the cell.

In Chapter 5, we study the effects of calponin on the mechanics of fully crosslinked actin networks using bulk rheology. In such networks, we find that basic calponin delays the strain stiffening onset and subsequent network failure, increasing both the maximal strain and maximal stress the networks can withstand before failing. We also investigate the effects of basic calponin on tropomyosin-actin networks and find that this increase in tensile strength occurs in both plain actin and tropomyosin-decorated actin networks, suggesting that calponin can affect both populations of actin in the cell. We compare our results to an affine network model and show that the effects are consistent with and explained by the calponin-induced reduction in actin persistence length observed in single filament studies (Chapter 4). Together, these data suggest a simple mechanism through which calponin mechanically stabilizes actin in cells under external strain by making actin filaments more flexible and in turn making the

actin cytoskeleton more compliant. This model explains the qualitative behavior observed in cells and tissues using only a single parameter, the actin flexural rigidity, and is the first model explaining mechanistically calponin function of actin stabilization.

The work presented here elucidates the possible functional roles of calponin and caldesmon and gives insight into the physical mechanisms by which they function. In Chapter 6, we summarize our findings and discuss further applications of such *in vitro* model systems in understanding complex biological systems.

2 Experimental Methods and Theoretical Framework

2.1 Protein preparations

C-terminal fragment H32K of smooth muscle caldesmon for use in actin polymerization and branching experiments is purified in bacteria and phosphorylated as previously described [Huang et al., 2010].

Arp2/ 3 complex is isolated from bovine brain [Boczkowska et al., 2008].

Smooth muscle calponin isoform (h1CaP) from ferret used for single actin flexural rigidity and rheology experiments is expressed in E. Coli as previously described [Appel et al., 2010].

Smooth muscle tropomyosin isoform Tm6 for rheology studies is purified from freshly isolated bovine aorta as previously described [Bretscher, 1984; Gallant et al., 2011].

Actin is purchased from Cytoskeleton (Denver, CO). Lyophilized rabbit skeletal muscle G-actin (100% α-skeletal isoform) labeled with rhodamine on surface lysine residues to a labeling ratio of about 0.5 dyes/ monomer or unlabeled is purchased and stored at -80 °C until use. In both cases, the >99% purity product is used. Experiments involving non-muscle actin use Cytoskeleton >99% pure lyophilized G-actin from human platelets, which consists of about 85% non-muscle β-actin and about 15% non-muscle γ-actin.

Alternatively, G-actin is purified from chicken pectoralis muscle, an actin isoform completely identical in sequence to rabbit skeletal muscle [Elzinga et al.,

1973; Vandekerckhove & Weber, 1979]. This purification protocol is very similar to established muscle actin purification protocols [Spudich & Watt, 1971; Pardee & Spudich, 1982], which themselves differ very little from the originally used methods [Straub, 1942] with modifications [Drabikowski & Gergely, 1962]. The prep is outlined below. Note that all equipment and solutions should be pre-cooled and all procedures carried out in a cold room on ice to slow protease activity.

Preparation of acetone powder from chicken pectoralis muscle:

- Remove pectoralis breast muscle from a freshly killed chicken. It is important that the chicken be freshly killed to avoid deterioration of proteins by proteases after sacrificing the animal. Avoid the lower muscle. Keep extracted muscle meat on ice.
- Using a scalpel pre-rinsed with 0.2 M EDTA, trim off tendons and fat and cut the muscle into several thin pieces. The connective tissue on the surface of the muscle is removed using a pre-rinsed pair of scissors.
- Pass sliced muscle through a pre-chilled meat grinder that has been rinsed with 0.2 M EDTA. Re-grind and remove tissue from inside grinder.
- Add 2 mL extraction buffer (0.3 M KCl, 0.15 M KPi, 20 mM EDTA, 5 mM $MgCl_2$, 3.3 mM ATP, 5 mM DTT, pH 6.7) per gram of tissue and stir gently with a large stir bar for 12 minutes.

- Add an equal amount of cold distilled water quickly, and then add cold distilled water again to dilute to half again; the total volume is now 4x the original volume after adding extraction buffer.
- Filter through 4 layers of cheesecloth into a large beaker. Change cheesecloth if necessary. Save the pulp in the cheesecloth for actin purification.
- From the pulp, extract a pellet of actin by washing 2 times with 500 mL 50 mM $NaHCO_3$ for 12 minutes. Stir gently using an overhead stirrer.
- Filter through 4 layers of cheesecloth after each extraction, squeezing out liquid.
- Extract pellet 2 times with 500 mL distilled cold water for 5 minutes.
- Filter through cheese cloth after each extraction.
- In a fume hood, extract pellet 4 times with 500 mL cold acetone for 10 minutes, and filter between each iteration.
- Filter the pellet through a Buchner filter.
- Dry acetone powder in hood overnight.
- Weigh and store at -20 °C.

Purification of actin from acetone powder:

- Mix 20 mL of resuspension buffer (2.0 mM Tris, 0.2 mM ATP, 0.5 mM DTT, 0.1 mM $CaCl_2$, and 1.0 mM NaN_3, pH 8.0) with each gram of acetone

powder and extract with stirring on ice for 30 minutes. The final yield is about 20 mg of actin per gram of acetone powder.

- Centrifuge for 30 minutes at 30,000*g* and 4 °C.
- Filter the supernatant with actin monomers through cheese cloth into a graduated cylinder and measure the volume.
- Resuspend pellets in a volume of resuspension buffer identical to the originally used volume, and repeat the centrifugation and filtration.
- While stirring the combined supernatants from the two centrifugation/ filtration steps, add 2.5 mL of 2 M KCl per 100 mL (final concentration 50 mM KCl) and then 0.2 mL of 1 M $MgCl_2$ per 100 mL (final concentration 2 mM $MgCl_2$). This will induce polymerization of the actin. Cover and stir slowly for 1 hour at room temperature.
- After 1 hour, bring to 0.8 M KCl by adding 5.6 g of KCl per 100 mL while stirring in the cold room. This dissociates any contaminating tropomyosin from the actin filaments.
- After 30 minutes, centrifuge for 2 hours at 140,000*g* to pellet the actin filaments.
- Discard the supernatant and gently wash off surface of pellets with resuspension buffer. Remove pellets by scraping them into a small volume of resuspension buffer with a stainless steel spatula.

- Gently resuspend the pellets in about 3 mL of resuspension buffer per original gram of acetone powder using a Dounce homogenizer.
- Dialyze actin for 2-3 days against 3-4 changes of 500 mL resuspension buffer to depolymerize the actin.
- Clarify the depolymerized actin solution by centrifugation at 140,000*g* for 2 hours. Keep the supernatant containing the depolymerized actin monomers.
- Gel-filter on a G-75 Sephadex size exclusion column in resuspension buffer to remove actin oligomers, capping proteins, and other minor contaminants.
- Aliquot the collected G-actin into smaller tubes and snap-freeze in a dry ice-ethanol bath. The aliquots are stored at -80 °C until use and should not be refrozen once thawed from -80 °C.

2.2 Glass cleaning and flow cell preparation

Imaging experiments involving actin assembly require ultraclean glass. If cleaning is omitted or insufficiently done, actin accumulation and aggregation on the glass surface will be evident during fluorescence imaging. Autofluorescence from grease and natural oils on the slides, if not properly cleaned, will also be noticeable during imaging. Gloves should be worn when handling the slides at all times to prevent oils from the skin from depositing on the glass., microscope cover slips purchased from Corning Glass (Corning, NY) undergo a series of

cleaning steps to avoid non-specific interactions with G-actin during the experiment. The cover slides are placed individually in a slide holder, after which they undergo the following procedure:

- Plasma clean under vacuum for 10 minutes.
- Sonicate bathe in glassware soap 20 minutes (1% 7x glassware cleaning solution, MP Biomedicals, Solon, OH).
- Sonicate bathe in ultraclean Millipore-filtered water 5 minutes.
- Sonicate bathe in acetone 15 minutes.
- Sonicate bathe in 1 M KOH 20 minutes.
- Clean each slide with ultraclean Millipore-filtered water.
- Dip and soak each slide in ethanol for 5 minutes.
- Remove from ethanol and leave to dry in dust-free environment for at least 2 hours.

At this point, the cover slips are assembled into sample flow chambers with double-sided tape and microscope slides (see Figure 2.1), which are stored away from dust until use. Flow chambers prepared using this procedure are used for all TIRF and confocal fluorescence microscopy in this work.

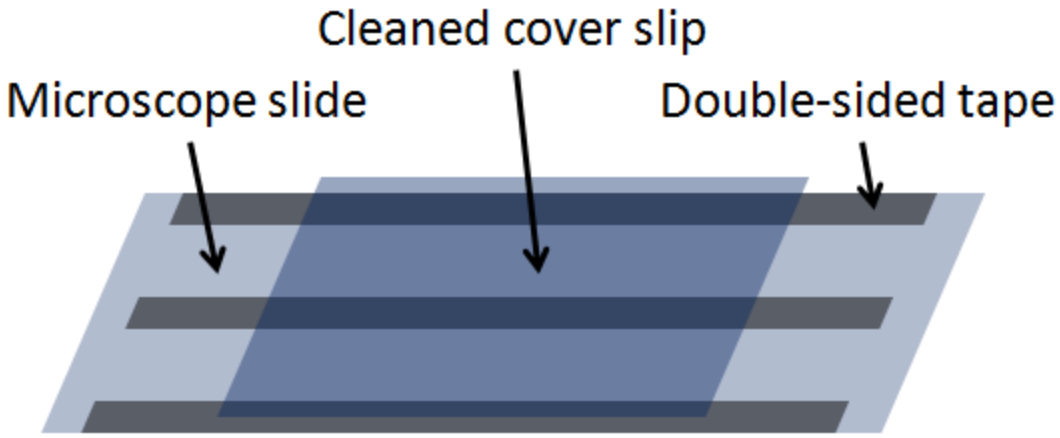

Figure 2.1: Assembly of sample flow chambers.
Flow chambers are assembled from cleaned glass cover slips using double-sided tape. Once assembled, the slides can be used several months later if carefully kept away from dust.

2.3 Microscopy techniques

Epifluorescence experiments in this work are done using a Nikon Eclipse TE-2000U inverted microscope (Nikon; Melville, NY) with a Mercury lamp as the excitation source. While regular epifluorescence microscopy suffices for imaging when there is no excessive background fluorescence present, the imaging of actin assembly requires microscopy techniques which reduce the background intensity and thus enhances the signal-to-noise ratio. Since *in vitro* actin polymerization typically needs to be done at G-actin concentrations of at least a few 100 nM to exceed the barbed end critical concentration, assembly of fluorescently labeled actin is imaged using either total internal reflection fluorescence microscopy (TIRF microscopy) [Amann & Pollard, 2001; Kuhn & Pollard, 2005; Breitsprecher

et al., 2009] or confocal fluorescence microscopy [Ichetovkin et al., 2002]. In our studies of actin assembly, we utilize both techniques.

TIRF excitation is achieved by directing a beam of excitation light, typically from a laser source, onto a sample substrate at an incidence angle beyond the critical angle of refraction. Although no intensity can be transmitted deep into the sample substrate for incidence angles beyond the critical angle, the boundary conditions of the magnetic and electric fields prevent all of the electromagnetic wave from simply reflecting directly at the interface; rather, an attenuated evanescent wave must penetrate partway into the sample substrate.

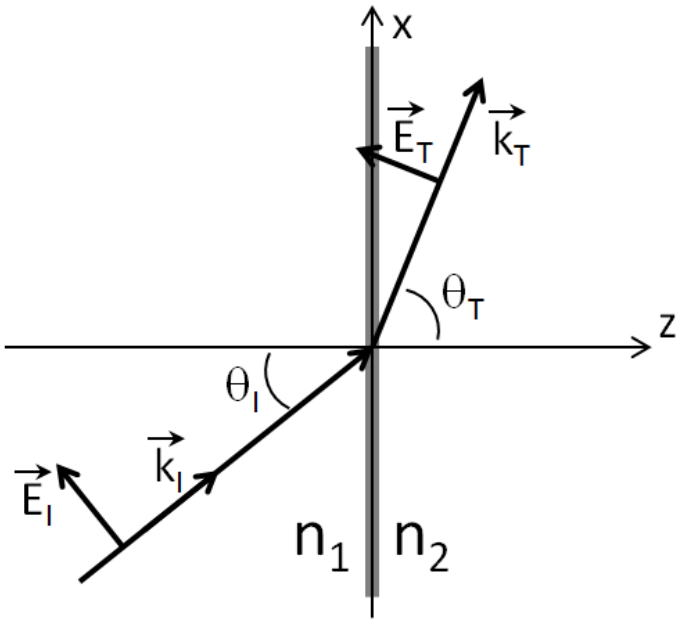

Figure 2.2: Electromagnetic wave incident on a material interface.
Medium 1 has a higher index of refraction than medium 2, making total internal reflection of the wave possible.

Consider a plane electromagnetic wave traveling through a medium with index of refraction n_1 incident on a material with index n_2, with $n_1 > n_2$ (see Figure 2.2). In terms of the angle of transmission, the transmitted electric field is

$$\vec{E}_T(\vec{r},t) = E_{T0}e^{i(\vec{k}_T\cdot\vec{r}-\omega t)} \tag{2-1}$$

In Cartesian coordinates, this can be written as

$$\begin{aligned}\vec{k}_T\cdot\vec{r} &= k_T(\sin\theta_T\,\hat{x} + \cos\theta_T\,\hat{z})\cdot(x\hat{x}+y\hat{y}+z\hat{z}) \\ &= k_T(x\sin\theta_T + z\cos\theta_T) = xk_T\sin\theta_T + zk_T\sqrt{1-\sin^2\theta_T} \\ &= xk_T\sin\theta_T + izk_T\sqrt{\sin^2\theta_T - 1} \equiv kx + i\delta z\end{aligned} \tag{2-2}$$

where

$$k \equiv k_T\sin\theta_T = \frac{\omega n_2}{c}\frac{n_1}{n_2}\sin\theta_I = \frac{\omega n_1}{c}\sin\theta_I \tag{2-3}$$

and

$$\begin{aligned}\delta &\equiv k_T\sqrt{\sin^2\theta_T - 1} = \frac{\omega n_2}{c}\sqrt{\left(\frac{n_1}{n_2}\right)^2\sin^2\theta_I - 1} \\ &= \frac{\omega}{c}\sqrt{{n_1}^2\sin^2\theta_I - {n_2}^2}\end{aligned} \tag{2-4}$$

The transmitted electric field is then

$$\vec{E}_T(\vec{r},t) = E_{T0}e^{i(kx-\omega t)}e^{-\delta z} \tag{2-5}$$

If $\sin\theta_I$ is below the sine of the critical angle $\sin\theta_c = \frac{n_2}{n_1}$, δ becomes imaginary, and $\vec{E}_T$ becomes purely a plane wave with x- and z-components. If $\theta_I > \theta_c$, δ is real, and $\vec{E}_T$ is an evanescent wave propagating in the x-direction (along the interface) and attenuated exponentially in the z-direction with an attenuation

depth of $1/\delta$ [Griffiths, 1999]. For an interface between typical microscope immersion oils ($n_1 = 1.56$) and water ($n_2 = 1.33$), the critical angle is 58.5°. As the incidence angle is increased slightly beyond this angle the penetration depth quickly becomes comparable to or smaller than the wavelength of excitation light used (see Figure 2.3). This allows for fluorescence excitation at very shallow depths, meaning that only labeled sample very close to the surface of the microscope slide will be illuminated, while labeled sample further into solution will not.

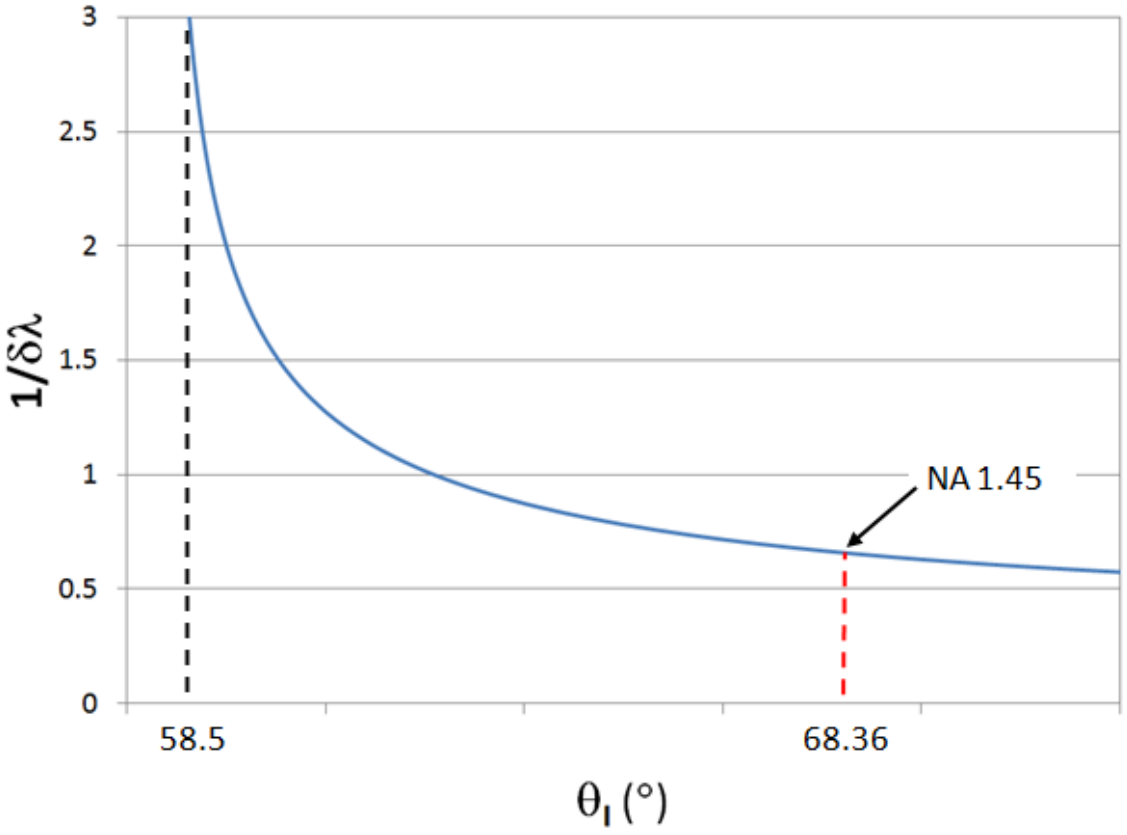

Figure 2.3: Attenuation depth of an evanescent wave.
For reference, the angle a 1.45 numerical aperture objective is shown. This numerical aperture is sufficient for TIRF microscopy and is typically the lowest common oil immersion NA used for objective-based TIRF microscopy. While a 1.40 NA objective ($\theta_I = 63.82°$) is theoretically possible, it leaves much less room for error in alignment and is not practical; a 1.30 NA oil immersion objective, another common NA objective, is insufficient for TIRF microscopy ($\theta_I = 56.44°$).

TIRF excitation can be obtained experimentally either by bringing the excitation beam through a prism optically coupled to the sample, or by bringing the excitation beam onto the edge of a high-numerical aperture objective. To image actin assembly using TIRF microscopy, we build a custom setup around a Nikon Eclipse TE-2000U inverted microscope (Nikon; Melville, NY) using a 532

nm Nd:YAG laser as the excitation source (see Figure 2.4). The objective used is an oil immersion objective with a numerical aperture of 1.45. This means that for a laser beam brought in at the edge of the objective parallel to the optical axis of the objective, the angle of incidence onto the sample will be 68.4°, corresponding to an exponential attenuation depth of about 300 nm (see Figure 2.3). In practice, a somewhat smaller incidence angle is obtainable, meaning the excitation light will penetrate deeper into solution.

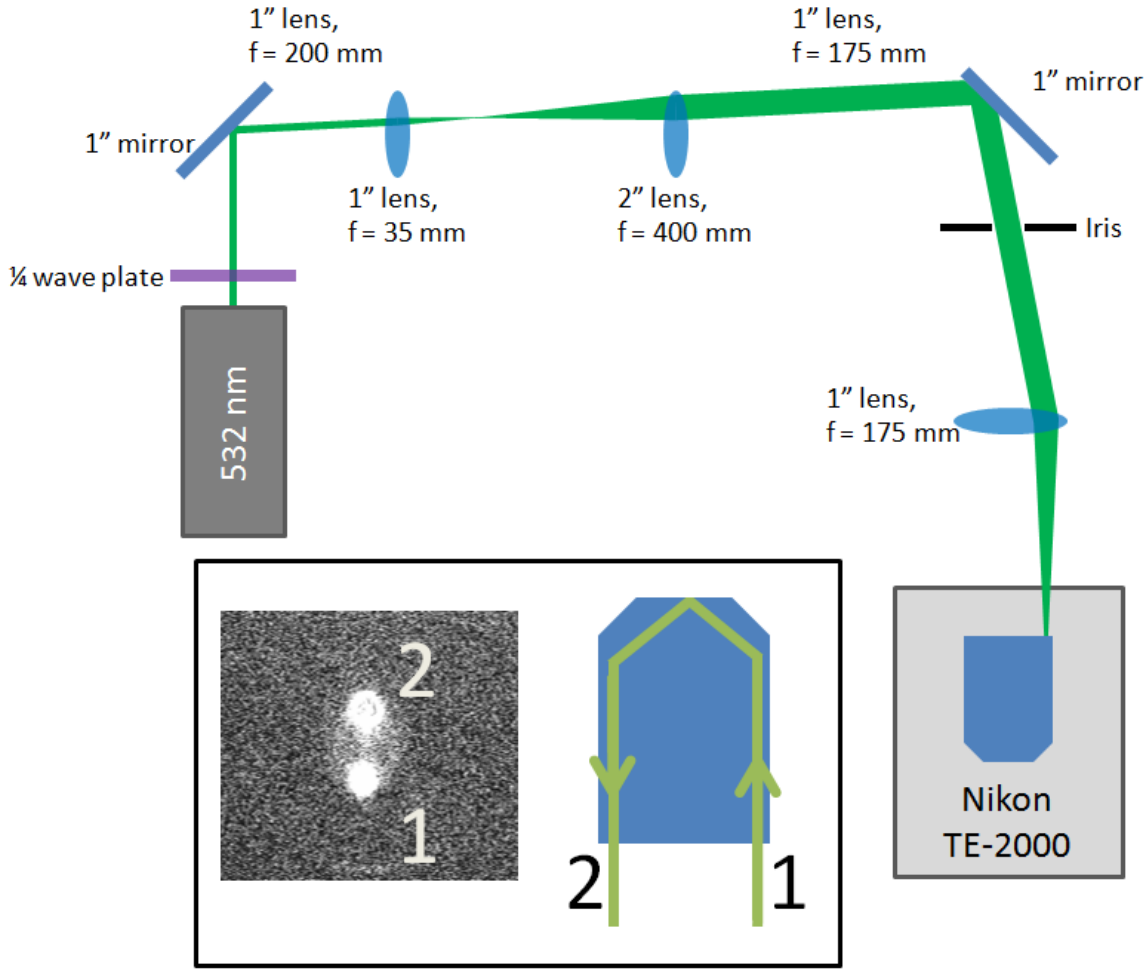

Figure 2.4: Experimental TIRF microscopy setup.
The ¼ wave plate ensures circular polarization of the laser excitation light, after which the beam is expanded and steered to the edge of the microscope objective. The inset shows reflections off the objective lens of the incoming and totally internally reflected beams, indicating total internal reflection has been achieved.

The laser beam is first sent through a ¼ wave plate to circularly polarize the light. Two mirrors are used to steer the beam through a Keplerian beam expander. A third lens is placed before the back port of the microscope with one focal point at the objective image plane. At the second focal point of this lens is

placed an iris aperture. This aperture is used for aiming purposes; when the beam is steered through the iris, its placement guarantees that the beam will enter the objective parallel to its optical axis. To align the TIRF excitation beam, the two mirrors are used to walk the beam towards the edge of the objective while monitoring the back focal plane with a camera mounted on the microscope camera port. Reflections from the objective mark the incoming beam; once the incoming angle reaches the critical angle, the internally reflected beam will be visible as well, as shown on the inset of Figure 2.4. At this point, TIRF illumination is fine-tuned using the two mirrors while imaging a flow chamber with fluorescent sample on the surface. After this, the setup is aligned and ready for use. On this setup, imaging is done using a Scion frame grabber (Frederick, MD) and an ICCD camera (PCI IC 310B, Birmingham, NJ).

Confocal fluorescence microscopy can be used to achieve a similar effect as with TIRF microscopy, in which only a narrow field of fluorescent sample is excited. By placing a pinhole in the path of the fluorescence emission, only light emitted from the focal plane will reach the detector. As a result, only a narrow plane is imaged, while the fluorescence background from out-of-plane sources is eliminated. While confocal microscopy allows for three-dimensional imaging by scanning and stacking several confocal planes, we use confocal microscopy in a single plane near the surface of the sample chamber. Multi-color fluorescence imaging is done using a Leica SP5 conventional confocal microscope, a 100x 1.4

numerical aperture oil immersion objective, a 488 nm argon ion laser (for excitation of Alexa Fluor 488 dye), and a 543 nm helium neon laser (for excitation of rhodamine dye). These lasers are scanned across the region of interest, allowing photomultiplier tubes to build an image of the area. Dynamic filtering, in which the emitted light is broken into its spectral components using a prism and distributed onto several different photomultiplier tubes, allows for simultaneous imaging of Alexa Flour 488-labeled actin and rhodamine-labeled actin simultaneously. Since actin polymerization is a fairly slow process, the signal-to-noise ratio is improved by scanning each line of the image 16 times and averaging the lines. On the Leica SP5 microscope, a 512x512 image with 16-fold line averaging takes about 10 seconds to capture.

2.4 Image processing

All image processing is done in ImageJ (rsbweb.nih.gov/ ij). Captured images are processed to either extract a single-pixel skeleton (for use in flexural rigidity analysis or determination of actin filament lengths in polymerization experiments), or to enhance the image quality through smoothening and contrast enhancement (for fluorescence experiments involving Arp2/ 3 complex-induced branching on actin).

To skeletonize a stack of images each containing a filament, the following process is used:

- Crop the original stack of images to reduce the processing time in the following steps
- Subtract background to help flatten the image; for an image of original resolution of 640x480 pixels, a rolling ball average of 50 pixels (corresponding to about 7 μm) is used
- Enhance contrast by 0.5%, normalizing the intensity across all slices
- Apply a Gaussian blur with σ of 0.25 μm
- Magnify the image 5-fold, using a bicubic interpolation
- Threshold the image stack to create a black/white representation of the filament
- After removing any stray objects still in any frames, skeletonize the black/white representation; ensure that no spokes are created in the process
- To ensure a successful skeletonization, overlay the resulting skeleton with the 5x magnified fluorescence images (see Figure 2.5)

The magnification step is a simple way of creating a skeleton with sub-pixel resolution. Any level of magnification could be used, so long as the original image is of good enough quality that the final skeleton accurately overlays with the original image. The resulting image can either be used to extract a filament length, or to computationally parameterize the filament in terms of its tangent angle and arc length anywhere along the length of the filament.

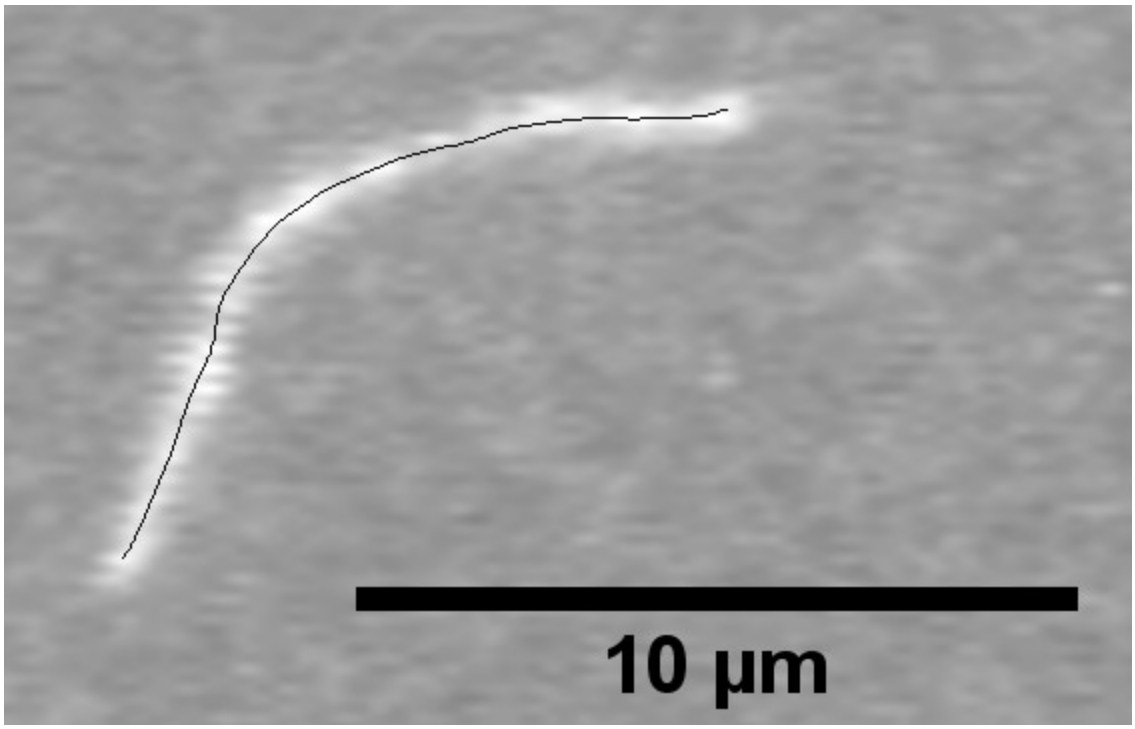

Figure 2.5: Filament skeleton overlaid with unprocessed fluorescence image. *Overlays of skeletonized images with the unprocessed originals are done for every frame to visually ensure agreement before computing the persistence length from the skeleton.*

Images of Arp2/3-induced branches taken with confocal fluorescence microscopy are processed in a similar way. A lower Gaussian blur radius of 0.025 µm is used to smoothen out any pixel noise caused by the scanning of the excitation laser. Due to the more complex images, with multiple objects and many intersecting or overlapping filaments, branch points are counted manually, and the length of filaments is quantified by hand using the "segmented line" tool in ImageJ.

2.5 Bulk rheology

Rheology is the study of how materials deform or flow in response to an external force (for a recent review of bulk rheological applications to biopolymer networks, see [Gardel et al., 2008]). In a shear rheometer, a shear stress σ can be applied, and the resulting shear strain response γ can be measured. If the material is purely elastic, any given applied stress with correspond to a certain strain, the ratio of which corresponds to the linear shear elastic modulus:

$$G' = \frac{\sigma}{\gamma} \tag{2-6}$$

In contrast, if the material behaves as a Newtonian fluid, the applied stress determines the strain rate rather than the strain, and the proportionality between the two is the fluid viscosity η:

$$\eta = \frac{\sigma}{\dot{\gamma}} \tag{2-7}$$

In practice, most biological samples exhibit some degree of both elasticity and viscosity, and the linear shear modulus is a combination of these two behaviors.

The mechanical properties of a sample can be probed by applying a sinusoidal oscillation $\sigma(\omega) = \Sigma \sin(\omega t)$ at an angular frequency ω and amplitude Σ about equilibrium and monitoring the resulting strain $\gamma(\omega) = \Gamma \sin\big(\omega t + \delta(\omega)\big)$. If the material is purely elastic, the two will be in phase, whereas a viscous material (in which the stress is proportional to the strain rate $\dot{\gamma}$) will exhibit a $\frac{\pi}{2}$ phase difference between stress and strain. A viscoelastic material will exhibit a

combination of these two behaviors, and the elastic and viscous moduli can be determined as [Gardel et al., 2008]:

$$G'(\omega) = \frac{\Sigma}{\Gamma}\cos\big(\delta(\omega)\big) \tag{2-8}$$

$$G''(\omega) = \frac{\Sigma}{\Gamma}\sin\big(\delta(\omega)\big) \tag{2-9}$$

$$\tan\big(\delta(\omega)\big) = \frac{G''(\omega)}{G'(\omega)} \tag{2-10}$$

Here, G' denotes the linear elastic (storage) shear modulus, and G'' denotes the linear viscous (loss) shear modulus.

If the material response is non-linear over the range of applied stresses, the linear elastic moduli will no longer accurately represent the material viscoelasticity. Instead, a pre-stress σ_0 can be applied if the material does not flow substantially, and oscillatory bulk rheology can then be applied around σ_0 instead of about 0 stress. This will yield the non-linear differential elastic and viscous shear moduli:

$$K'(\omega) = \frac{\Delta\Sigma}{\Delta\Gamma}\cos\big(\Delta\delta(\omega)\big) \tag{2-11}$$

$$K''(\omega) = \frac{\Delta\Sigma}{\Delta\Gamma}\sin\big(\Delta\delta(\omega)\big) \tag{2-12}$$

$$\tan\big(\Delta\delta(\omega)\big) = \frac{K''(\omega)}{K'(\omega)} \tag{2-13}$$

(2-11) – (2-13) are identical in appearance to the linear moduli (2-8) – (2-10) in the absence of an applied pre-stress, but describe the viscoelasticity when materials

exhibit non-linearities. As we will see in Chapter 5, actin networks behave in a highly non-linear fashion at sufficiently high stresses, and the differential moduli will be used to describe their behavior in these cases.

Finally, the material response can also be investigated by applying variations of creep tests and monitoring the stresses and strains. For example, in samples exhibiting a high degree of transient flow, a creep test can be performed in which a constant stress σ_0 is applied and the resulting strain $\gamma(t)$ is monitored. This also allows for relaxation times to be investigated by applying and removing the stress in a step-wise fashion. In this work, we will make use of the strain ramp, in which the sample is strained at a constant rate $\dot{\gamma}$. This approach is especially convenient because, as will be discussed in more detail in Chapter 5, actin networks permanently crosslinked with biotin-neutravidin are predominantly elastic and thus exhibit little strain rate dependence. Furthermore, using a permanent crosslinker, the networks experience very little creep under stress. Applying a strain ramp at constant strain rate therefore allows for the determination of the network elastic properties over a range of linear and non-linear regimes. At low strain rates (i.e., for low viscous contribution), the differential elastic modulus can be determined along the entire stress-strain curve as

$$K' = \frac{\partial \sigma}{\partial \gamma} \tag{2-14}$$

This approach is equivalent to pre-stressed oscillatory rheology in determining K', but the strain ramp is preferable in this study, as we are also interested in determining the yield stress and strain (γ_{max} and σ_{max}), both of which are directly apparent from the strain ramp. The moduli and rheological measurements discussed here are summarized in Figure 2.6.

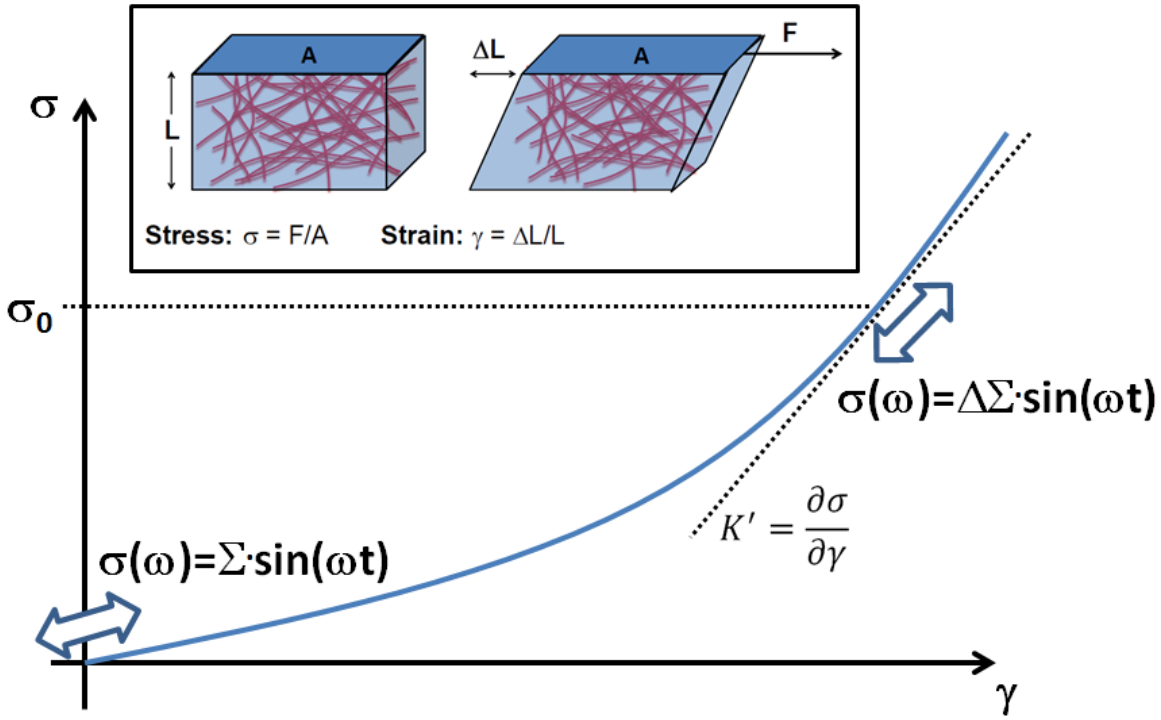

Figure 2.6: Graphical representation of bulk rheological measurements.
The linear moduli G' and G'' are measured by applying an oscillatory shear about equilibrium. Beyond the linear response, the differential moduli K' and K'' can be measured by applying a pre-stress σ_0 and oscillating about this non-zero stress. The slope along the stress-strain curve for an elastic material (or, equivalently, for a quasistatic strain ramp with $\dot{\gamma} \to 0$) is the differential modulus K', which at zero stress equals G'. The inset defines stress and strain in terms of the geometry and applied shear force.

All bulk rheology in this work is done on an Ares-G2 stress-controlled rheometer (TA Instruments; New Castle, DE) using custom made top and bottom geometries of roughened stainless steel. The top geometry is a parallel plate geometry with a diameter of 40 mm. The bottom plate is attached over the standard rheometer plate by heating the plate to 65 °C and melting paraffin onto the plate (the melting point of paraffin is 52-54 °C). Once the stainless steel plate is attached, the plate is cooled and the paraffin hardens, holding the bottom geometry in place (see Figure 2.7).

The inertia of the top geometry is calibrated and a rotational mapping performed before a series of experiments. At this point, the distance is zeroed by bringing the top geometry down onto the bottom plate, after which the geometry is retracted and the sample can be loaded (see Chapter 5.2.1 for details on sample preparation). No further calibrations or mappings are done between samples to avoid introducing systematic error during a series of measurements, although the gap is zeroed between samples and cleanings of the geometries.

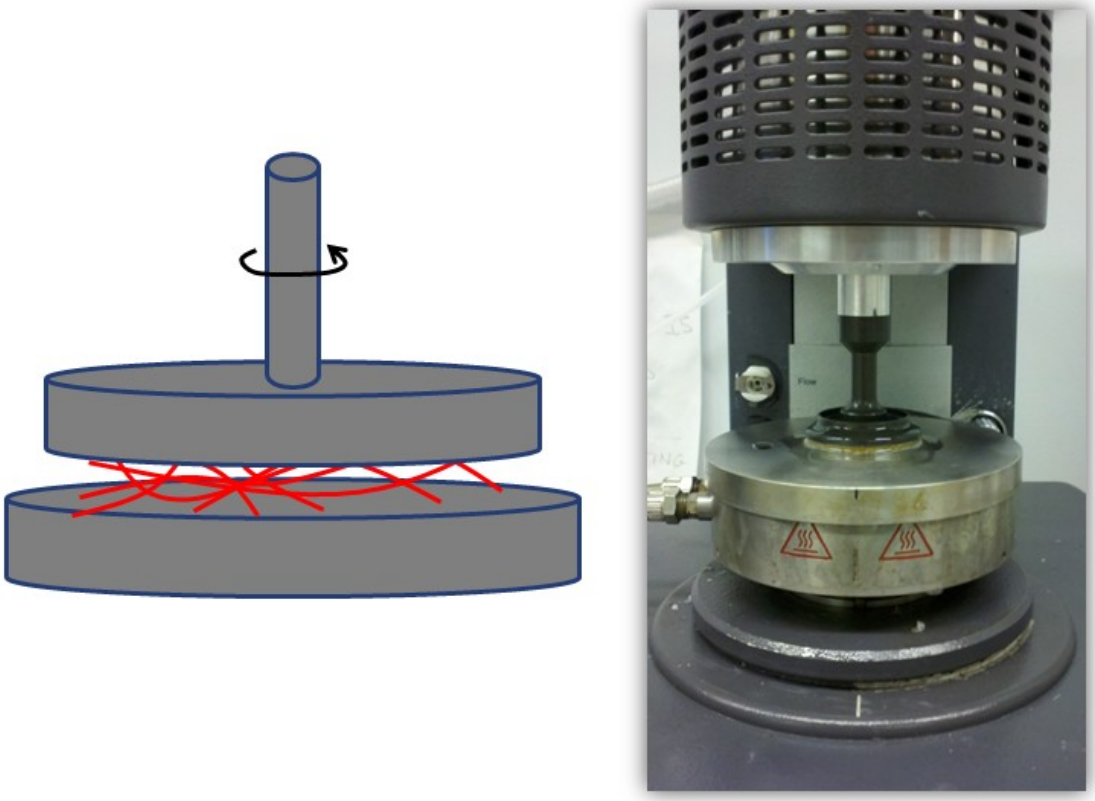

Figure 2.7: Rheometer setup used for actin bulk rheology.
The rheometer consists of a movable top geometry and a stationary bottom geometry, on which the normal force is measured. The actin sample is polymerized between these plates and the top geometry rotated to measure the network properties, as sketched to the left. To the right is shown the rheometer setup. The top geometry is lowered to the desired gap size above the bottom plate, which is attached using paraffin wax. The liquid visible is mineral oil used to seal the sample from evaporation.

2.6 Single filament flexural mechanics

2.6.1 The beam equation and energy of bending of a rod

As a basis for quantifying the bending mechanics of biopolymers, consider a rod bent into a radius of curvature R (Figure 2.8) [Howard, 2001]. The torque τ

required to bend the rod is proportional to the curvature, with a constant of proportionality describing the flexural rigidity of the rod:

$$\tau = \kappa \frac{1}{R} \tag{2-15}$$

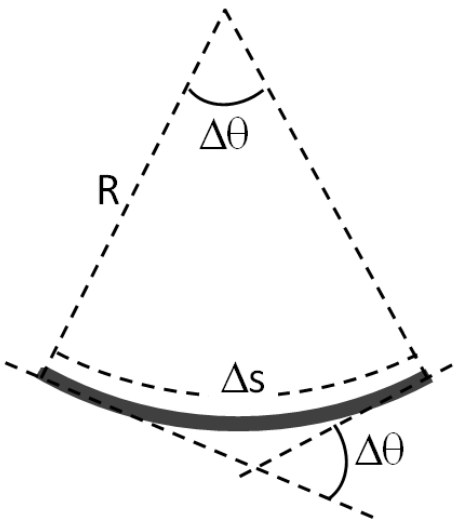

Figure 2.8: Bending of a rod through an angle Δθ.
The arc length Δs is $R\Delta\theta$ for any angle $\Delta\theta$. For a small enough $\Delta\theta$, the required torque to bend the rod can be expressed in terms of $\frac{d^2y}{dx^2}$, since $\frac{dy}{ds} \approx \frac{dy}{dx}$.

To rewrite this beam equation into a more useful form, consider the tangent angle anywhere along the beam's arc length *s*. (See Figure 2.9.) In Cartesian coordinates, this angle is

$$\frac{dx}{ds} = \cos\theta \quad ; \quad \frac{dy}{ds} = \sin\theta \tag{2-16}$$

It also follows from Figure 2.8 that

$$\frac{d\theta}{ds} = \frac{1}{R} \tag{2-17}$$

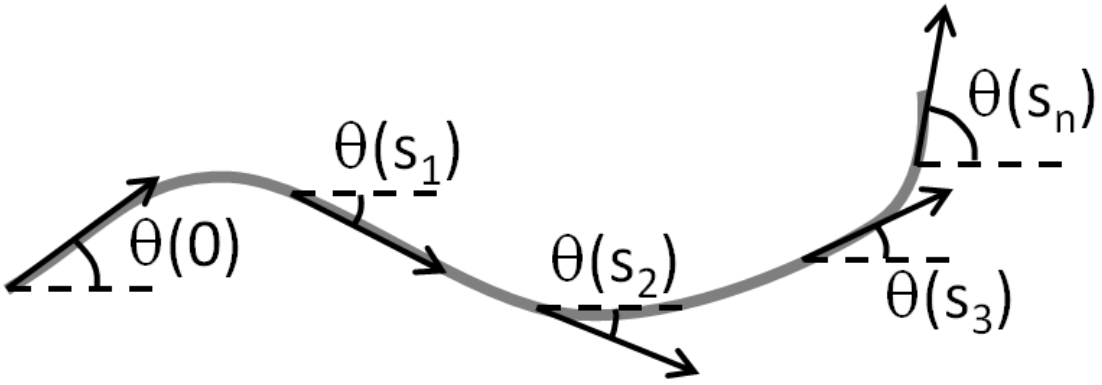

Figure 2.9: Parameterization of a rod in terms of its tangent angle.
The horizontal direction is arbitrarily chosen as $\theta = 0$.

If the deflection in angle is not too large, $x \approx s$, and

$$\frac{dy}{dx} \approx \frac{dy}{ds} = \sin\theta \approx \theta \tag{2-18}$$

which means that the beam equation can be rewritten as

$$\tau = \kappa \frac{d\theta}{ds} = \kappa \frac{d}{ds}\left(\frac{dy}{ds}\right) = \kappa \frac{d^2y}{ds^2} = \kappa \frac{d^2y}{dx^2} \tag{2-19}$$

The potential energy of bending of this rod is calculated as the integral of the torque over the total curvature [Howard, 2001]. Rewriting the curvature $\frac{1}{R} = \frac{d\theta}{ds} \equiv \rho$ for convenience and using the expression for torque from the beam equation (2-19), the energy of bending becomes

$$dU = \left[\int_0^{\rho_0} \tau \cdot d\rho\right] ds = \left[\int_0^{\rho_0} \kappa\rho \cdot d\rho\right] ds = \frac{1}{2}\kappa\rho^2 ds \tag{2-20}$$

or

$$\frac{dU}{ds} = \frac{1}{2}\kappa\left(\frac{d\theta}{ds}\right)^2 \tag{2-21}$$

2.6.2 Polymer persistence length and the cosine correlation function

To relate the average shape of an actin polymer fluctuating thermally, the polymer is parameterized in terms of tangent angles $\theta(s)$ on any point along the filament arc length *s*. (See Figure 2.9.) Below, we assume $\theta(0) = 0$ without loss of generality. Consider the temporal mean of the cosine of θ at arc length *s*, written $\langle\cos[\theta(s)]\rangle = c(s)$:

$$\begin{aligned} c(s+\Delta s) - c(s) &= \langle\cos[\theta(s+\Delta s)] - \cos[\theta(s)]\rangle \\ &= \langle\cos[\theta(s+\Delta s) + \theta(s) - \theta(s)] - \cos[\theta(s)]\rangle \\ &= \langle\cos[\Delta\theta + \theta(s)] - \cos[\theta(s)]\rangle \end{aligned} \tag{2-22}$$

where we have introduced $\Delta\theta = \theta(s+\Delta s) - \theta(s)$. The tangent angles are statistically independent because the thermal forces acting on the different segments are independent. Using this, as well as trigonometric identities, we obtain:

$$\begin{gathered} c(s+\Delta s) - c(s) = \\ \langle\cos[\theta(s)]\cdot\cos[\Delta\theta] - \sin[\theta(s)]\cdot\sin[\Delta\theta]\rangle - \langle\cos[\theta(s)]\rangle = \\ \langle\cos[\theta(s)]\rangle\cdot\langle\cos[\Delta\theta]\rangle - \langle\sin[\theta(s)]\rangle\cdot\langle\sin[\Delta\theta]\rangle - \langle\cos[\theta(s)]\rangle = \\ \langle\cos[\theta(s)]\rangle\cdot(\langle\cos[\Delta\theta]\rangle - 1) \end{gathered} \tag{2-23}$$

Above, we the average values of the sine terms are 0, because the angles are equally distributed about 0. For a small step Δs,

$$c(s+\Delta s) - c(s) \approx \frac{dc(s)}{ds}\Delta s \tag{2-24}$$

Combining (2-23) and (2-24), and using the Taylor expansion of $\cos[\Delta\theta] \approx 1 - \frac{1}{2}\Delta\theta^2$ for small $\Delta\theta$:

$$\begin{aligned} \frac{dc(s)}{ds} &\approx \frac{\langle\cos[\Delta\theta]\rangle - 1}{\Delta s} c(s) \\ &\approx -\frac{1}{2}\left\langle\frac{\Delta\theta^2}{\Delta s}\right\rangle c(s) \end{aligned} \tag{2-25}$$

Comparing this to (2-21) and using the principle of energy equipartition, we can rewrite this as a first-order differential equation and solve by direct integration:

$$\begin{aligned} \frac{dc(s)}{ds} &= -c(s)\frac{\langle\Delta U\rangle}{\kappa} = -\frac{1}{2}k_B T\frac{c(s)}{\kappa} \\ \int\frac{dc}{c} &= -\int\frac{1}{2}\frac{k_B T}{\kappa}ds \end{aligned} \tag{2-26}$$

or

$$\langle\cos[\theta(s) - \theta(0)]\rangle = e^{-\frac{k_B T}{2\kappa}} = e^{-\frac{1}{2L_p}} \quad ; \quad L_p \equiv \frac{\kappa}{k_B T} \tag{2-27}$$

(2-27) is referred to as the cosine correlation function of a worm-like chain polymer. Note that the expression above is derived for a filament in two dimensions with one degree of flexural freedom and energy $\frac{1}{2}k_B T$. The same expression would apply to a polymer free to fluctuate in three dimensions with two degrees of flexural freedom and energy $k_B T$, only without the factor of $\frac{1}{2}$ in the exponent. The quantity $\frac{\kappa}{k_B T}$ has units of length and is termed the polymer

persistence length [Landau & Lifshitz, 1980; Howard, 2001]. It can be geometrically interpreted as the length over which two tangential segments become decorrelated; polymers of lengths much larger than their persistence lengths, such as DNA, are considered flexible [Bednar et al., 1995], while polymers of lengths much shorter than L_p, such as microtubules, are considered rigid [Gittes et al., 1993]. Actin filaments, as will be discussed in more detail in Chapter 4, have lengths similar to L_p, and are considered semiflexible [Gittes et al., 1993; Isambert et al., 1995]. (2-27) can be directly applied to sequential images of a thermally fluctuating actin filament to extract its persistence length. Note, however, that we assume the polymer to be straight under no thermal forces. If this is not the case and the polymer has an intrinsic shape, L_p in (2-27) can be thought of as an apparent persistence length, and will differ from the actual, or dynamic, persistence length; for example, this has been noted for strands of smooth muscle tropomyosin [Sousa et al., 2010].

2.6.3 Mode variance analysis

In addition to the cosine correlation analysis, a second common form of analysis uses the variance in amplitudes of filament fluctuations to extract the persistence length [Howard, 2001]. Referring to Figure 2.9, the parameterization $\theta(s)$ is written as a superposition of orthogonal Fourier modes:

$$\theta(s) = \sqrt{\frac{2}{L}} \sum_{n=0}^{\infty} a_n \cos\frac{n\pi s}{L} \quad ; \quad a_n = \sqrt{\frac{2}{L}} \int_0^L \theta(s) \cos\frac{n\pi s}{L} ds \tag{2-28}$$

Here, L is the contour length of the filament, and a_n denotes the amplitude of the n^{th} Fourier mode. From (2-21), the total energy of bending of a rod is:

$$U = \int_0^L \frac{1}{2}\kappa \left(\frac{d\theta}{ds} - \frac{d\theta^0}{ds}\right)^2 ds \tag{2-29}$$

Since $\frac{d\theta}{ds} = -\sqrt{\frac{2}{L}} \sum_{n=0}^{\infty} \frac{n\pi}{L} a_n \sin\frac{n\pi s}{L}$, (2-29) becomes

$$\begin{aligned} U &= \frac{1}{2}\kappa \int_0^L \left(\frac{2}{L} \sum_{n=0}^{\infty} \left(\frac{n\pi}{L}\right)^2 \sin^2\left(\frac{n\pi s}{L}\right) (a_n - {a_n}^0)^2\right) ds \\ &= \frac{1}{2}\kappa \sum_{n=0}^{\infty} \left(\frac{n\pi}{L}\right)^2 (a_n - {a_n}^0)^2 \end{aligned} \tag{2-30}$$

Above, we use that $\int_0^L \sin^2\left(\frac{n\pi s}{L}\right) ds = \frac{L}{2}$. Considering the n^{th} mode and using the principle of energy equipartition for a polymer with one degree of flexural freedom, we obtain:

$$U_n = \frac{1}{2}\kappa \left(\frac{n\pi}{L}\right)^2 (a_n - {a_n}^0)^2 \tag{2-31}$$

$$\langle U_n \rangle = \frac{1}{2} k_B T = \frac{1}{2}\kappa \left(\frac{n\pi}{L}\right)^2 \langle (a_n - {a_n}^0)^2 \rangle = \frac{1}{2}\kappa \left(\frac{n\pi}{L}\right)^2 \mathrm{Var}(a_n) \tag{2-32}$$

$$\frac{\kappa}{k_B T} = L_p = \frac{L^2}{n^2 \pi^2 \mathrm{Var}(a_n)} \tag{2-33}$$

The final simplification uses the definition of persistence length from (2-27).

As might be intuitively expected, a stiffer polymer will exhibit a smaller amplitude variance under thermal forces. (2-33) takes advantage of the fact that

the Fourier modes of $\theta(s)$ are orthogonal, and hence the variance of the amplitude of each mode can be used to determine the persistence length. In practice, this can either be done by calculating L_p for each mode and ensuring that each mode converges to the same value, or by noting that $\mathrm{Var}(a_n) = {L_p}^{-1}\left(\frac{n\pi}{L}\right)^{-2}$ and determining L_p from a best fit over a range of modes [Gittes et al., 1993; Greenberg et al., 2008; Brangwynne et al., 2007]. In contrast to cosine correlation analysis, mode variance analysis does not require the filament to be intrinsically straight; however, it is important to ensure that images of a fluctuating filament are temporally uncorrelated, as the analysis will otherwise underestimate the mode variance.

2.6.4 Hydrodynamic relaxation of filament shapes

To properly image and interpret the shapes of thermally fluctuating actin filaments, the time it takes the filament to relax in a viscously damped environment must be taken into consideration. The temporal correlation time is highly nonlinear in both the filament length L, as well as in the mode number n.

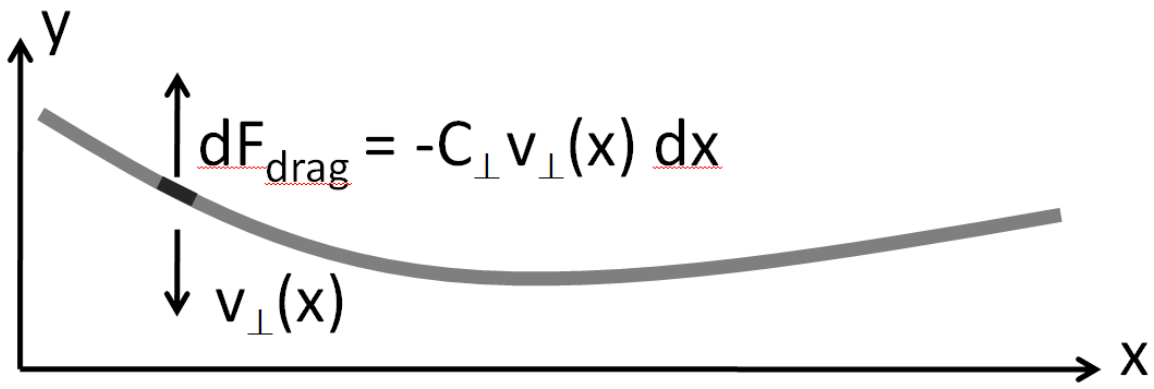

Figure 2.10: Perpendicular hydrodynamic drag force on a straightening rod
The restoring spring force straightening the rod is given by the beam equation (2-19), while the drag force per unit length is velocity dependent and acts to dampen this straightening.

To see how the temporal correlation time scales with filament length, we consider a bent filament represented as a homogeneous rod (Figure 2.10) relaxing under its own flexural rigidity in a viscously damped environment [Howard, 2001]. The total torque τ on the segment at position x' due to perpendicular drag forces on the right-hand side of the segment is

$$\tau(x') = \int_{x'}^{L} f_{\perp}(x)\,(x - x')dx \tag{2-34}$$

Differentiation gives

$$\frac{\partial^2 \tau}{\partial x^2} = f_{\perp}(x) = -C_{\perp}\frac{\partial y}{\partial t} \tag{2-35}$$

Here, $f_{\perp}$ is a velocity-dependent viscous drag force per unit length perpendicular to the filament, and $C_{\perp}$ is a drag coefficient per unit length of the filament. Combining this result with the beam equation (2-19) yields

$$\frac{\partial^2 y}{\partial x^2} = \frac{\tau}{\kappa} \tag{2-36}$$

$$\frac{\partial^4 y}{\partial x^4} = \frac{\partial^2 \tau}{\partial x^2}\frac{1}{\kappa} = -\frac{C_\perp}{\kappa}\frac{\partial y}{\partial t} \tag{2-37}$$

(2-37) is referred to as the hydrodynamic beam equation. This equation can be solved using separation of variables:

$$y(x,t) = X(x)\cdot T(t)$$

$$T\frac{\partial^4 X}{\partial x^4} = -\frac{C_\perp}{\kappa}X\frac{\partial T}{\partial t} \tag{2-38}$$

$$\frac{1}{X}\frac{\partial^4 X}{\partial x^4} = -\frac{C_\perp}{\kappa}\frac{1}{T}\frac{\partial T}{\partial t} \equiv \lambda$$

This yields two differential equations in x and t:

$$\frac{\partial^4 X}{\partial x^4} = \lambda X \tag{2-39}$$

$$\frac{\partial T}{\partial t} = -\frac{\lambda\kappa}{C_\perp}T \tag{2-40}$$

The temporal part (2-40) is easily solved by integration to yield an exponentially decaying function with relaxation constant t:

$$\int \frac{1}{T}\partial T = \int \frac{\lambda\kappa}{C_\perp}\partial t \tag{2-41}$$

$$T(t) = Ae^{-t/t} \quad ; \quad t \equiv \frac{C_\perp}{\lambda\kappa} \tag{2-42}$$

The spatial part (2-39) has the general solution

$$X(x) = Be^{\lambda^{1/4}x} + Ce^{-\lambda^{1/4}x} + De^{i\lambda^{1/4}x} + Ee^{-i\lambda^{1/4}x} \tag{2-43}$$

For a filament with unconstrained ends, the following boundary conditions apply:

$$\frac{\partial^2 X(0;L)}{\partial t^2} = 0 \tag{2-44}$$

$$\frac{\partial^3 X(0;L)}{\partial t^3} = 0 \tag{2-45}$$

(2-44) ensures that the torque at both filament ends is 0, while (2-45) ensures that the shear force at the ends is 0. This yields the solutions

$$\lambda = \left(\frac{2\alpha_n}{L}\right)^4$$
$$\tan\alpha_n = (-1)^n \tanh\alpha_n \quad ; \quad n = 1,2,3,\ldots \tag{2-46}$$

Approximate values for the constants α_n are

$$\alpha_n \approx \left(n + \frac{1}{2}\right)\frac{\pi}{2} \tag{2-47}$$

The temporal relaxation constant then becomes

$$t_n \approx \frac{C_\perp}{\kappa}\left(\frac{L}{\pi\left(n+\frac{1}{2}\right)}\right)^4 \tag{2-48}$$

In the case of actin, a 10 μm filament will have a perpendicular drag coefficient per unit length of [Howard, 2001; Tirado & García de La Torre, 1979]:

$$C_\perp = \frac{2\pi\eta}{\ln\left(\frac{L}{2r}\right) - 0.20} = \frac{2\pi \cdot 1\ \text{mPa·s}}{\ln\left(\frac{10\ \mu\text{m}}{7\ \text{nm}}\right) - 0.20} \approx 1\ \text{mPa·s} \tag{2-49}$$

Then, assuming a persistence length of about 17 μm [Gittes et al., 1993], the first-mode temporal relaxation constant at room temperature ($T = 300$ K) is

about 0.25 seconds. The strong length dependence quickly exacerbates the slow relaxation for longer filaments; furthermore, the above estimate of the drag coefficient assumes no nearby boundaries, and is an underestimation in experiments in which actin is imaged near a glass surface. In this work, where fluctuating actin filaments are imaged between two glass coverslips no more than a few microns apart, a frame rate of 0.2 fps is used to minimize temporal correlation between frames.

2.6.5 A note regarding the interpretation of actin persistence length

For the most part of this study, F-actin is treated as a semiflexible worm-like chain when discussing the mechanics of the polymer. Since most of the actin filaments we will be considering are long enough to contain several helical repeats, and long enough to be considered semiflexible, quantifying the rigidity of actin in terms of its persistence length is appropriate throughout this study.

However, if actin is treated as a homogeneous rod, its flexural rigidity can be further related to its Young's compression modulus E and the second moment of inertia I by [Landau & Lifshitz, 1986; Howard, 2001]

$$\frac{\Delta F}{\Delta A} = E\frac{\Delta L}{L} = E\frac{r}{R} \tag{2-50}$$

where r is the radius of the rod, and R is the radius of curvature of the rod, as shown in Figure 2.8. The torque is then

$$\tau = \int d\tau = \int r dF = \int r \frac{dF}{dA} dA = \frac{E}{R} \int r^2 dA = \frac{EI}{R} \tag{2-51}$$

where $I \equiv \int r^2 dA$ and $\kappa = EI$. In this framework, actin is often treated as a rod with an elliptical cross-section and second moment of inertia $I = \frac{\pi}{4} r_a^2 r_b^2$, resulting in a Young's modulus on the order of 1 GPa, similar to that of Plexiglas [Gittes et al., 1993; McCullough et al., 2008].

Especially when discussing the effects of actin-binding proteins on flexural mechanics of actin, we will avoid this further interpretation of $\kappa = EI$ in this study. The interactions between actin monomers and the potentially complicated ways in which these are modified by actin-binding proteins does not obviously lend itself to a simplified interpretation as a change in E. Perhaps most importantly, the binding of actin-binding proteins to F-actin does also not create a single material with a simple, geometrically interpretable second moment of inertia; for example, tropomyosin binds to actin by forming a chain which wraps around the filament and only loosely connects to the interface of actin in some places [Li et al., 2011]. Therefore, we do not use the interpretation of $\kappa = EI$ beyond order-of-magnitude estimates of E here, and discuss instead actin flexibility simply in terms of the polymer persistence length and changes thereof induced by actin-binding proteins.

2.7 Actin network mechanics

2.7.1 Actin as an entropic spring

Consider a single semi-flexible actin filament suspended between two nodes, as shown in Figure 2.11. At $T = 0$, the polymer will assume an end-to-end length equal to its arc length, but at higher temperatures, the end-to-end length will be shortened by Δ due to transverse thermal fluctuations of amplitude L [MacKintosh et al., 1995; Gardel et al., 2004a; MacKintosh, 2006]. This end-to-end contraction depends on the polymer bending stiffness and can be estimated by considering the thermal energy density and equating it to the bending energy (2-21):

$$\frac{k_B T}{l} \sim \kappa \left(\frac{L}{l^2}\right)^2 \tag{2-52}$$

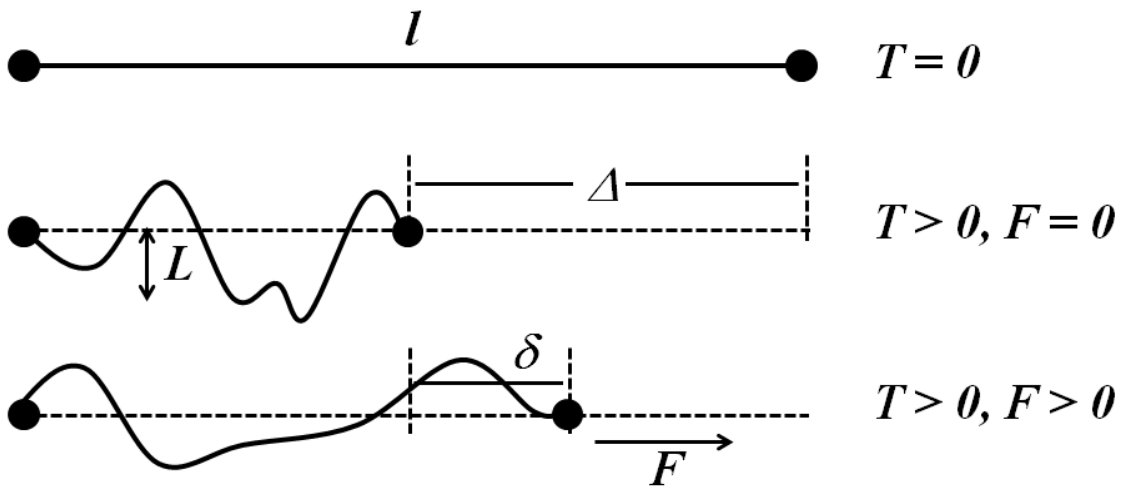

Figure 2.11: Actin as an entropic spring.
At zero temperature, the end-to-end length equals the full arc length, whereas thermal fluctuations will cause the filament end-to-end length to contract by a distance Δ for $T > 0$. Applying a force F will pull out entropy of the system, and the spring will exert a restoring force, which for small displacements is linear in δ.

Geometrically, $\Delta \sim \frac{L^2}{l}$ for $l \gg L$, which, combined with (2-52), yields

$$\Delta \sim l^2 \frac{k_B T}{\kappa} = \frac{l^2}{L_p} \tag{2-53}$$

Thus, the equilibrium end-to-end length contraction in the absence of an external force is inversely proportional to the rigidity of the polymer.

If a force is applied, the filament will be partially extended by a distance δ (Figure 2.11, bottom panel). This results in a decrease in the amplitude of transverse fluctuations. The work (or energy) per unit length associated with this extension is

$$U_F \sim F \frac{\Delta}{l} \sim F \left(\frac{L}{l}\right)^2 \tag{2-54}$$

Thus, under an applied force,

$$U_F + U_B = \frac{k_B T}{l} \tag{2-55}$$

Since the contour length of the filament is unchanged as it gets stretched, it can be determined geometrically that

$$\left(\frac{L}{l}\right)^2 \sim \frac{(\Delta - \delta)}{l} \tag{2-56}$$

which yields

$$F\left(\frac{L}{l}\right)^2 + \kappa\left(\frac{L}{l^2}\right)^2 \sim F\frac{(\Delta - \delta)}{l} + \frac{\kappa(\Delta - \delta)}{l^3} \sim \frac{k_B T}{l} \tag{2-57}$$

or

$$F \sim \frac{k_B T}{(\Delta - \delta)} - \frac{\kappa}{l^2} \tag{2-58}$$

Note that the force diverges as $\delta \to \Delta$, that is, when the polymer is pulled towards full extension. Thus, a single entropic spring will exhibit strain stiffening under linear extension. However, for small extensions δ, the force-extension is linear. Taylor expanding and keeping only the lowest non-trivial term of δ gives

$$F \sim \frac{k_B T}{\Delta} + \frac{\delta k_B T}{\Delta^2} - \frac{\kappa}{l^2} \sim \frac{k_B T}{l^2 k_B T/\kappa} + \frac{\delta k_B T}{(l^2 k_B T/\kappa)^2} - \frac{\kappa}{l^2} \sim \frac{\kappa^2}{k_B T l^4}\delta \tag{2-59}$$

2.7.2 Mesh size and entanglement length

The mesh size ξ of a polymer network is a geometrical parameter defined as the side length of a cubic box so that the box is as large as can be while only

containing a single filament (see Figure 2.12). Physically, this length corresponds to the typical spacing between polymers in solution. In the limit of rigid rods ($L_p \gg \xi$), ξ depends only on the polymer volume fraction ϕ and the molecular size of the monomers making up the polymer solution [De Gennes et al., 1976; MacKintosh, 2006].

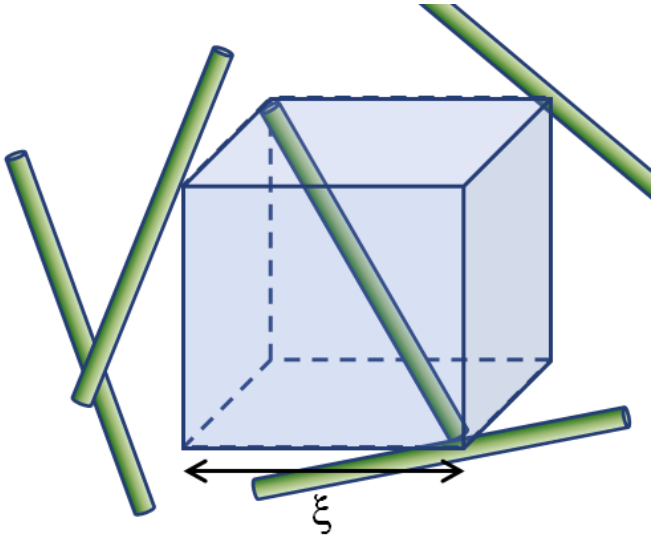

Figure 2.12: Geometrical definition of mesh size.
For a network of rigid polymers, the mesh size is defined as the largest size of a box still only containing a single filament.

From Figure 2.12, the volume fraction can be related to the mesh size as

$$\phi = \frac{\sqrt{3}\xi\pi r^2}{\xi^3} \tag{2-60}$$

where r is the radius of the polymer. By definition, the volume fraction is also the volume of each monomer v times the concentration of monomers cN_A. This yields:

$$vcN_A = \frac{\sqrt{3}\xi\pi r^2}{\xi^3}$$
$$\xi = \left(\frac{\sqrt{3}\pi r^2}{vN_A}\right)^{1/2} c^{-1/2} \tag{2-61}$$

For actin, assuming a volume per monomer of 92 nm^3 and a filament diameter of 7 nm, the above expression reduces to

$$\xi = 3.5 \cdot 10^{-8} \sqrt{\frac{\text{mol}}{\text{m}}} \cdot c^{-1/2} \tag{2-62}$$

or, using units of μm and μM for ξ and c,

$$\xi(\mu\text{m}) = 1.10 \cdot [c(\mu\text{M})]^{-1/2} \tag{2-63}$$

This scaling relation has been experimentally verified, but with proportionality constant between ξ and $\sqrt{c}$ of 1.46 instead of the 1.10 in (2-63) [Schmidt et al., 1989]; this experimental proportionality constant will be used in this work when estimating mesh sizes of polymer networks.

To describe the average distance between points at which polymers cross and physically interact (entanglements), the thermal fluctuations must be taken into consideration; these in turn depend on the persistence length of the polymer [Odijk, 1983; MacKintosh, 2006].

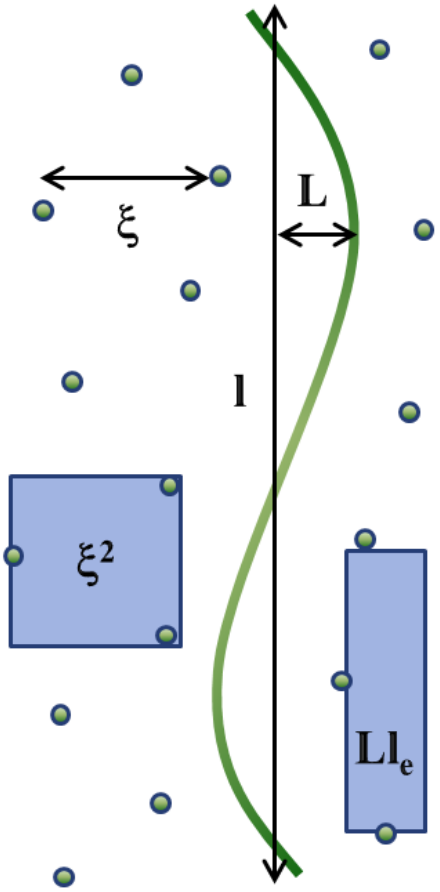

Figure 2.13: Geometrical definition of entanglement length.
Since the polymer needs to intersect two polymers over the distance l_e the area Ll_e swept out by the polymer by thermal fluctuations must be about equal to ξ^2.

Consider a polymer fluctuating thermally in a network of mesh size ξ (see Figure 2.13). The area swept out by the polymer will be roughly the length of the polymer l times the amplitude of the fluctuation, denoted on Figure 2.13 as L. If the entanglement length is defined as the distance between two points at which the polymer crosses and interacts with another polymer in the network, the probability of another polymer being within the area $l \cdot L$ must be ≈ 1, which is

true if this area is comparable to ξ^2. In this case, l becomes l_e (the entanglement length), and

$$\xi^2 \sim L l_e \tag{2-64}$$

The transverse fluctuations of a filament of length l_e can be shown from a scaling argument to be $L^2 \sim \frac{{l_e}^3}{L_p}$ [MacKintosh, 2006], and so

$$\xi^2 \sim \sqrt{\frac{{l_e}^3}{L_p}} l_e \sim {l_e}^{5/2} {L_p}^{-1/2} \tag{2-65}$$

$$l_e \sim \xi^{4/5} {L_p}^{1/5} \tag{2-66}$$

For semiflexible polymers ($L_p \gg \xi$ or equivalently $l_e \gg L$), the entanglement length is larger than the mesh size.

2.7.3 Affine models of actin networks

The elasticity of actin networks can be understood in terms of the properties of the filaments themselves (their persistence length) and the geometrical properties of the actin network (the mesh size and entanglement lengths, which in turn depend on the actin concentration). All models discussed here assume an affine deformation of the network, meaning the contributions to the elasticity are entropic in nature, and that the deformations are uniformly scaling with the bulk strain throughout the sample. This is true for networks of sufficiently long polymers and high enough concentrations to ensure full percolation, while networks of a low concentration of short filaments will have a mechanical, non-affine response [MacKintosh, 2006].

For an entangled actin network, the network elasticity arises from the entanglements between filaments [Isambert & Maggs, 1996]. A filament confined by the surrounding network to a volume of $\xi^2 l_e$ will have two degrees of bending freedom, corresponding to an energy of $k_B T$. This energy per volume results in a linear modulus of

$$G' \sim \frac{k_B T}{\xi^2 l_e} \sim \frac{k_B T}{\xi^2 \left(\xi^{4/5} {L_p}^{1/5}\right)} \sim k_B T {L_p}^{1/5} \xi^{-14/5}$$
$$G' \sim k_B T {L_p}^{1/5} c^{7/5} \tag{2-67}$$

where in the final steps we have used the expressions for mesh size (2-61) and entanglement length (2-66) found earlier.

A crosslinked affine actin network is expected to exhibit a somewhat stronger concentration dependence [MacKintosh et al., 1995]. Considering the force-extension relation expected for an entropic spring of original extension l_c (the distance between crosslinkers) being stretched by a force F over a distance δ (2-59), the linear elastic modulus can be written in terms as the stress σ and stress γ as

$$G' = \frac{\sigma}{\gamma} \sim \frac{F/\xi^2}{\delta/l_c} \sim \frac{\delta k_B T {L_p}^2}{{l_c}^4} \frac{l_c}{\xi^2 \delta} \sim \frac{k_B T {L_p}^2}{\xi^2 {l_c}^3} \sim k_B T {L_p}^2 \xi^{-2} (n l_e)^{-3}$$
$$G' \sim k_B T {L_p}^2 \xi^{-2} n^{-2} \xi^{-12/5} {L_p}^{-3/5} \sim k_B T {L_p}^{7/5} n^{-2} \xi^{-22/5} \tag{2-68}$$

or

$$G' \sim k_B T {L_p}^{7/5} n^{-2} c^{11/5} \tag{2-69}$$

where n is determined by the crosslinking density. Above, we use (2-61) and (2-66) to substitute for mesh size and entanglement length.

The non-linear behavior of actin networks depends on whether the networks are fully percolated or not. While entanglements provide elasticity in the linear regime, the entanglements are pulled out and the filaments flow when subjected to external strain. In contrast, a network percolated by crosslinkers exhibits a strong strain stiffening, which can result in elasticities many times larger than G' [Gardel et al., 2004a]. The origin of this strain stiffening can be explained within the affine model by noting that the full force-extension curve for an entropic spring is linear for small extensions (2-59) but diverges as the filament nears full extension [MacKintosh, 2006]. While models for strain stiffening will not be discussed in detail here, we note that an alternative model, in which filaments are recruited in a non-affine fashion to stiffen the overall network, has also been proposed [Onck et al., 2005].

In terms of the extension Δ of a single filament due to thermal forces (2-53), the maximal strain a crosslinked network can withstand before failing is

$$\gamma_{\max} \sim \frac{\Delta}{l_c} \sim \frac{l_c}{L_p} \tag{2-70}$$

Thus, the excess chain length in the form of thermal undulations decreases with increasing persistence length, meaning there is less chain slack available to "pull out" under an applied stress [MacKintosh et al., 1995]. Similarly, the onset of

strain stiffening γ_{crit} scales as l_c/L_p in the affine model, as has been noted previously [Tharmann et al., 2007].

3 Caldesmon and Actin Filament Dynamics

3.1 Introduction

Caldesmon is an actin-binding protein present in almost all vertebrate cells. There are two major caldesmon isoforms: the heavy isoform, which uniquely exists in smooth muscle cells, and the light isoform, which exists in all non-muscle cells [Wang, 2008]. The two isoforms are similar in sequence, with the non-muscle isoform lacking a central alpha-helical spacer region [Stafford et al., 1990]; however, the two isoforms share similar actin-binding regions. Smooth muscle caldesmon is a long, thin molecule that can span 14 actin monomers and is thought to decorate actin axially, matching its molar ratio in smooth muscle of 1:14 to actin [Graceffa et al., 1988; Mabuchi & Wang, 1991; Lehman et al., 1989; Moody et al., 1990].

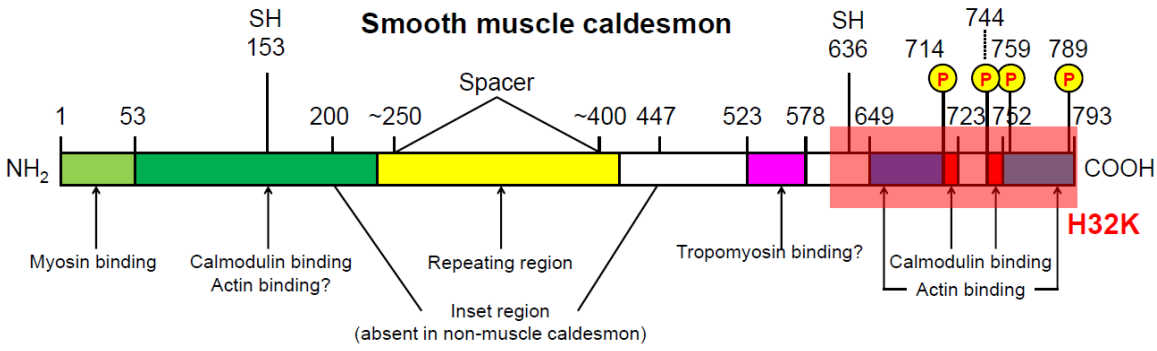

Figure 3.1: Domain structure of smooth muscle caldesmon.
The C-terminal fragment used in this work, H32K, is highlighted in red. Also shown are phosphorylatable residues within the C-terminal fragment.

After its discovery in the 1980s, smooth muscle caldesmon was initially studied as a possible actomyosin regulator in smooth muscle. Caldesmon was

found to inhibit the sliding velocity of actin in *in vitro* actomyosin motility assays [Shirinsky et al., 1992] and actomyosin ATPase activity [Chalovich, 1987] in a phosphorylation-dependent manner, but it was unclear whether this or other mechanisms, such as myosin regulatory light chain phosphorylation, was the primary regulatory mechanism of smooth muscle contraction [Chalovich, 1988; Trybus, 1991]. Electron micrograph reconstructions placed caldesmon near weak myosin-binding sites on actin, and showed that caldesmon was well situated to compete sterically with other actin-binding proteins, but also made it clear that caldesmon did not fit with the established troponin-tropomyosin framework of regulation in striated muscle [Lehman et al., 1997]. This left the primary role and mechanism of caldesmon unclear and also left unexplained the role of the non-muscle caldesmon isoform nearly ubiquitous in vertebrates.

Caldesmon has since been implicated in regulation of actin assembly and dynamics and has been implicated in cellular motility [Lin et al., 2009], including processes such as cell migration [Jiang et al., 2010], the assembly of focal adhesions which anchor motile cells to their substrate [Helfman et al., 1999], and the dynamics of podosomal structures [Eves et al., 2006]. When cells are stimulated to migrate, caldesmon is phosphorylated and translocated from the cytosol to the cell periphery [Kordowska et al., 2006], including regions of membrane ruffling at the leading edge [Bretcher & Lynch, 1985]; however, while actin nucleation and polymerization drives membrane protrusions and cell

motility in this region, the involvement and mechanism of caldesmon in these processes is unknown.

Recently, caldesmon has been suggested to stabilize a structural state of actin filaments, termed the “nascent” state [Huang et al., 2010], preventing actin from irreversibly transitioning to a separate “mature” state after polymerization. The notion that actin exists in multiple structural states is not a new one [Oda & Maéda, 2010]; indeed, some studies have proposed that filamentous actin can exhibit as many as six distinct structures, each of which can coexist within a filament [Galkin et al., 2010]. The concept of transient structural actin maturation from an initial nascent state following polymerization has also been previously proposed [Steinmetz et al., 1997; Bryan & Rubenstein, 2005; Kueh et al., 2008; Galińska-Rakoczy et al., 2009], but because this nascent state is relatively short-lived, it has been poorly characterized, and its significance remains controversial. Caldesmon stabilization of nascent actin opens the door to more detailed studies of this actin structure.

Arp2/ 3 is a protein complex consisting of seven polypeptides [Goley & Welch, 2006]. Capable of binding to the side of an actin filament (termed the “mother filament”), the complex nucleates a new filament (a “daughter filament”) which grows from the mother filament at a 70° angle [Amann & Pollard, 2001]. The Arp2/ 3 complex plays an important role at the leading edge of motile cells, where Arp2/ 3-driven dendritic nucleation of actin helps drive

membrane protrusions and directed cell motility [Lai et al., 2008]. While also regulated by several associated proteins, called Arp2/3 activators, the specific targeting of Arp2/3 complex to actin at the leading edge of the motile cell has been proposed to involve a preferential binding to ATP- or ADP-Pi-actin over ADP-actin [Ichetovkin et al., 2002]; however, the exact mechanisms by which Arp2/3 complex targets this specific actin population are not well understood. Since phosphorylated caldesmon is abundant near the leading edge of motile cells during cell motility [Kordowska et al., 2006; Bretcher & Lynch, 1985], any interactions with caldesmon-decorated actin and the Arp2/3 complex are of particular interest, and any insight into mechanisms through which Arp2/3 complex targets specific actin filaments would be illuminating not just in light of the actin maturation hypothesis, but also in better understanding the targeting mechanisms of actin-binding proteins such as the Arp2/3 complex to specific cellular populations of actin.

In this chapter, we study the role of caldesmon in regulating actin polymerization and maturation, and investigate a novel biological mechanism of caldesmon in cell motility. The C-terminal fragment of caldesmon, H32K, when added before initiation of polymerization, attenuates the pyrene fluorescence intensity of polymerizing actin, which is usually used as a measure of actin polymerization [Huang et al., 2010; Collins et al., 2011]. However, we show using TIRF microscopy that H32K does not affect the polymerization rate of

actin, suggesting that the changes in pyrene fluorescence reflects a different structural maturation transition in the filament, which is inhibited by the early addition of H32K [Collins et al., 2011]. The notion that H32K delays a maturation transition in actin and prolongs its nascent state is consistent with electron micrographs, showing a change in the staining of actin that evolves over time into the smooth-looking canonical electron micrograph actin appearance, and that this transition is delayed upon addition of H32K to G-actin prior to polymerization (see Figure 3.2.)

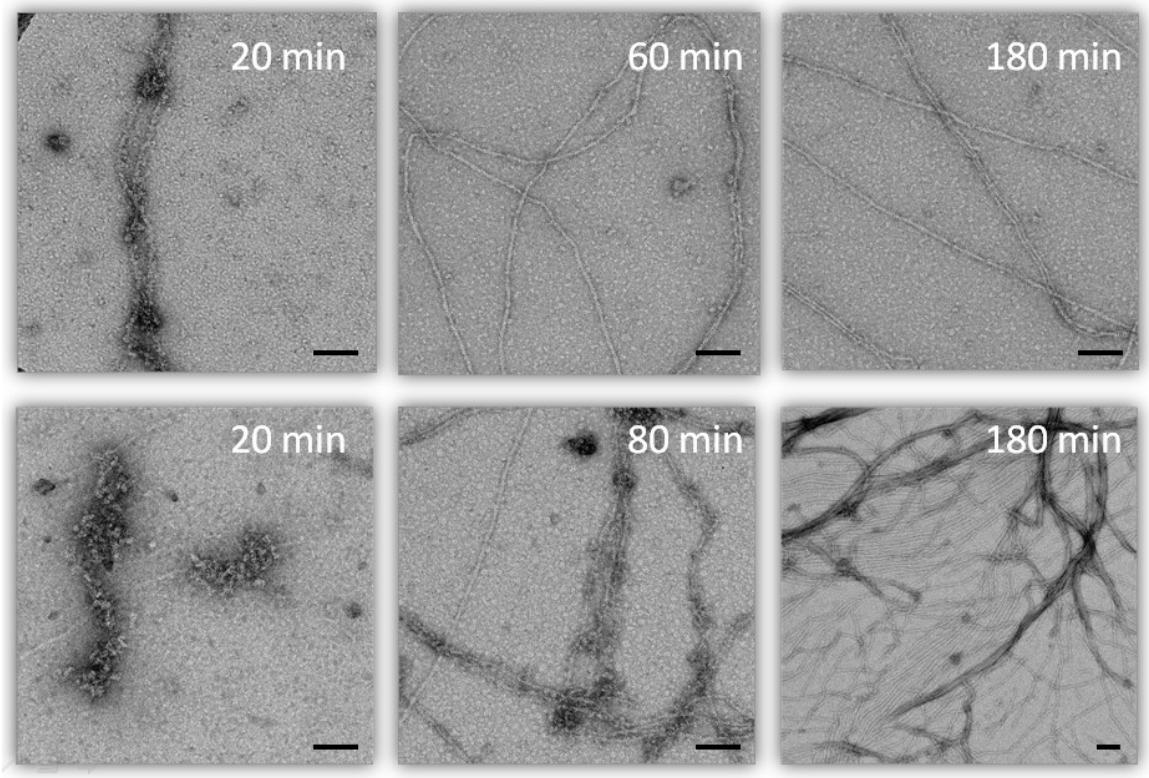

Figure 3.2: Electron micrographs of actin polymerized with or without H32K. *Plain actin filaments (top panels) transition to from a "rough" appearance to the canonical "smooth" filament stain in tens of minutes. In contrast, actin polymerized in the presence of H32K (bottom panels) maintains the "rough" appearance over longer time scales. Eventually, the appearance of individual filaments cannot be discerned due to H32K-induced actin bundling. Scale bars are 100 nm. Time indicates time after initiation of polymerization.*

To investigate the possible biological role of such a prolonged nascent structural state stabilized by H32K, we compare the ability of nascent actin filaments stabilized by phosphorylated H32K and mature actin in binding Arp2/ 3 complex and forming actin branches. We find that H32K-decorated actin more readily binds Arp2/ 3 complex and forms branches, but only when H32K is present during initial actin polymerization [Jensen et al., 2012a]. These data are

consistent with a delay of an irreversible maturation process of actin independent of other transient markers of actin polymerization, such as ATP hydrolysis in the filament. This suggests a novel regulatory mechanism by which the state of actin determines the interactions with Arp2/ 3 complex, and is to our knowledge the first reported direct functional importance of nascent actin filaments.

3.2 Methods

3.2.1 Determining actin polymerization rates with H32K

For actin polymerization rate experiments, lyophilized G-actin from rabbit skeletal muscle labeled with rhodamine on surface lysine residues to a labeling ratio of roughly 0.5 is purchased from Cytoskeleton (Denver, CO) and stored at -80 °C until use. Two days before the experiment, 50 mL of low-salt buffer (0.2 mM CaCl2, 0.2 mM ATP, 10 mM DTT, and 5 mM Tris-HCl, pH 8.0) is added to a vial of 20 mg lyophilized actin, which is left to resuspend on ice for 1 hour. The actin was cycled to F-actin by adding a polymerization inducer buffer (final concentration of 50 mM KCl, 2 mM MgCl2, 1 mM ATP, and 1 mM DTT) and letting the actin polymerize at room temperature for 2 hours. At this point, the actin was converted back to G-actin by dialyzing it against 500 mL of G-buffer (0.005% NaN_3, 0.2 mM $CaCl_2$, 0.2 mM ATP, 1 mM DTT, and 2 mM Tris-HCl, pH 8.0). Dialysis is performed at 4 °C while gently stirring the dialysis buffer. The

dialysis buffer is changed every 12 hours over two days, for a total of four buffer changes.

On the day of the experiment, a vial of column-purified unlabeled actin prepared from acetone powder is thawed and put on ice. The dialyzed rhodamine-labeled actin is removed from dialysis and put on ice. Note that with actin labeled on surface lysines to a low enough ratio, mixing labeled and unlabeled actin is not necessary, and polymerization will still proceed normally; this is not the case if actin is labeled on residue Cys-374, in which case polymerizing actin with a fraction of unlabeled actin is crucial [Kuhn & Pollard, 2005]. The labeled and unlabeled actin is mixed to a ratio of 30% labeled:70% unlabeled and are mixed into an oxygen scavenger buffer consisting of 100 mM dextrose, 160 U glucose oxidase, 2 μM catalase, 10 mM DTT, 50 mM KCl, 0.5 mM ATP, and 2 mM $MgCl_2$. The buffer also contains 12.5 mM imidazole to buffer pH, 7 μM BSA to help coat the glass and block non-specific actin-surface interactions, and 0.5% methyl cellulose to slow the diffusion of actin filaments during the experiment. These samples are compared to similar samples containing pH32K in a molar ratio of 1:3 pH32K:actin. The use of phosphorylated H32K minimizes the problem of actin bundling, which is promoted by unphosphorylated caldesmon [Arias & Pacaud, 2001]. In practice, samples are most easily prepared by mixing an oxygen scavenger buffer at 2x concentration and mixing it equally with G-actin at twice the desired

concentration. Mixing is done quickly, as the addition of salts initiates polymerization, and the sample is loaded into a flow chamber constructed from pre-cleaned glass cover slips and imaged immediately.

Imaging is done using TIRF microscopy at ambient room temperature. Images are captured every 4-15 seconds depending on the actin concentration used, with laser excitation shuttered between frames to avoid excessive photobleaching. Imaging continued until polymerization proceeded to crowd the surface (10-30 minutes, depending on the actin concentration). Each image is then processed in ImageJ to extract the filament length, and the growth rate for each filament is determined as the best linear fit to a length vs. time graph. Occasionally, we observe pauses in elongation rate, presumably due to defective monomers being incorporated at the filament barbed end or due to filament interactions with residual surface debris [Kuhn & Pollard, 2005]; these pauses are excluded from the final analysis. Any bundles of actin or aggregated protein are omitted from analysis.

3.2.2 Quantifying Arp2/3 branching on actin filaments with H32K

To determine the effect of H32K on actin branching induced by Arp2/ 3 complex, a similar protocol to that described to determine actin polymerization rates is used, with slight changes in the actin polymerization steps.

G-actin labeled on surface lysine residues with Alexa Fluor 488 is polymerized in 25 mM KCl, 25 mM imidazole, 1 mM EGTA, 4 mM $MgCl_2$,

1 mM ATP, and 10 mM DTT at 1.5 μM either alone or with pH32K added at a 1:3 pH32K:actin molar ratio. These are left for 3 hours at room temperature to ensure that all actin has hydrolyzed its nucleotide, and that all filaments are either fully mature or fully nascent. Immediately before imaging, final samples are prepared by mixing rhodamine G-actin (final concentration 500 nM), Arp2/ 3 complex (final concentration 300 nM), and Alexa Fluor 488 F-actin obtained from the prepolymerized stock described above (final concentration 15 nM). Additional pH32K is also added to samples using Alexa Fluor 488 actin prepolymerized with pH32K, in order to maintain a 1:3 molar ratio. The constituents are then mixed in an oxygen scavenger buffer (described above), loaded into a flow chamber prepared from pre-cleaned glass cover slips, and imaged immediately using confocal fluorescence microscopy at ambient room temperature. Controls are performed in which Arp2/ 3 complex or pH32K is absent entirely, or in which pH32K is added immediately before imaging but not during the prepolymerization of the Alexa Fluor 488 actin. Single images were captured at random locations on the flow chamber surface until actin polymerization caused too much crowding, which occurred after about 10 minutes. After processing in ImageJ, branching of rhodamine actin ("daughter filaments") on Alexa Fluor 488 actin filaments ("mother filaments") are counted, provided they (1) form a 70°±10° angle with the mother filament [Amann & Pollard, 2001], (2) branch towards the barbed end of the mother filament [Volkmann et al., 2001],

if discernable, and (3) are not discernibly elongating or branching off of other filaments. Any bundled actin is omitted from analysis.

3.2.3 Computational simulation of branching distributions on actin

To characterize the spatial distribution of Arp2/3 complex-induced branches on actin, the experimentally determined numbers of branches and the lengths of every observed Alexa Fluor 488 actin filament are fed into a custom-written Matlab simulation (MathWorks, Natick, MA). Since the filaments do not necessarily have equal length distributions between experiments, simply looking at the distance between branches, the number of branches per filament, or the distance from branch points to mother filament ends is insufficient to distinguish if pH32K-stabilized actin exhibits different branching distributions. We therefore establish the expected distributions for random Arp2/3-induced branching in the absence of binding cooperativity computationally as a point of reference. For each experimental condition, the program uses the observed lengths of Alexa Fluor 488 mother filaments and randomly places the experimentally observed number of branches on these filaments. The program is repeated until the resulting distributions converge, which occurred after 100,000 iterations. A total of 280 branches and 613 separate mother filaments are measured and input into the simulation for pH32K-stabilized nascent actin, while 276 branches and 985 filaments are measured and input for plain actin. An annotated copy of the Matlab code can be found in Appendix B.

3.3 Results

3.3.1 H32K does not affect actin elongation, but affects structure

When added to pyrene-labeled G-actin before polymerization is initiated, H32K has been shown to suppress the rise in bulk pyrene fluorescence intensity typically associated with actin assembly [Huang et al., 2010; Collins et al., 2011]. This attenuation only occurs when H32K is added to G-actin prior to polymerization, suggesting that H32K cannot reverse actin to its low-pyrene fluorescence intensity state once actin has polymerized and matured.

In general, the change in fluorescence intensity arises from a change in the hydrophobic environment of the pyrene probe, and indicates that a structural change is occurring near the probe. While this structural change, in the case of actin, is typically interpreted as a G-actin to F-actin transition, we use TIRF microscopy to directly determine the effect of pH32K on the polymerization rates of actin, and thus to determine whether the altered structural transition is related to changes in actin polymerization rates.

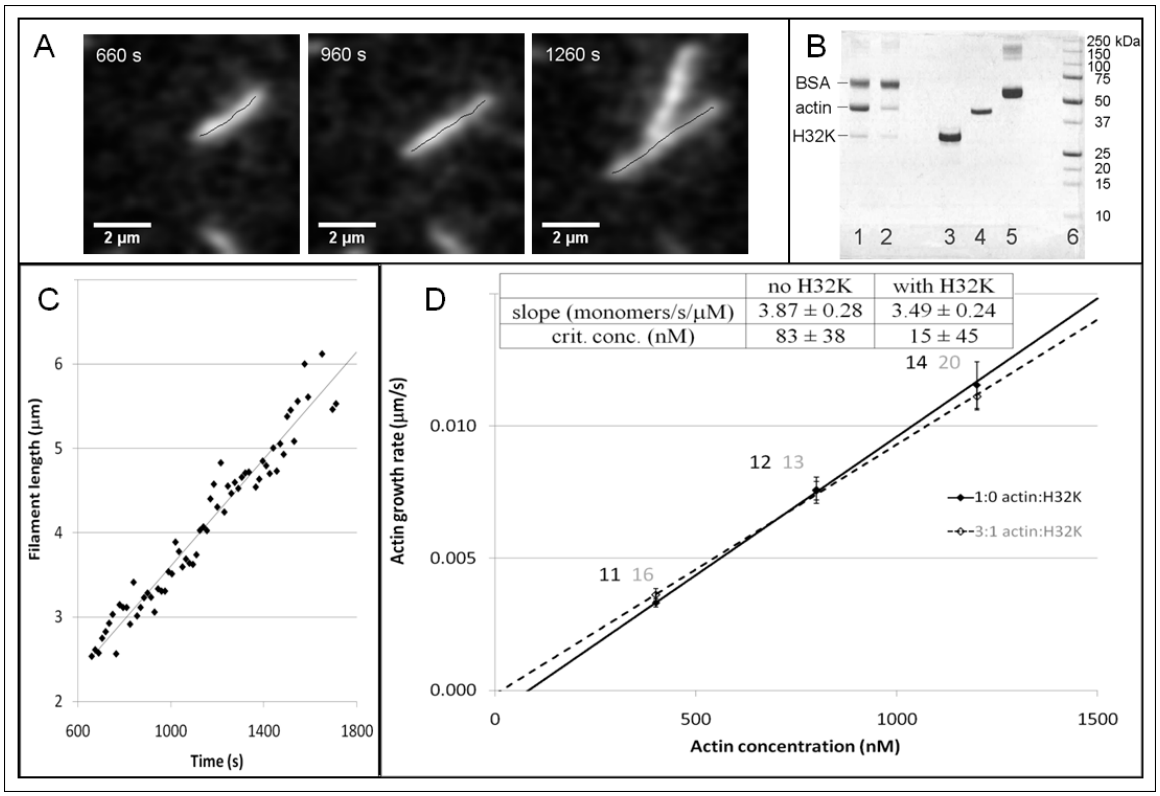

Figure 3.3: H32K does not affect actin polymerization rates.

(A) Representative TIRF microscopy image of an elongating F-actin filament, with G-actin concentration of 400 nM and pH32K concentration of 133 nM. Time indicated is since sample mixing. (B) G-actin polymerized as described in Chapter 3.2.1 is pelleted at 100,000g and run on a 12.5% SDS-PAGE gel to confirm binding of pH32K to actin. 9 μg actin with 3 μg pH32K (lane 1); 5 μg actin with 5 μg pH32K (lane 2); or actin, pH32K, or BSA (lane 3) are shown. Lane 6 is BioRad standard 161-0363. (C) Filament length trace of the filament shown in panel A. The growth rate is determined from the slope of the linear fit. (D) Actin growth rates as a function of actin concentrations, with (open circles; dashed line) and without (closed circles; solid line) pH32K. Error bars on individual data points represent standard errors, based on the number of analyzed filaments at each concentration, which is indicated adjacent to each data point. Length scales are converted from μm to G-actin monomers using as estimate of 370 monomers/μm [Huxley & Brown, 1967]. The concentration dependence of the growth rate, the critical concentrations, and their uncertainties are determined from a weighted least-squares linear fit to the data, with weights chosen as the inverse of the standard error squared. Neither the individual data points nor the fitting parameters show any statistically significant differences.

TIRF microscopy allows us to visualize growing actin filaments with minimal fluorescence background from the labeled G-actin in solution, both in the presence and absence of ERK-phosphorylated H32K (pH32K). A representative TIRFM image of a growing actin filament at concentrations of 400 nM G-actin and 133 nM pH32K, with the ImageJ-generated skeleton overlaid, is shown in Figure 3.3A. The time since mixing the constituents is shown in the upper left corners of each frame. By monitoring the filament length over time, the filament growth rate is determined, as shown in Figure 3.3C.

Growth rates of several filaments are measured in this fashion at concentrations of 0.4, 0.8 and 1.2 μM G-actin, both in the presence and absence of pH32K (Figure 3.3D). As expected, the growth rate is linear with concentration,

with a critical concentration of about 100 nM [Kuhn & Pollard, 2005]. Here, error bars represent the standard error in elongation rates, based on the number of observed filaments, which is indicated next to each data point. Length scales are converted from μm to G-actin monomers using an estimate of 370 G-actin monomers/ μm [Huxley & Brown, 1967]. The concentration dependence of the growth rate (slope), the critical concentrations (crit. conc.), and their uncertainties are determined from a weighted least-squares linear fit to the data, with weights for each data point chosen as the inverse of the standard error squared. Based on these error bars, neither the data points at each individual concentration nor the linear fit parameters show any significant difference between samples with and without pH32K, confirming that the initial addition of H32K to G-actin does not affect the resulting filament growth rate

Finally, binding of pH32K to actin is ascertained by SDS-PAGE after centrifugation of the actin sample polymerized in the presence of pH32K as in the TIRF microscopy assays (Figure 3.3B; lanes 1 and 2). G-actin is polymerized with phosphorylated H32K and centrifuged at 100,000*g*. The polymerization is carried out in the same oxygen scavenger buffer used for TIRF microscopy assays. The pellet is collected and run on 12.5% SDS-PAGE to confirm the binding of pH32K to actin. Two ratios are incubated and spun: 9 μg G-actin with 3 μg pH32K (Lane 1) and 5 μg G-actin with 5 μg pH32K (Lane 2). The top band present in both lanes is residual BSA from the buffer. Lanes 3–5 are controls

containing only 3 μg pH32K, 5 μg actin, and 5 μg BSA, respectively. Lane 6 contains the BioRad standards 161-0363, with molecular weights indicated on the far right.

These data show that the addition of pH32K to actin during the initial polymerization does not affect the polymerization rate of actin, and thus the changes observed in pyrene fluorescence intensity caused by H32K do not reflect changes in actin polymerization rates.

3.3.2 H32K transiently enhances branching by Arp2/3 complex

To investigate the dynamic properties of actin filaments before and after maturation as well as their interaction with Arp2/ 3 complex, we visualize actin filament assembly using fluorescently labeled actin of two different colors similarly to previous studies [Amann & Pollard, 2001; Ichetovkin et al., 2002], except that pH32K is added to interfere with the actin maturation process.

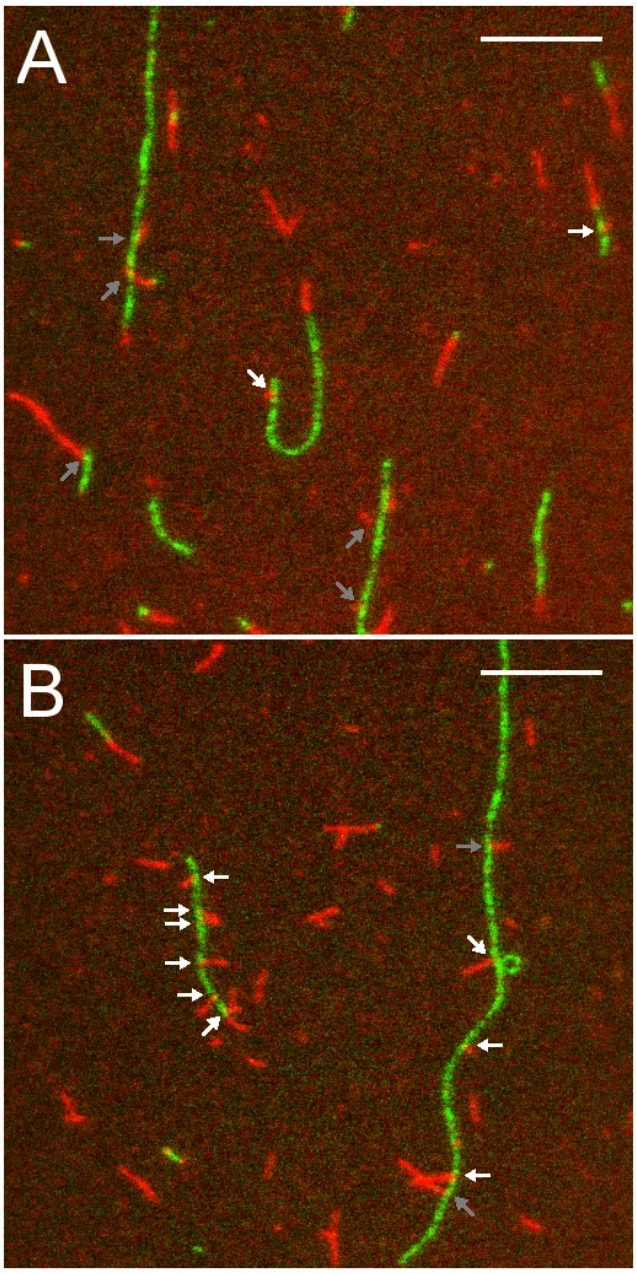

Figure 3.4: Two-color actin assembly assay with Arp2/3.
Alexa Fluor 488 actin (green) is first polymerized without (A) or with (B) pH32K for 3 hours. A combination of rhodamine G-actin (red) and Arp2/3 complex, prepolymerized Alexa Fluor 488 F-actin, and additional pH32K (maintaining a 1:3 molar ratio to actin) is then added. White arrows indicate counted branches, while gray arrows indicate branches that were discarded (see Chapter 3.2.2). Note the barbed ends of several Alexa Fluor 488 actin filaments discernible by the growing red actin caps. Scale bars: 5 μm.

Two-color fluorescence confocal microscopy imaging of actin assembly is carried out with prepolymerized Alexa Fluor 488 F-actin while rhodamine-actin is assembling (Figure 3.4) until the field of view becomes too crowded with polymerized actin. To quantify the effects of pH32K on Arp2/3 complex-mediated branching, rhodamine-actin (red) branches originating from prepolymerized Alexa Fluor 488 actin mother filaments (green) are counted. Although considerable branching off of newly polymerized red mother filaments is also observed [Ichetovkin et al., 2002], we only consider branching on prepolymerized green F-actin in our analysis, as the lengths of these are constant during the experiment, and as we can control their age and interaction with pH32K during the prepolymerization step.

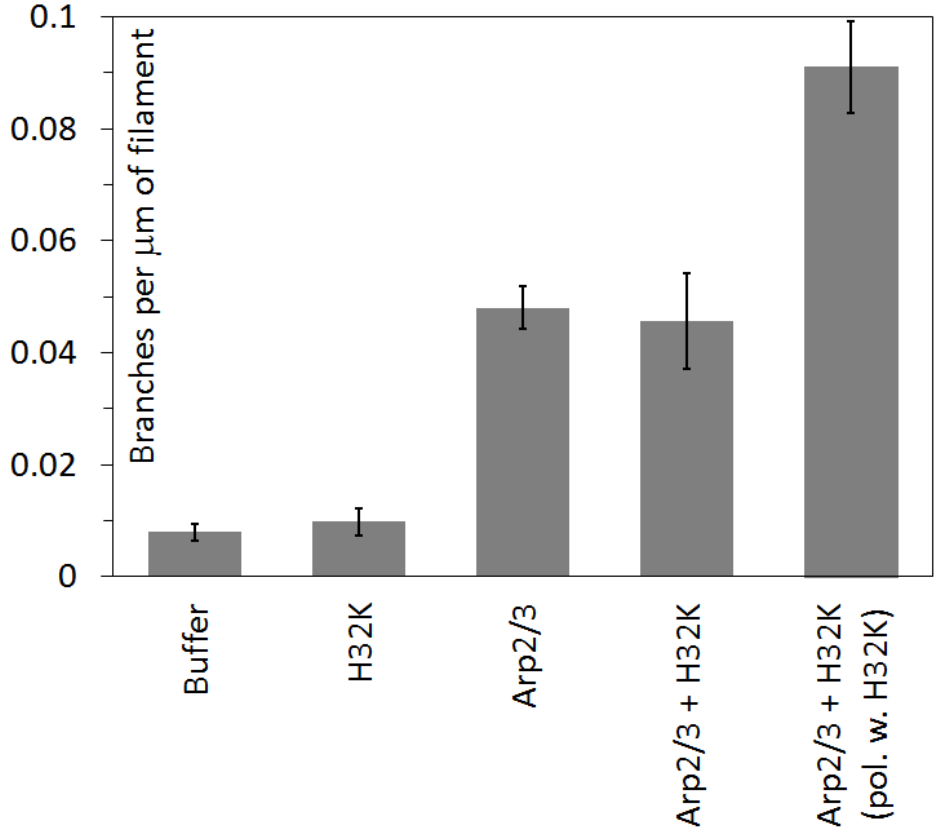

Figure 3.5: pH32K transiently enhances the branching activity of Arp2/3.
Branching is quantified as the number of branches on Alexa Fluor 488 actin per unit length. Bars represent mean values for all imaged fields (between 23 and 61 for each condition) weighted by the amount Alexa Fluor 488 actin present ±S.E. "Buffer" and "H32K" are control experiments and indicate apparent branching in the absence of Arp2/3 complex, either with or without pH32K. The last three bars indicate, from left to right: branching with Arp2/3 complex alone; with Arp2/3 complex and pH32K present using Alexa Fluor 488 F-actin prepolymerized without pH32K; and with Arp2/3 complex and pH32K present using Alexa Fluor 488 F-actin prepolymerized with pH32K.

The level of branching is quantified as the number of red branches per unit length of green filaments polymerized either in the presence or in the absence of pH32K. As compared with the branching activity in the absence of pH32K, we observe a 2-fold increase in dendritic branching density on Alexa

Fluor 488 actin filaments prepolymerized in the presence of pH32K (Figure 3.5). However, when pH32K is instead added right before imaging at a ratio of 1:3 to Alexa Fluor 488 actin filaments prepolymerized in the absence of pH32K, the level of branching is indistinguishable from the caldesmon-free control.

3.3.3 Distribution of Arp2/3 on nascent filaments

Several actin-binding proteins have been shown to cooperatively interact with actin, including the actin-binding proteins tropomyosin [Yang et al., 1979], myosin [Orlova & Egelman, 1997], cofilin [Hawkins et al., 1993; Hayden et al., 1993], and gelsolin [Prochniewicz et al., 1996]. Although we show above that actin polymerized with pH32K more readily forms Arp2/3-induced branches (Figure 3.5), the branching density alone is insufficient to determine whether the increased branching arises from a change in affinity only, or from a change in cooperativity of the Arp2/3 complex binding to actin. If the degree of cooperativity is altered, we expect to see a difference in the distribution of branches on the Alexa Fluor 488 actin, evident either as clusters of branches on the Alexa Fluor 488 actin or as a few Alexa Fluor 488 actin filaments with a high density of branches, thus increasing the overall average branching density. To determine whether the additional branch formation is a result of changes in cooperative binding of Arp2/3 complex to actin, we compare the cooperativity of branching activity between pH32K-stabilized nascent actin filaments and actin alone in two ways.

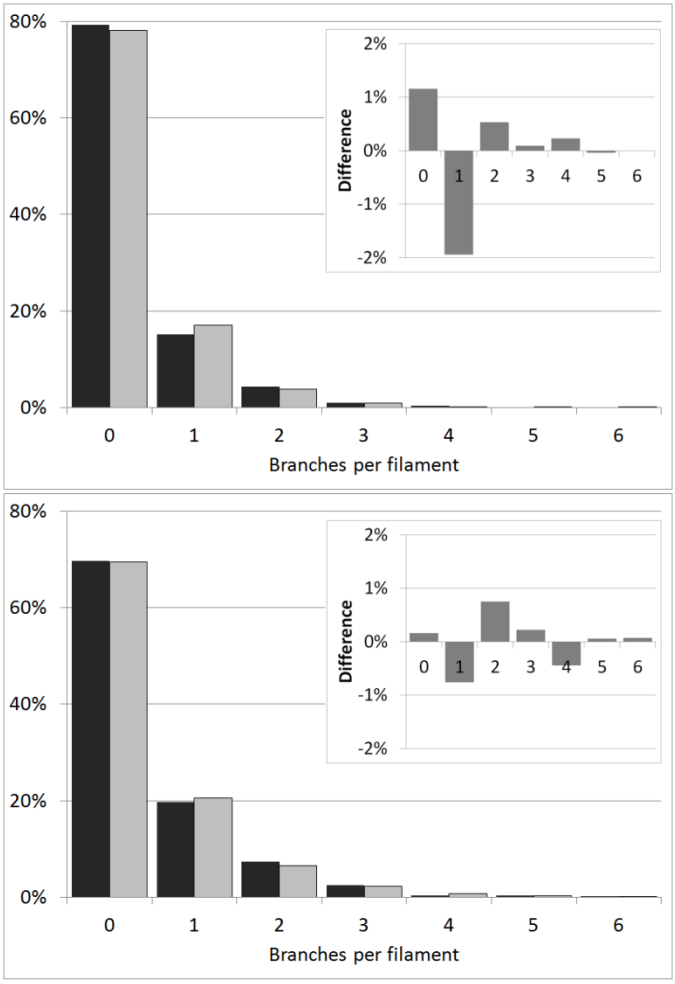

Figure 3.6: Branches per mother filament with and without pH32K.
Each bar represents the measured (black bars) or simulated (grey bars) number of filaments with 0-6 branches. The top panel shows Arp2/3-induced branching on actin without any pH32K present; the bottom panel shows Arp2/3-induced branching on actin polymerized with pH32K present at a ratio of 1:3. Insets show the difference between measured and simulated distributions.

First, we count the number of branches per filament to see whether a few filaments with many branches are responsible for the increased branching density observed when actin is polymerized with pH32K. Most mother filaments with branches have only one branch, whereas fewer filaments have

multiple branches per filament (Figure 3.6, top panel). Furthermore, polymerizing actin with pH32K has no discernible effect on this distribution (Figure 3.6, bottom panel), suggesting that the increased branching density does not originate from a few filaments with a disproportionally high number of branches. Because the exact distributions depend on the length distributions of mother filaments in each experiment, we run a simulation to generate the distribution of Arp2/3-induced branches representing random, noncooperative binding of the Arp2/3 complex. As noted in the insets of Figure 3.6, the observed distributions hardly differ from this random distribution, suggesting that Arp2/3 complex exhibits little cooperativity in binding to actin both with and without pH32K present.

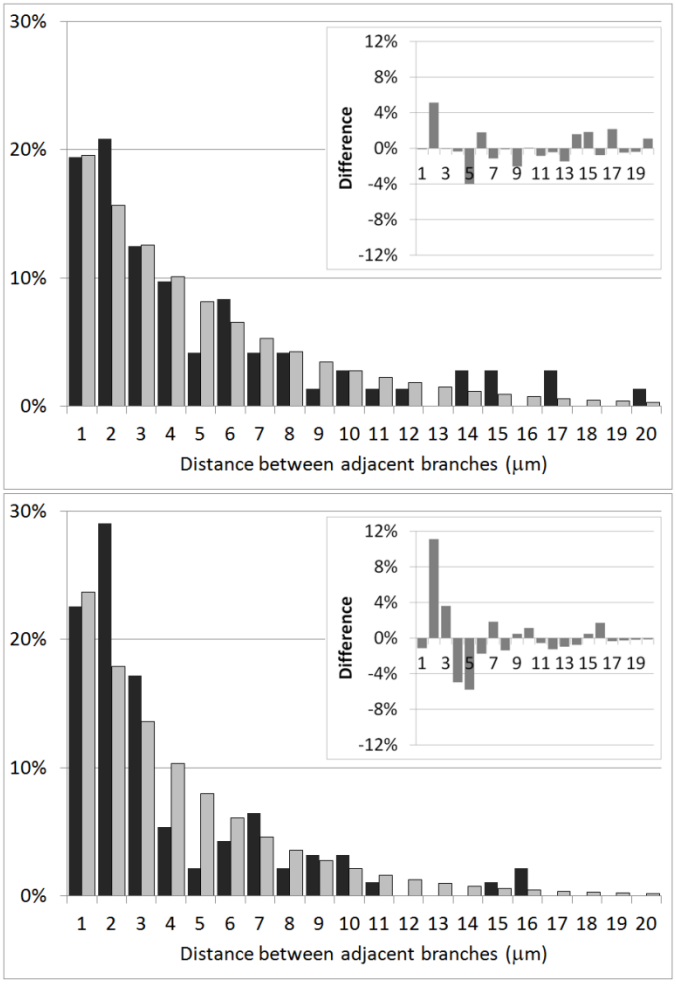

Figure 3.7: Distance between branches with and without pH32K.
The distribution of branches is measured as the distance between adjacent branching points on every actin filament without pH32K (top panel) or on every actin filament polymerized with pH32K at a 1:3 molar ratio. Only filaments with two or more branches are contributing to this statistic. Shown are both the measured (black bars) and simulated (grey bars) distributions. Insets show the difference between measured and simulated distributions.

Secondly, we quantify the distance between adjacent Arp2/ 3 branches to look for clusters of branches (Figure 3.7). As above, the observed distributions are compared with a simulation-generated random distribution, each of which is

specific to the particular filament lengths observed. Because a polymer in dynamic equilibrium, such as actin, tends to have an exponential length distribution with more short filaments and fewer long ones, the simulated random distribution is not even across all mother filament lengths [Howard, 2001]. This disproportionate abundance of shorter filaments in turn makes randomly placed branch points more likely to be more closely spaced, explaining the asymmetric shape of the simulated data in Figure 3.7. Importantly, when comparing the simulated and measured distributions, no marked differences are evident without pH32K, suggesting that the actin polymerized without pH32K does not produce more regions with closely spaced branches than would be expected from a random distribution (Figure 3.7, top panel). With pH32K, slightly more closely-spaced branches are found than expected from a purely random distribution (Figure 3.7, bottom panel); it is therefore possible that pH32K-stabilized nascent actin filaments have a slightly higher cooperativity in Arp2/ 3 complex binding, although we do not explore any such possible change in cooperative unit further in this study.

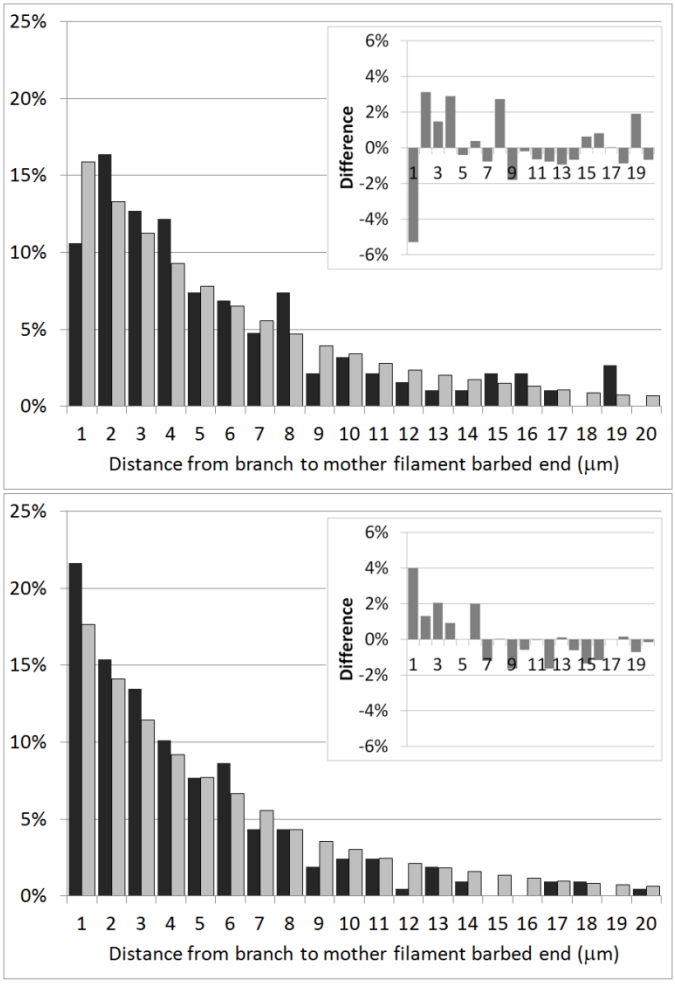

Figure 3.8: Distance between branches and mother filament barbed end.
The distance between all branches and their mother filament barbed ends are measured both for actin alone (top panel) and for actin prepolymerized with pH32K at a 1:3 molar ratio (bottom panel). Only mother filaments whose barbed ends are discernible are counted. Shown are both the measured (black bars) and simulated (grey bars) distributions. Insets show the difference between measured and simulated distributions.

Finally, we also compare the relative locations of branches to their mother filament barbed end (Figure 3.8). As noted for Figure 3.7, the simulated random distribution is skewed toward shorter distances due to the exponentially decaying length distribution of actin mother filaments in dynamic equilibrium

[Howard, 2001]. We observe little difference in the distribution of branches along the mother filament as compared with a simulated random distribution of branches for both pH32K-stabilized nascent actin (Figure 3.8, bottom panel) and mature actin filaments (Figure 3.8, top panel). We expect to see no effect on branching due to actin filament polarity, as all mother filaments in the experiment are either fully nascent or fully mature and thus would have no internal heterogeneity to bias Arp2/3 binding. Although the barbed end of growing actin consists of an ATP-actin or ADP-Pi-actin cap, which has been noted to exhibit a higher affinity for the Arp2/3 complex [Ichetovkin et al., 2002], our mother filaments have no such structural asymmetry and thus do not preferentially form branches along certain regions of the mother filament.

Together, these data show that the branch distributions on both mature and pH32K-stabilized actin are very close to those expected for a random distribution of branches, suggesting that Arp2/3 complex binds with little or no cooperativity to both mature and nascent actin filaments.

3.4 Discussion and conclusions

This work lends further credence to the idea that actin exists in a transient nascent state after transitioning from G- to F-actin and shows that the C-terminal fragment of caldesmon, H32K, prolongs the lifetime of this nascent state. We also explore the functional importance of this actin state and show that H32K-stabilized nascent actin more readily forms Arp2/3-induced branch

structures. This is to our knowledge the first direct functional effect of nascent actin reported in the literature.

Our data addresses the time dependent morphological differences between two transient actin structures; the pre-transitional state, and mature actin filaments. Newly polymerized, pre-transitional actin filaments have a rough, irregular appearance under negative-stain electron microscopy, while over time, these actin filaments mature into the typical smooth F-actin. When caldesmon is included at early stages of polymerization, the resulting filaments maintain the rough and irregular appearance for a longer time than control filaments. It appears that when added early, caldesmon delays the maturation process of actin filaments [Huang et al., 2010; Collins et al., 2011] (Figure 3.2). It is clear that the electron micrographs of the proposed nascent actin filaments, in some places showing filaments many times wider than the canonical actin filament with a diameter of about 7 nm, cannot represent a slight structural modification and may in fact represent differences in staining; however, even if a filament structure cannot be discerned from the images, the very fact that the electron microscopy stain interacts differently with the actin filaments suggests that the structural details between nascent and mature actin must be different. On the basis of the pyrene fluorescence intensity of the same sample, we then propose that the rough filaments represent the low fluorescence, pre-transitional state of polymerized actin, whereas the smooth filaments represent the high

fluorescence, post-transitional state of mature F-actin [Huang et al., 2010]. However, to support this claim, we must first show that the pyrene fluorescence differences are not due to differences in actin polymerization rates induced by caldesmon. We accomplish this using TIRF microscopy to directly visualize actin polymerizing with or without pH32K and show that pH32K does not affect the elongation rates. This substantiates the argument that the electron micrographs and in particular the pyrene fluorescence data do indeed represent a transient structural maturation in actin, which is modulated by caldesmon.

Several structural transitions besides those related to the nucleotide state are known for polymerizing actin, which in turn could modulate the affinity of actin-binding proteins for actin. For example, FRET measurements have revealed that individual actin monomers within a filament alternate on a time scale of seconds between structural states that are discernible by differences in myosin binding [Kozuka, 2006]; electron microscopy has also shown distinct structural states existing within F-actin [Egelman & Orlova, 1995]. ATP hydrolysis and subsequent phosphate release by actin occurs on a time scale of a few minutes [Carlier, 1987]; however, these time scales are inconsistent with the time scales over which pH32K affects actin, and given that caldesmon does not affect the phosphate release rate from F-actin [Huang et al., 2010], this distinct nascent state of actin appears unrelated to any of these, and in particular does not appear linked to the nucleotide state of actin.

While this work adds evidence to the emerging idea of a novel nascent actin state [Steinmetz et al., 1997; Bryan & Rubenstein, 2005; Kueh et al., 2008; Galińska-Rakoczy et al., 2009; Huang et al., 2010; Collins et al., 2011] which can be regulated by caldesmon (and potentially other actin-binding proteins as well), the functional role of such a nascent actin state is unclear. Our comparison of canonical mature actin to pH32K-stabilized nascent actin in the presence of Arp2/3 complex gives direct evidence of a potential functional role of nascent actin filaments in cells. While Arp2/3 complex has previously been suggested to target actin in a nucleotide-dependent fashion [Ichetovkin et al., 2002], our results, combined with the abundance of phosphorylated caldesmon near the leading edge of motile cells [Bretcher & Lynch, 1985; Kordowska et al., 2006], suggests a novel mechanism by which Arp2/3 complex preferentially targets the newly formed actin filaments at the cell leading edge and thus helps induce local actin polymerization to form membrane protrusions and facilitate cell motility. The fact that pH32K only enhances Arp2/3 complex-induced branching when present during the mother filament polymerization (Figure 3.5) is also consistent with the fact that caldesmon binding to actin filaments does not revert mature filaments to their nascent state [Huang et al., 2010].

This work also demonstrates that the state of the actin filament itself can be a determining factor of the affinity of actin-binding proteins for actin. A number of actin-binding proteins (e.g., cofilin) are thought to target actin

depending on its nucleotide state [Pollard & Borisy, 2003]. Our work demonstrates that at least one additional mechanism besides the state of the nucleotide of actin should be considered as a filament age marker for binding by actin-binding proteins. The pH32K-stabilized nascent actin filament structure studied here is stable over at least several hours, providing transient regulation well beyond the time scale of the filament nucleotide state or any previously studied transient actin structure. The enhanced interaction of Arp2/3 complex with actin nascent filaments transiently regulated by phosphorylated caldesmon is, to our knowledge, the first functionally important role of the nascent actin filament structure.

4 Calponin and Single Actin Filament Mechanics

4.1 Introduction

Calponin is an actin-binding protein present in both smooth muscle and non-muscle cells. At the time of its discovery, the regulation of actomyosin contraction in smooth muscle was poorly understood, and while smooth muscle was known to contain tropomyosin, troponin, the regulator of skeletal muscle contraction, was not found. Upon its discovery in smooth muscle in the mid-80s [Lehman & Kaminer, 1984; Takahashi et al., 1986], calponin was proposed to be a calcium-binding troponin-analogous protein in smooth muscle that could play the role of troponin in actomyosin regulation, hence the name calponin [Winder & Walsh, 1990; Shirinsky et al., 1992; Winder et al., 1998; Takahashi et al., 1988a; Takahashi et al., 1988b]. Calponin was found to inhibit actomyosin ATPase activity and actin sliding velocity in *in vitro* motility assays; however, electron micrograph reconstructions later showed that calponin interactions with tropomyosin shifts tropomyosin position towards the closed, rather than the blocked, position, exposing strong myosin-binding sites on actin that were previously covered by tropomyosin [Hodgkinson et al., 1997]. Despite calponin not being particularly troponin-like, the name remains. Its role and importance in actomyosin contractile regulation in smooth muscle also remains somewhat unclear, as other mechanisms, e.g., myosin light chain phosphorylation

[Chalovich, 1988; Trybus, 1991], later became apparent, and as the absence of calponin does not abolish smooth muscle contractility [Nigam et al., 1998].

In recent years, studies of both basic calponin (the smooth muscle-specific isoform of calponin) and the two non-muscle calponin isoforms (neutral and acidic calponin, all named after their respective isoelectric points) have revealed a significant involvement of calponin in cellular mechanotransduction and cytoskeletal regulation, both as an end product and as an intermediary part of mechanosensory regulatory pathways. (For a recent review of our understanding of the biological role of calponin, see [Rozenblum & Gimona, 2008].) Basic calponin, or h1CaP, has been shown to respond to agonist-induced smooth muscle contraction by relocating to the cortical actin, away from contractile actin filaments [Parker et al., 1994]. This translocation was later found to accompany changes in cytoskeletal remodeling, resulting in larger amounts of F-actin in the cortical regions of the cell [Kim et al., 2008]. A recent study demonstrated the importance of acidic calponin in the rearrangement and regulation of the actin cytoskeleton to facilitate cell fusion [Shibukawa et al., 2010]. As acidic calponin was knocked down, actin cytoskeletal rearrangements and subsequent cell fusion was promoted, suggesting that acidic calponin is an actin cytoskeleton stabilizer which negatively regulates cell fusion. The neutral calponin isoform has also been shown to regulate cytoskeletal actin and is itself regulated by mechanical cellular stimuli [Hossain et al., 2005], and influences cell

migration and vascular development [Tang et al., 2006] and cytokinesis through regulation of cytoskeletal actin networks [Hossain et al., 2003]. Basic calponin expression upregulated by vitamin C in smooth muscle tissue was recently found to alter smooth muscle mechanical properties by increasing the tensile strength of the tissue but reducing its stiffness [Arrigoni et al., 2006], an effect potentially important for proper function of smooth muscle tissue under strain. Basic calponin has also been found to stabilize actin in cultured smooth muscle cells and reduce the actin turnover induced by exogenously added chemical stimuli.

Despite the growing body of work implicating calponin as a cytoskeletal regulator and actin stabilizer in cells and tissues under stress, very little insight into the physical mechanism of calponin function has been gained so far. Most of the published studies so far have focused on the cell or tissue level, on which it is difficult to discern specific mechanisms or other proteins involved. While it is becoming clear that calponin plays a role in stabilizing cytoskeletal actin network structures in cells, it is unclear how this occurs, or whether calponin acts in concert with other actin-binding proteins.

The approach taken in this work is a bottom-up approach, in which simple reconstituted systems are used to characterize the effects of calponin on actin mechanics and stability. The goal is to gain sufficient mechanistic insight from these *in vitro* model systems to propose a physical mechanism of calponin

stabilization of actin *in vivo*. In this chapter, we study single actin filaments with and without calponin and quantify the flexural rigidity as a first step in understanding how calponin alters the mechanics of actin. We measure the flexural rigidity of two actin isoforms (α-skeletal muscle actin and non-muscle β-actin) and compare our measurements to published values. We then show that basic calponin reduces the flexural rigidity of both α-skeletal muscle actin and non-muscle β-actin, suggesting that the slight differences between the actin isoforms does not affect the gross mechanical changes induced by calponin and suggests that either actin isoform can be used as a basis for a more intricate model system. (This will be explored further in Chapter 5) Actin filaments decorated with calponin are found to be more susceptible to shear during sample preparation. We compare these results to reconstructions of calponin-decorated actin from cryo-electron microscopy images and argue that changes around actin subdomain 2 could account for the mechanical changes observed on the filament level [Jensen et al., 2012b].

These results show that calponin alters the mechanics of F-actin without other cellular constituents present and points to regulation of filament rigidity as a possible parameter of importance in understanding calponin's effects on actin in the cell. In Chapter 5 we use these results as a basis for understanding the effects of calponin on reconstituted actin networks and present a model for calponin stabilization of actin *in vivo*.

4.2 Methods

4.2.1 Measuring the persistence length of actin

To determine the flexural rigidity of actin filaments, lyophilized rabbit skeletal muscle G-actin (100% α-skeletal muscle actin) or non-muscle G-actin (85% non-muscle β-isoform and 15% non-muscle γ-isoform) are both purchased from Cytoskeleton (Denver, CO). Both unlabeled G-actin and G-actin labeled with rhodamine on surface lysine residues to approximately 0.5 dyes/ monomer is used.

In experiments involving rabbit skeletal muscle actin, the day before the experiment, a vial of unlabeled lyophilized G-actin is resuspended in 0.2 mM $CaCl_2$, 0.2 mM ATP, 10 mM DTT, and 5 mM Tris-HCl, pH 8.0 to a concentration of 5 mg/ mL and left at 4 °C until the day of the experiment. The day before the experiment, a vial of labeled lyophilized G-actin is also resuspended on ice to a concentration of 0.4 mg/ mL in the same buffer. The vial is left to resuspend on ice for 1 hour, after which half the sample is removed to a separate vial and polymerized at room temperature for 2 hours in 50 mM KCl, 2 mM $MgCl_2$, 1 mM ATP, and 1 mM DTT. The polymerized actin is then vortexed at low speed for 30 seconds with a table top vortexer to shear the F-actin into smaller filaments. These smaller filaments are mixed with a 4-fold excess of unpolymerized rhodamine G-actin to a final actin concentration of 500 nM and left at 4 °C overnight in a final buffer of 25 mM KCl, 25 mM imidazole, 1 mM EGTA, 4 mM

$MgCl_2$, 1 mM ATP, and 10 mM DTT, allowing filaments to grow from the vortexed actin seeds. Doing this second polymerization step at 4 °C reduces the rate of nucleation of new filaments and creates a smaller pool of longer filaments growing from the existing F-actin seeds.

Experiments involving non-muscle actin from human platelets also uses both labeled and unlabeled actin from Cytoskeleton (Denver, CO) and is prepared as described above, but with doubled actin concentrations in the polymerization steps, using 0.8 mg/ mL actin to form F-actin seeds and a final polymerization at 1 μM actin in order to exceed the higher critical concentration of the non-muscle actin isoform [Gordon et al., 1977; Rubenstein, 1990; Herman, 1993].

Unlabeled G-actin prepared in this way is stored at 4 °C for experiments for no longer than two weeks, while labeled G-actin is stored at 4 °C after resuspension for no longer than 5 days.

As a precaution, the amount of calponin needed for each flexural rigidity experiment is centrifuged for 30 minutes at 100,000*g* to pellet any damaged protein forming aggregates in solution the day before the experiment. The supernatant is stored in 100 mM DTT overnight at 4 °C to minimize oxidative damage. A spectroscopic Bradford protein assay is used to show that no calponin is pelleted for calponin less than 2 weeks old. To avoid any potentially subtle artifacts from oxidative damage or other forms of protein degradation,

calponin is therefore safely used in experiments within 2 weeks of purification. Calponin stored in DTT after centrifugation is used within 5 days, after which it is discarded.

On the day of the experiment, microscope slides and coverslips (Corning Glass; Corning, NY) are dipped and rinsed in 1 mM BSA twice to limit actin interactions with the glass surface and left to dry on the bench under a dust cover. Rabbit skeletal actin and calponin are mixed in an oxygen scavenger buffer to final concentrations of 2 mM dextrose, 160 U glucose oxidase, 2 μM catalase, 10 mM DTT, 1 mM ATP, 100 mM KCl, 25 mM imidazole, 1 mM EGTA, and 4 mM $MgCl_2$ either with or without calponin. The final concentration of labeled F-actin is 15 nM (low enough to visualize the actin under epifluorescence microscopy), while the final concentration of unlabeled G-actin is 85 nM for a total actin concentration of 100 nM, close to the barbed end critical concentration of α-skeletal muscle actin to help stabilize the filaments from depolymerization during imaging without significantly adding to their length [Isambert et al., 1995]. Experiments involving non-muscle actin are prepared in a similar fashion, except that the final concentration of unlabeled G-actin is 485 nM for a total actin concentration of 500 nM, to account for the higher barbed end critical concentration [Gordon et al., 1977; Rubenstein, 1990; Herman, 1993].

After allowing the sample an incubation time at room temperature for 30 minutes, 3 μL of the sample is deposited onto a BSA-coated microscope slide,

and a BSA-coated coverslip is gently set on top using a gloved hand and gently compressed using a pair of soft rectangular rubber erasers to form a narrow (~1-2 μm wide) flow chamber. The sample is then taken directly to the microscope for imaging. If necessary, imaging is delayed a few minutes to allow convective currents in the flow cell to settle, minimizing artifacts in filament shape due to fluid flow.

F-actin filaments freely fluctuating in two dimensions are visualized using standard epifluorescence illumination. The sample temperature is kept at 30 °C using an objective heater (Bioptechs; Butler, PA). Images of filaments 4-15 μm in length are captured 5 seconds apart to avoid excessive temporal correlation between subsequent frames. (See Chapter 2.6.4.)

To extract the persistence length, filaments are analyzed using a cosine correlation analysis of tangent angles (Chapter 2.6.2) after skeletonization in ImageJ (Chapter 2.4) using a custom-written Matlab script (see Appendix A). As a control, these results are compared to a mode variance analysis (Chapter 2.6.3) using a different sub-pixel fitting algorithm to fit a Gaussian shape across the filament, using a code provided by Dr. Thomas Angelini [Jensen et al., 2012b].

4.3 Results

4.3.1 Calponin reduces actin persistence length

To establish whether any differences in filament mechanics exist between α-skeletal muscle actin and non-muscle actin isoforms, we perform flexural

rigidity assays on both actin from rabbit skeletal muscle and on non-muscle actin from human platelets. As a control, two different analysis techniques, cosine correlation function (ccf) analysis and mode variance (mv) analysis, are employed. (See Figure 4.1 and Figure 4.2.)

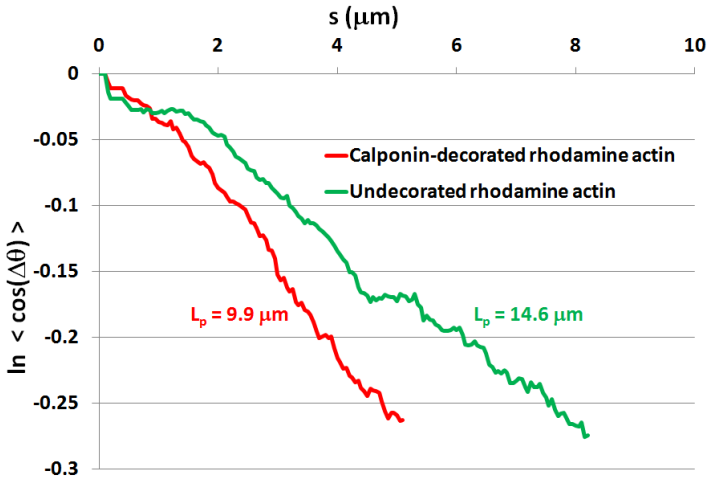

Figure 4.1: Cosine correlation function persistence length analysis.
Shown are two example filaments, one with and one without calponin. On a single-logarithmic plot, (2-27) predicts a linear curve, the slope of which is directly related to the persistence length. The steeper the slope on such a plot, the lower the persistence length.

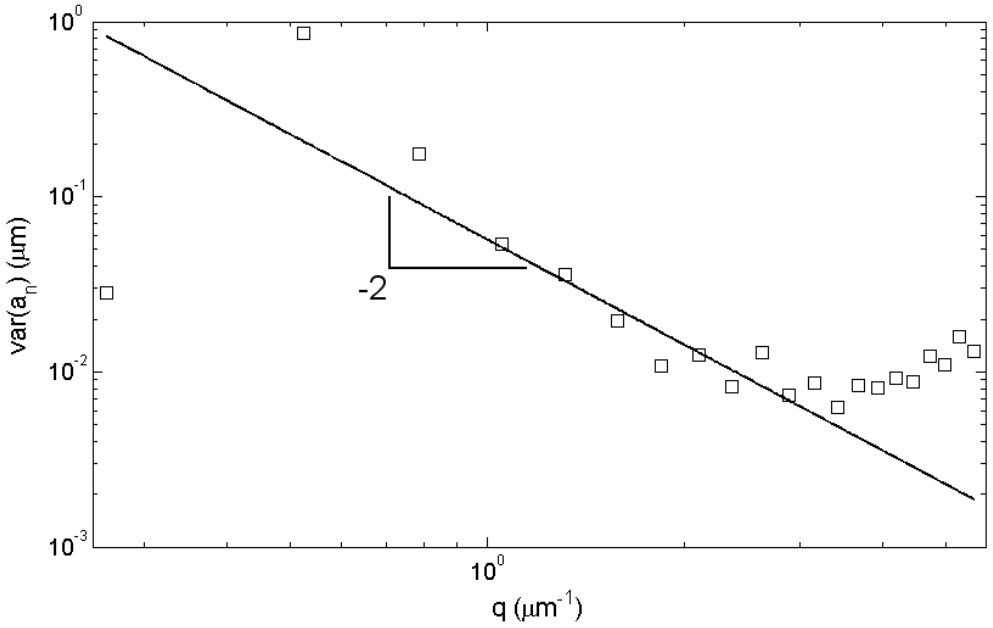

Figure 4.2: Mode variance persistence length analysis.
Once a filament is parameterized in terms of its tangent angle θ and arc length s (see Figure 2.9), the parameterization is decomposed into orthogonal cosinusoidal modes, the amplitude variance of which is shown here as a function of $q \equiv \frac{n\pi}{L}$. The persistence length is extracted by fitting (2-33) to the data. The higher modes are not used in fitting, as the are limited by the resolution noise floor. The lower modes are vulnerable to drift artifacts, while the lowest mode consistently exhibited a lower than expected amplitude, like due to moderate temporal correlation between frames.

The effects of calponin are assessed on both isoforms. The results are summarized in Figure 4.3. The data show good agreement between the cosine correlation function analysis and the mode variance analysis techniques. Slight differences in results are not surprising, especially since the cosine correlation function analysis uses a skeleton derived manually from ImageJ (Chapter 2.4), while the mode variance analysis uses a skeleton derived from the raw images by computationally fitting a Gaussian across the filament to locate the filament

backbone. Notably, the data show a statistically significant reduction in persistence length of both rabbit skeletal muscle (RS) actin and non-muscle human platelet (HP) actin when bound to calponin.

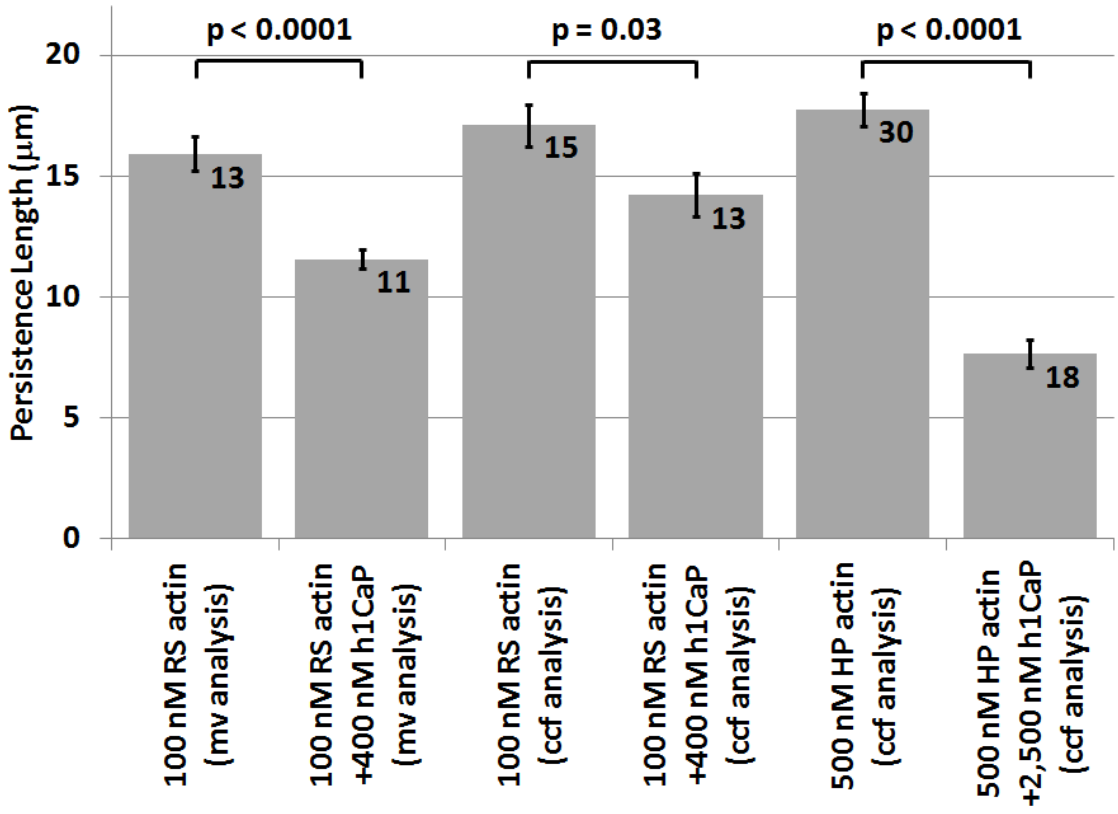

Figure 4.3: Persistence length measurements.
Shown are 100 nM rabbit skeletal with or without 4:1 molar excess of h1CaP, analyzed either using mode variance analysis (first and second bars) or cosine correlation function analysis (third and fourth bars). The last two bars are 500 nM human platelet actin with or without 5:1 molar excess of h1CaP analyzed using cosine correlation function analysis. Error bars are standard errors, based on the number of observed filaments, which is indicated on each bar.

Finally, we note that calponin is not fully decorating actin during the experiments with rabbit skeletal actin, despite being incubated at a 4:1 ratio,

consistent with previously measured dissociation constants of calponin from actin [Lu et al., 1995]. This is confirmed by pelleting the actin-calponin samples prepared for flexural rigidity experiments by ultracentrifugation for 30 minutes at 100,000*g* and running the pellet on a 12.5% SDS-PAGE gel (Figure 4.4). Lane 1 shows a BioRad standard 161-0363, with molecular weights indicated on the far left. Lanes 2 and 3 are control lanes loaded with 4 μg of actin or 4 μg of calponin, respectively. Lanes 4-6 are 500 nM F-actin incubated and pelleted with 0, 2.5 μM, or 5 μM h1CaP, respectively. Molar binding ratios are derived from densitometry measurements of each band and are shown above each lane as h1CaP:actin. The results show that persistence length changes occurred at sub-saturating calponin binding ratios.

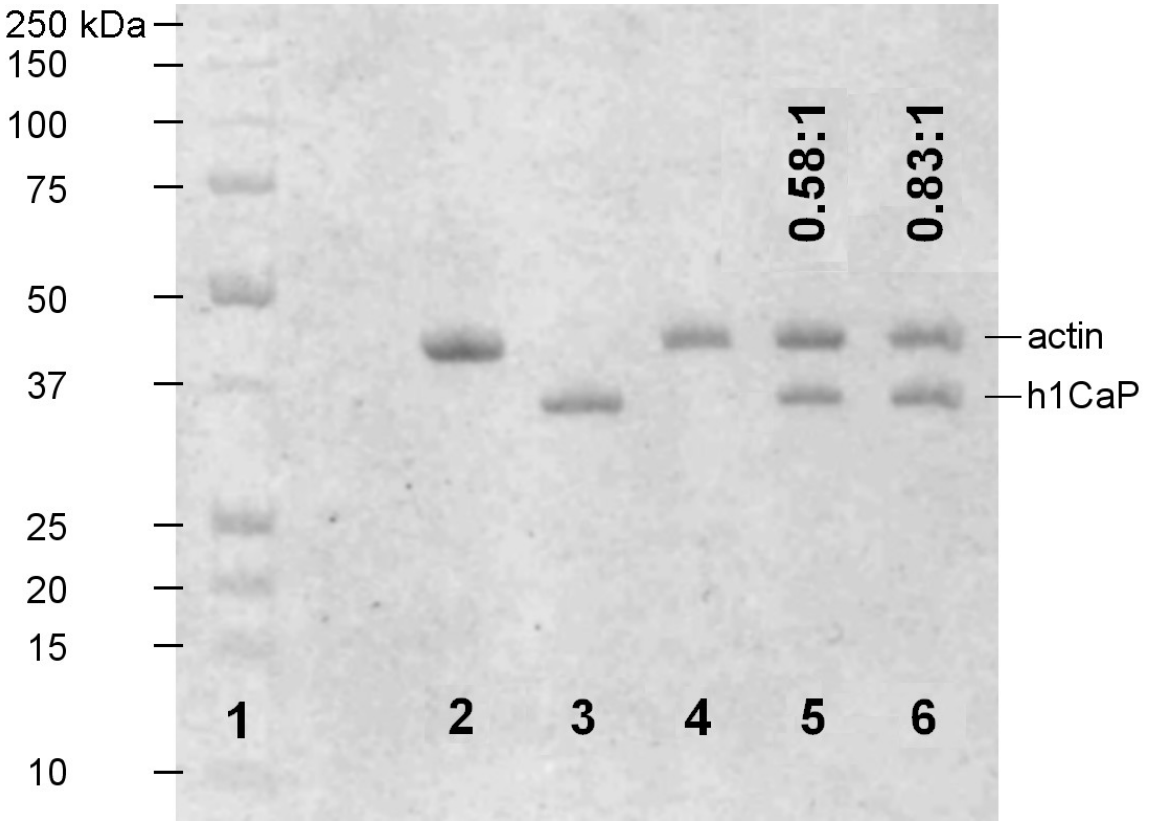

Figure 4.4: SDS-PAGE gel of actin-calponin samples.
Rabbit skeletal muscle F-actin is incubated with basic calponin under conditions similar to those of the flexural rigidity assay (see Chapter 4.2.1) and ultracentrifuged at 100,000g. The pellet is collected and run on a 12.5% SDS-PAGE gel. Lane 1: BioRad standard 161-0363, with molecular weight markers shown to the left; lane 2: control lane with 4 μg actin; lane 3: control lane with 4 μg h1CaP; lanes 4-6: 500 nM rabbit skeletal muscle F-actin incubated and pelleted with 0, 2.5 μM, or 5 μM h1CaP. Molar binding ratios are indicated as h1CaP:actin above each lane. The results show that persistence length changes for rabbit skeletal muscle actin reported in Figure 4.3 occur at sub-saturating calponin binding, while the filament rupture discussed in Chapter 4.3.2 persists to full decoration.

4.3.2 Calponin increases shear susceptibility of actin filaments

When preparing samples of 100 nM rabbit skeletal actin incubated with varying amounts of calponin and compressing the BSA-covered glass slides to

form a two-dimensional flow chamber, we note that actin filaments are shorter when incubated with increasing amounts of calponin (Figure 4.5). This effect is exacerbated with calponin concentration over the range investigated (0-5 μM h1CaP, corresponding to 0 to 50 times molar excess). Shown in Figure 4.5 are a 0:1 ratio (Figure 4.5A), an 8:1 ratio (Figure 4.5B), and a 50:1 ratio (Figure 4.5C). The histograms show normalized length counts of observed filaments, binned into 0.5 μm groups. 250-800 filaments were counted for each condition. Insets represent representative fluorescence microscopy images of each condition, with a scale bar of 10 μm shown for reference. The length distributions at each concentration of h1CaP are not seen to evolve over time. While not shown in the figure, this effect is found to be dependent on the amount of force applied when compressing the two glass slides together by varying the compressive force between experiments, suggesting that the shorter filaments are a result of shear-induced filament rupture. While the applied force is not quantified here, we find that calponin always reduces the actin filament length as compared to plain actin under the same force.

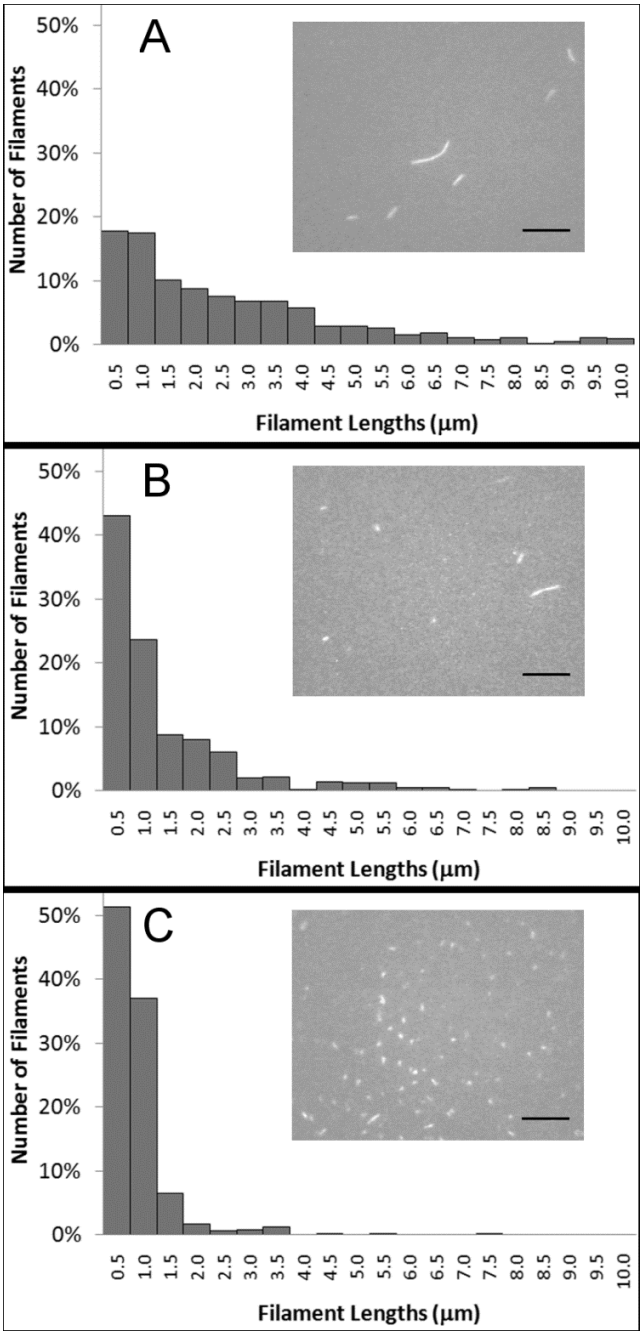

Figure 4.5: Changes in filament lengths with calponin.

Histograms show normalized length counts, binned into 0.5 μm groups, for 100 nM calponin-free RS actin (panel A), 100 nM RS actin with 800 nM h1CaP (panel B), and RS actin with 5,000 nM h1CaP (panel C). 250-800 filaments are counted for each condition. Insets show representative fluorescence microscopy images of each condition. Scale bar is 10 μm.

4.4 Discussion and conclusions

The main findings of this study are that calponin reduces the persistence length of single F-actin filaments while also making these filaments more susceptible to shear. Here, we discuss the implications of this finding and explore a possible mechanism behind this mechanical change involving actin subdomain 2.

Our persistence length measurements using plain actin are in fair agreement with previously reported values in the literature, which range around 1-20 μm (see Table 4.1). These measurements have been done using light scattering techniques, electron microscopy, and fluorescence microscopy mainly on α-skeletal muscle actin, since this actin isoform is very easily purified from vertebrates like rabbit or chicken. Still, the exact sources and treatments of the actin differ between the published studies. For example, some research has used resuspended lyophilized actin, while other labs exclusively use freshly purified never frozen or lyophilized protein. It is also worth noting that changes in persistence lengths derived from imaging of thermally fluctuating actin filaments can arise from skeletonization artifacts. For example, the data shown in Figure 4.1 and Figure 4.3 based on the cosine correlation function analysis are derived

by drawing secant lines starting at one end pixel and moving forward 10 pixels, corresponding to 0.3 to 0.4 μm. This length scale is large enough to avoid oversampling the data, but still short enough to accurately represent the actin filament. Lowering this parameter lowers the observed persistence length; for example, a secant step of 3 pixels instead of 10 reduces the measured persistence length of the rhodamine-labeled F-actin from 17.1 μm to 13.9 μm. Importantly, the change in persistence length induced by calponin is robust to the different skeletonization and analysis techniques explored in this work.

While many different actin sources, methods, and analyses were employed in these previously published studies, resulting in a range of values reported, it is worth noting that studies using the exact same source of rabbit skeletal muscle actin as is used in this work obtain a very similar persistence length to that found here [Köster et al., 2005]. We also see no difference in the persistence length of the investigated α-skeletal muscle actin from rabbit and the mixture of β and γ non-muscle actin from human platelets, suggesting that the amino acid differences between these isoforms do not significantly affect the flexural mechanics of the polymerized F-actin.

L_p, *actin* (μm)	*Source*	*Notes*
6.25	Takebayashi et al., 1977	w/ o phalloidin
31.25	Yanagida et al., 1984	w. phalloidin
17.7	Gittes et al., 1993	w. phalloidin
0.5	Käs et al., 1993	w. phalloidin
16.7	Ott et al., 1993	w. phalloidin
8.5 – 11	Isambert et al., 1995	w/ o phalloidin
15.5 – 19	Isambert et al., 1995	w. phalloidin
1.8	Käs et al., 1996	w. phalloidin
15.7	Goff et al., 2002	w. phalloidin
19	Köster et al., 2005	w/ o phalloidin
17	Brangwynne et al., 2007	w. phalloidin
18.2	Greenberg et al., 2008	w/ o phalloidin corrected for factor of 2 in analysis
35.4	Greenberg et al., 2008	w. phalloidin corrected for factor of 2 in analysis
9.8	McCullough et al., 2008	w/ o phalloidin

Table 4.1: Previously published values of actin persistence lengths.
In cases where multiple actin isoforms or different methods of analysis were employed, a range of persistence length values are given. We distinguish between actin decorated with phalloidin (an actin-stabilizing drug) and plain actin, as indicated in the notes for each value.

We find that calponin reduces the persistence length of both α-skeletal muscle actin and of non-muscle actin from human platelets (Figure 4.3). Although we see a larger reduction in persistence length when calponin is added to human platelet non-muscle actin at a similar ratio used for rabbit skeletal muscle actin (Figure 4.3), this may be due to the fact that a higher actin concentration is used in the experiment rather than arise from actin isoform-dependent changes in binding. Since the off rate of calponin is

concentration-independent but the on rate depends on the concentrations, increasing the concentrations but keeping the ratios unchanged would increase the amount of actin-bound calponin. This is also consistent with previously reported dissociation constants of actin-calponin binding [Lu et al., 1995]. Importantly, the change for both actins is towards a lower persistence length, showing that calponin affects both isoforms of actin in a similar fashion.

In addition to a reduction in persistence length, we also observe a significant reduction in the length of calponin-actin filaments as compared to undecorated rhodamine actin (Figure 4.5). It is unlikely that this reduction in average filament length is caused by a change in the depolymerization rates or critical concentrations of actin, as we do not observe any discernable changes in filament lengths over the course of an experiment, and as the relative length differences are apparent immediately after sample preparation. The severity of the length reduction is also lessened if the flow chamber is not compressed, but instead assembled by resting the cover slip on top of the microscope slide and letting it slowly settle under its own weight, thus lessening the shear experienced by the actin. Furthermore, calponin has previously been reported to promote actin assembly and inhibit depolymerization through electrostatic interactions at low salt concentrations [Kake et al., 1995; Tang et al., 1997]. We therefore propose that the observed difference in filament lengths is caused by a shear-induced filament breakage to which calponin-decorated actin filaments are

more susceptible. The exponential distribution of filament lengths observed both in the absence and presence of calponin (Figure 4.5), which is characteristic of a double-stranded polymer in dynamic equilibrium [Howard, 2001], also supports this hypothesis.

While calponin bound to F-actin has previously been visualized by electron microscopy, it remains somewhat ambiguous exactly how and where calponin binds to actin, and whether it binds in a unique fashion or through multiple modes of binding [Galkin et al., 2006]. Rather than pointing to multiple binding modes, recent cryo-electron microscopy places calponin over actin subdomain 2 (Figure 4.6; [Jensen et al., 2012b]) and in agreement with previous negative stain electron microscopy reconstructions [Hodgkinson et al., 1997]. Actin subdomain 2 is a common actin-binding protein targeting site [McGough, 1998; Dominguez, 2004] and is known to be a relatively malleable part of actin, with structural changes in this subdomain rearranging the radial mass distribution of the filament, in turn affecting the flexibility of F-actin [Orlova & Egelman, 1993; Bremer et al., 1994; Isambert et al., 1995]. Interestingly, calponin is in contact with longitudinally adjacent monomers by reaching from subdomain 1 across subdomain 2 of one monomer to the edge of subdomain 1 of the longitudinally neighboring monomer (Figure 4.6). The connection between these subdomains is a known region of intermonomeric hydrophobic contact, as a hydrophobic region of subdomain 2 on one monomer inserts itself into a

hydrophobic cleft between subdomains 1 and 3 on the longitudinally neighboring monomer [Dominguez, 2004]; this places calponin in reach of important intermonomer contacts in F-actin. Calponin also reaches residues 43-48 in subdomain 2 [Hodgkinson et al., 1997], a region of actin previously discussed to be structurally involved in altering F-actin flexural rigidity by changing the structure of subdomain 2 [Isambert et al., 1995]. The changes in calponin-decorated actin flexural mechanics (Figure 4.3) together with this structural information suggests a model of calponin interactions with F-actin in which calponin induces structural changes in actin subdomain 2 and possibly affects intermonomer contacts to change the overall flexibility of the filament.

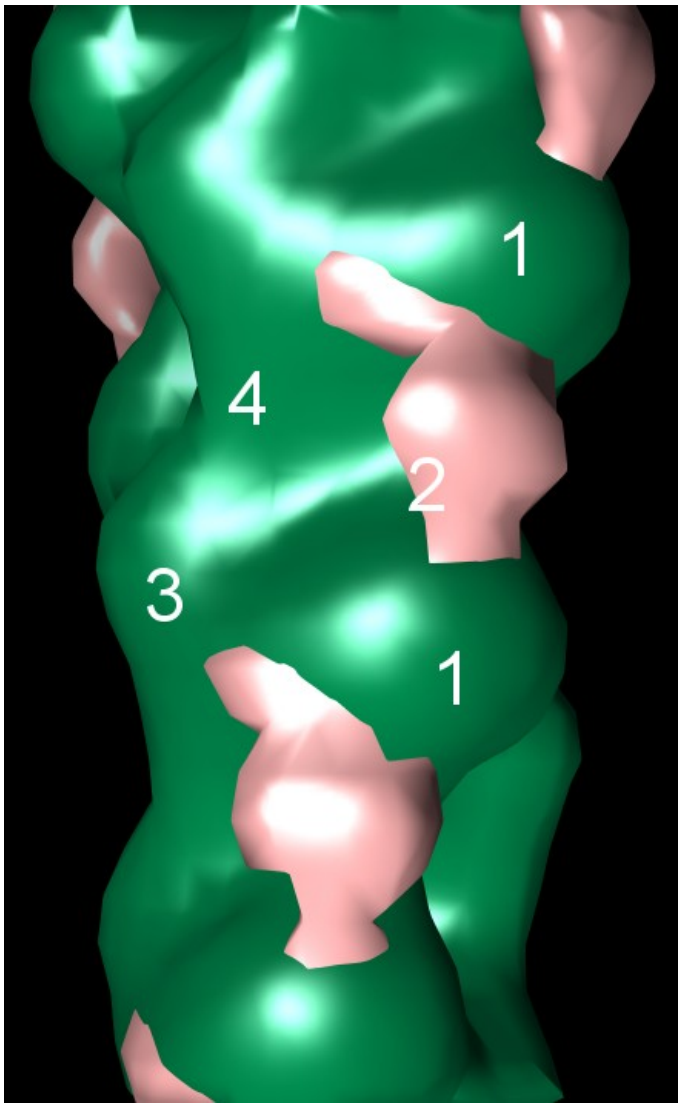

Figure 4.6: Electron micrograph reconstruction of calponin-actin.
Shown is the difference map of RS actin (green) with the basic calponin density (pink) over actin subdomain 2, bridging actin subdomains 1 of longitudinally neighboring actin monomers. The four subdomains of one monomer, as well as subdomain 1 of the neighboring monomer, are labeled for spatial reference. The reconstruction is done by Dr. William Lehman [Jensen et al., 2012b] from cryo-electron microscopy images.

A correlation between decreased actin filament rigidity and decreased filament stability has been observed for another ABP, cofilin, which has been

shown to both reduce actin rigidity and sever actin [Prochniewicz et al., 2005; McCullough et al., 2008]. Two models for cofilin severing of actin have been proposed: one in which increased flexibility allows actin monomers to explore a greater conformational space, making bond rupture within decorated regions more likely [Prochniewicz et al., 2005], and one in which severing occurs at ABP decoration boundaries due to a mismatch in mechanical properties between decorated and undecorated actin regions [De La Cruz, 2009]. This latter model is strongly supported by observations of cofilin-induced actin severing activity [Yeoh et al., 2002; Andrianantoandro & Pollard, 2006], as well as recent direct visualizations of single actin filament rupture in the presence of fluorescently labeled cofilin [Suarez et al., 2011]. In the case of calponin, our data show the observed actin filament breaking under shear being exacerbated with calponin concentration (Figure 4.5), and we observe no reduction in severing as the actin filaments near calponin saturation, as would be the case if severing were occurring at decoration boundaries rather than within regions of calponin decoration. The mechanism of the observed calponin-induced shear severing would therefore be one in which calponin reduces the flexural rigidity of actin, likely through interactions with actin subdomain 2, allowing a larger conformational space to be explored. This in turn makes severing in calponin-decorated regions more likely under external shear, such as that experienced during sample preparation.

A growing body of evidence is pointing to calponin as a cytoskeletal regulator stabilizing the actin cytoskeleton in cells (see Chapter 4.1). The data discussed here show that calponin has an effect on F-actin bending mechanics *in vitro* without additional binding partners or other cellular components present, reducing the actin persistence length. This suggests that the functional effects of calponin observed *in vivo* could be caused directly by calponin interactions with actin, rather than through action by multiple binding partners or other cellular components; however, the physical mechanism of *in vivo* calponin stabilization of actin is not apparent from just these single filament data. Still, the data point to actin flexural rigidity as a parameter of interest in understanding the effects of calponin on larger-scale actin systems more closely mimicking the cellular cytoskeleton, and will serve as the basis for the work discussed in Chapter 5, in which the work is extended to consider the mechanics of *in vitro* actin networks.

5 Mechanics of Actin Networks with Calponin

5.1 Introduction

While the data in Chapter 4 shed some light on how basic calponin can affect single actin filaments, it is not clear what implications this has for actin networks and cytoskeletal regulation *in vivo*. As discussed, calponin is seen to stabilize actin in cells [Parker et al., 1994; Hossain et al., 2003; Hossain et al., 2005; Arrigoni et al., 2006; Tang et al., 2006, Kim et al., 2008; Rozenblum & Gimona, 2008; Shibukawa et al., 2010]. For example, studies using smooth muscle tissues grown artificially in a medium with large amounts of vitamin C show that basic calponin expression was upregulated, while the tissue has a lower stiffness but a higher tensile strength [Arrigoni et al., 2006]. It is unclear whether calponin upregulation is the cause of the mechanical changes in the tissue or simply an intermediary of a signaling pathway, and whether other actin-binding partners are involved in the process. The mechanisms by which the tissue mechanics are regulated are also unclear from the published works.

To remedy this, we use a model reconstituted actin network and look for any mechanical changes induced by basic calponin. The underlying thesis of choosing an actin network system as a model system of study is that basic calponin is known to directly affect actin filament mechanics (see Chapter 4), and we therefore expect to see these changes propagate through to the whole network setting as well.

The reconstituted actin network is a minimalistic system in which one can still hope to gain an understanding of any mechanisms through which calponin functions. Despite the obvious lack of complexity found in a real cell, such systems have previously been shown not only to yield insights into the physics of semiflexible polymer networks, but also mimic some fundamental properties of the actin cytoskeleton with very few constituents present [Gardel et al., 2004a; Gardel et al., 2004b; Gardel et al., 2006; Thatmann et al., 2007; Kasza et al., 2009]. We therefore consider such a model system a natural extension of the bottom-up approach undertaken in Chapter 4. We use a model system in which we reconstitute *in vitro* actin networks permanently crosslinked with biotin-neutravidin crosslinkers and study their bulk rheological properties with and without calponin. As part of establishing this model system for our use, we explore the rheology of varying crosslinking ratios and actin isoforms. While it has previously been published that actin isoforms have greatly different rheological properties [Allen et al., 1996], we see only minor differences between α-skeletal and non-muscle actin isoforms, but none as dramatic as reported in this previously published study. We consider these differences likely to arise from impurities in actin used by previous researchers.

In a fully crosslinked network, we find that basic calponin delays the strain stiffening onset and subsequent network failure, increasing both the maximal strain and maximal stress the networks can withstand before failing.

Since tropomyosin is highly prevalent in most cells and could affect the mechanical effects induced by calponin (in fact, the two proteins are present in equal amounts in smooth muscle [Takahashi et al., 1986]), we also investigate the effects of basic calponin on tropomyosin-actin networks and find that this increase in tensile strength occurs in both plain actin and tropomyosin-decorated actin networks, suggesting that calponin can affect both types of filament in the cell. We compare our results to affine network models and show that the effects are consistent with and explained by the calponin-induced reduction in actin persistence length observed in single filament studies (Chapter 4). Together, these data suggest a simple mechanism through which calponin mechanically stabilizes actin in cells under external strain by making actin filaments more flexible and in turn making the actin cytoskeleton more compliant. This model explains the qualitative behavior observed in cells and tissues using only a single parameter, the actin flexural rigidity, and is the first model explaining one possible mechanism for calponin stabilization of actin.

5.2 Methods

5.2.1 Rheology of actin networks

Lyophilized G-actin from human platelets (85% non-muscle β-isoform and 15% non-muscle γ-isoform) lyophilized G-actin from rabbit skeletal muscle (100% α-skeletal muscle actin isoform), and lyophilized rabbit skeletal muscle G-actin biotinylated on surface lysine residues to a density of 1 biotin per monomer are

purchased from Cytoskeleton (Denver, CO). On the day before the experiment, G-actin is resuspended to a concentration of 4 mg/mL (plain actin) or 0.1 mg/mL (biotinylated actin) in G-buffer (0.2 mM $CaCl_2$, 0.2 mM ATP, 0.2 mM DTT, 0.005% NaN_3, and 2 mM Tris-HCl, pH 8.0).

To test the effects of basic calponin on actin network mechanics, actin networks at 0.5 mg/mL actin concentration are polymerized from these two G-actin sources at a ratio of biotinylated actin to plain actin of 1:100. Once the rheometer is prepared and calibrated (see Chapter 2.5), 37.5 μL plain actin is mixed with biotinylated actin and polymerization induced by adding 30 μL 10x F-buffer (20 mM $MgCl_2$, 2 mM $CaCl_2$, 1 M KCl, 5 mM ATP, 2 mM DTT, and 20 mM Tris-HCl, pH 7.5) and quickly mixing the actin and buffer. After 60 seconds, a second mixture of actin-binding proteins at the desired concentrations, neutravidin (Sigma Aldrich; St. Louis, MO), and additional G-buffer to bring the final volume to 300 μL are added, and the mixture is gently mixed by pipetting up and down five times at a consistently slow pace (taking 10 seconds to total) using a 20-200 μL sized pipette tip. The prepolymerization step is needed to incorporate the biotinylated actin uniformly into F-actin filaments before adding the neutravidin, as severe inhomogeneities would otherwise result. Consistent pipetting is also crucial here and throughout in order to form reliably reproducible networks. In these experiments, a ratio of 2:1 calponin:actin and 0.2:1 tropomyosin is used. These ratios, at the used actin

concentrations, should be sufficient to saturate actin (note that the concentration of tropomyosin refers to the coiled-coil dimer as a tropomyosin "monomer", and that this unit occupies seven actin monomers on the filament).

After mixing, 285 μL of the sample is immediately loaded onto the lower rheometer plate, and the upper parallel plate geometry is lowered to a gap size of 200 μm. The upper geometry is gently spun while lowering the gap to uniformly wet the two plates. The sample is sealed around the edge using mineral oil (Sigma Aldrich; St. Louis, MO) and left to polymerize for 1 hour at 25 °C while the polymerization is monitored using oscillatory rheometry at a frequency of 1 rad/ s and strain amplitude of 0.5%. After the polymerization, the sample is subjected to a slow strain ramp ($\dot{\gamma} = 0.25\ \%/\mathrm{s}$), during which the shear stress and strain are monitored. The sample is strained far enough to reach network failure, which is quantified in terms of the maximal strain $\gamma_{\max}$ and maximal stress $\sigma_{\max}$ the network can withstand. The differential modulus K' is extracted from the slope of the stress-strain curves in Matlab (MathWorks, Natick, MA) after smoothing the curves, as described in Chapter 2.5 and (2-14). In a fully crosslinked network, three regimes (a linear regime with $\frac{dK\prime}{d\gamma} = 0$, a strain stiffening regime with $\frac{dK\prime}{d\gamma} > 0$, and a failure regime with $\frac{dK\prime}{d\gamma} < 0$) are evident (Figure 5.1).

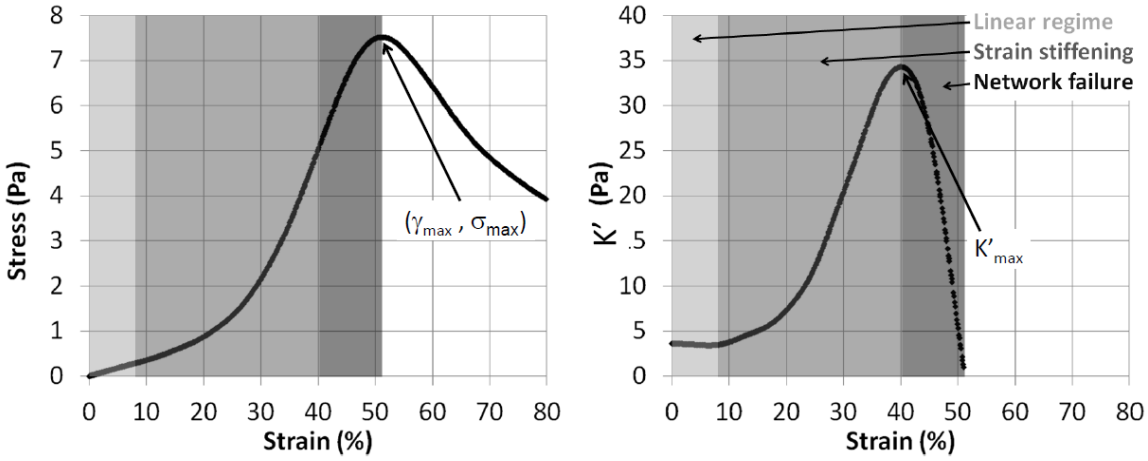

Figure 5.1: Stress-strain behavior of a fully crosslinked actin network.
The shown example is of a 0.5 mg/mL HP actin network with 1:100 biotin-actin and a 2x molar excess of h1CaP. For a fully crosslinked network, three distinct regimes are apparent, highlighted on both the stress-strain curve and the graph of the differential modulus $K'(\gamma) = \frac{\partial \sigma(\gamma)}{\partial \gamma}$. *Network failure is quantified in terms of* γ_{max} *and* σ_{max}, *which are also indicated on the figure. The graphs shown here have been smoothed in Matlab.*

The rheometer geometries are cleaned between samples by wiping them down with a volume of acetone, a volume of isopropanol, a volume of glassware dish soap, and three volumes of distilled water (10 mL each). The geometry gap is zeroed between samples, but rheometer mappings and inertia calibrations are kept unchanged to avoid introducing systematic errors between measurements.

In the data below, polymerization curves are unfiltered raw data, while stress-strain curves and differential modulus curves used in analysis have undergone smoothing. While this smoothing does not change the quantitative analysis of strain stiffening behavior and network failure, it is explicitly noted in the legend of each figure whenever smoothing has been applied. In the initial stages establishing the exact conditions from which to work, other actin

concentrations and crosslinking densities than those listed above are explored; the exact conditions are therefore also listed explicitly for each figure.

5.2.2 Simulating affine strain in an ensemble of linear springs

To help understand how changes in the actin filament persistence length can affect the behavior of an entire network under affine strain, we use a Matlab script to visualize qualitative changes in strain behavior of an ensemble of linear springs when the stiffness of each spring is changed (see Appendix C). This is purely meant as an aid in illustrating how changes in the mechanics of individual components can affect the qualitative behavior of the whole system, and is not meant to be taken as an accurate simulation of strain behavior in an actual actin network.

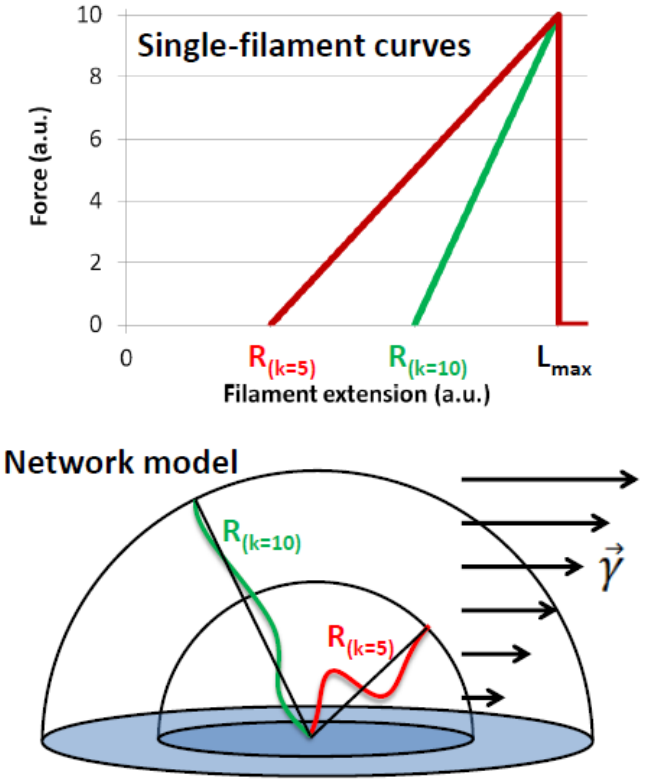

Figure 5.2: Simulation of ensemble of linear springs under affine strain. *Each spring is given a force-extension curve as shown in the top panel, and is assumed to be linear throughout. A softer spring will have a shorter starting end-to-end length R, as well as a lower spring constant k. All springs are defined to fail at a maximal extension* L_{max}*, after which their restoring force is 0. 100,000 springs are distributed isotropically on a hemisphere of radius R and subjected to an affine strain field* $\vec{\gamma}$*, during which the forces from each spring in the shear direction are added (bottom panel).*

The simulation, for which all variables are in arbitrary units, assumes that each spring component can be extended to a maximal extension $L_{max} = 3$ before breaking at a maximal force of $F = 10$, and that the restoring spring force after this maximal extension is 0 (Figure 5.2, top panel). Two arbitrary spring constants, $k = 5$ and $k = 10$, are chosen in the simulation. The springs with lower spring constant will have a shorter initial extension. While the simulation

makes no assumptions about the origin of the elasticity, note that this behavior, in which a softer spring will also have a shorter initial extension, is qualitatively consistent with an actin filament acting as an entropic spring having a shorter equilibrium end-to-end length and a lower spring constant when the flexural rigidity of the filament is lowered (see Chapter 2.7.1 for more details).

To simulate an ensemble of springs, 10^6 filaments are arranged on a hemisphere, with one end fixed at the center and the other end placed randomly a distance R away, creating a "pin cushion" of hemispherically isotropically distributed springs (Figure 5.2, bottom panel). The end-to-end length R is generated as a normal distribution with a standard deviation of 0.1; not doing so results in the same qualitative behavior, but a less smooth curve. An affine strain field $\vec{\gamma}$ is then applied, and the force in the plane of the strain is added up for each filament to build a stress-strain curve for the system. Note that no connectivity between springs is simulated, and that the failure of each spring is only dependent on its own extension, which in turn is entirely dependent on the strain field and not on any local spring connections. The model also does not capture any non-affine behavior that may occur in a network under high strain.

5.3 Results

5.3.1 Rheological properties of actin networks

As an initial step in the study, various actin network conditions are explored to establish a base model system from which to investigate the effects of

calponin. This section contains the results of these initial studies of actin network rheology.

The rheological behavior of actin networks is highly dependent on whether or not the networks are fully crosslinked. At the crosslinking ratio used in this study (1:50 or 1:100 biotin-actin:actin, corresponding to a crosslinking ratio of 1:100 or 1:200), 0.5-1 mg/ mL actin polymerizes into networks that are dominantly elastic. In contrast, actin networks without crosslinkers exhibit very little elasticity, although the networks still appear slightly elastic within the experimental resolution of the rheometer used here (Figure 5.3). Increasing the crosslinking density or the actin concentration resulted in networks of a higher stiffness, but all were around 2-4 Pa.

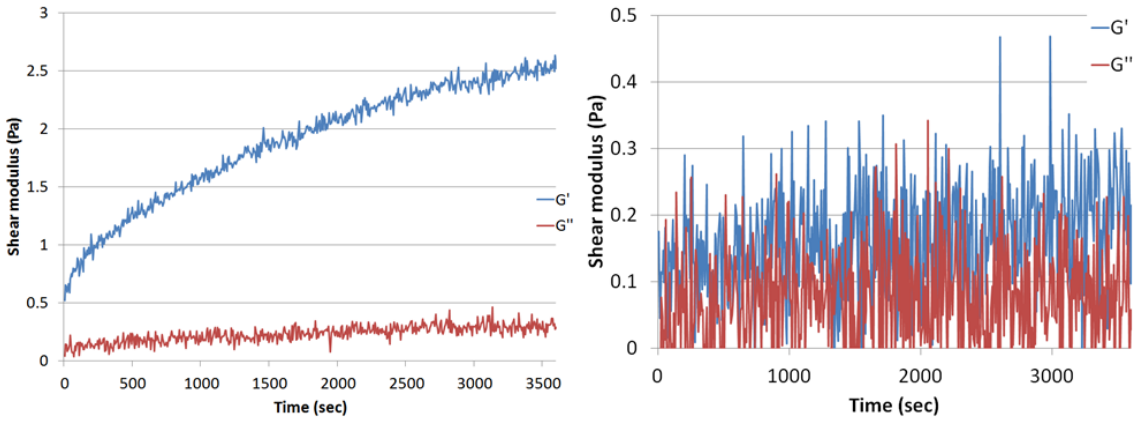

Figure 5.3: Polymerization of actin networks with and without crosslinkers. *Oscillatory rheology is used to monitor the polymerization of 1 mg/mL actin networks with (left panel) or without (right panel) 1:50 biotin-actin. While a crosslinked actin network polymerizes to a G′ of a few Pascal and forms a predominantly elastic network, entangled actin exhibits very low elasticity.*

The nonlinear behaviors of networks with and without crosslinkers also differ greatly; while crosslinked actin strain stiffens after going through a linear regime, entangled actin has a longer regime of linear behavior with elasticity similar to that seen in the linear oscillatory rheology, after which the entanglements giving rise to the elasticity are pulled out, and the network strain weakens and flows (Figure 5.4).

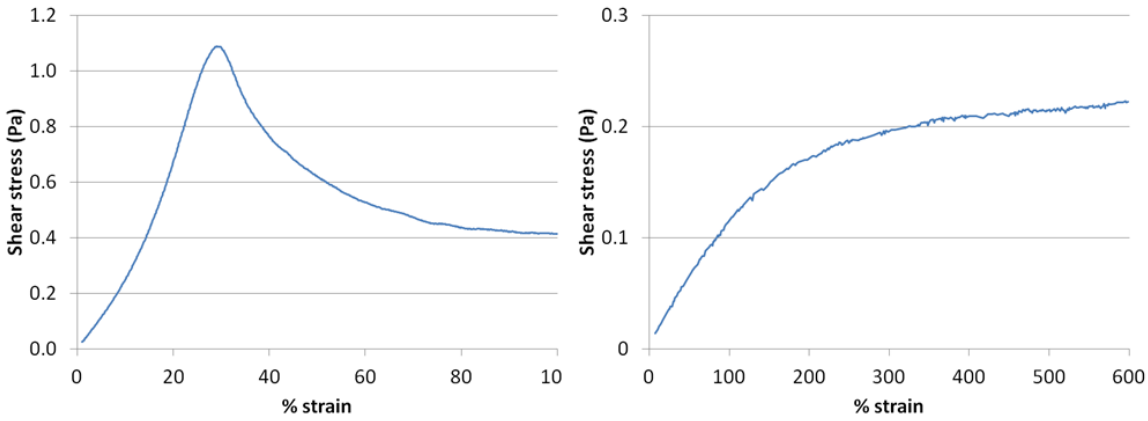

Figure 5.4: Strain ramps of actin networks with and without crosslinkers.
Strain ramps of the networks shown in Figure 5.3. The crosslinked actin network at 1 mg/mL undergoes strain stiffening after going through a linear regime, after which the network eventually fails (see also Figure 5.1); in contrast, an entangled actin network at 1 mg/mL has a long linear regime with low elasticity, after which the entanglements are pulled out and the filaments flow, causing the network to strain weaken.

To establish a model system for investigating calponin effects on actin network mechanics, we also investigate the changes in network strain behavior with varying amounts of biotinylated actin present. Two ratios of biotin-actin to plain actin are shown in Figure 5.5. Lowering the biotin-actin ratio from 1:100 (corresponding to a crosslinking ratio of 1:200) to a biotin-actin ratio of 1:200

(corresponding to a crosslinking ratio of 1:400) lowers the linear modulus and delays the onset of strain stiffening. As the crosslinking density is reduced, the network fails at a lower maximal stress, but a higher maximal strain.

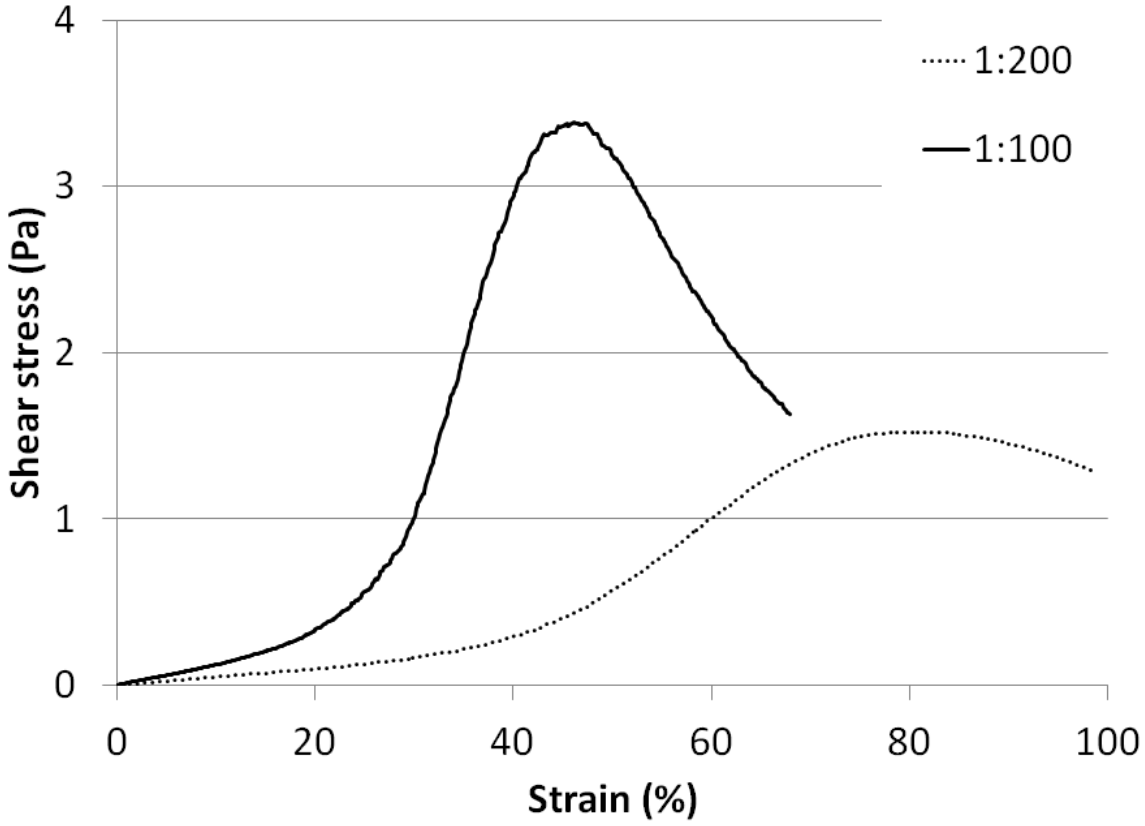

Figure 5.5: Strain ramps of actin networks of varying crosslinking density. *0.5 mg/mL RS actin crosslinked with biotin-neutravidin, with 1:100 biotin-actin (solid line) or 1:200 biotin-actin (dotted line). Lowering the crosslinking ratio lowers the linear elastic modulus, evident as a lower initial slope. The linear region is prolonged and the yield strain increased as predicted within an affine network model, while the yield strain is reduced.*

While we choose non-muscle actin (comprised primarily of non-muscle β-actin) as the basis for this study since the non-muscle actin isoforms are presumed to be more relevant to the smooth muscle calponin isoform studied

here, we compare α-skeletal muscle and non-muscle actin in bulk rheology. The results are summarized in Table 5.1, measuring both the linear modulus and the maximal stress and strain the networks withstand during a strain ramp. This comparison is done using actin networks at 1 mg/ mL concentration and using 1:50 biotin-actin, but which are otherwise prepared as described in Chapter 5.2.1.

	100% α-skeletal muscle (N=6)	85% β, 15% γ non-muscle (N=10)
Linear modulus G'	3.1±0.4 Pa	4.4±0.4 Pa
Max. strain γ_{max}	51.1±1.8 %	36.9±2.6 %
Max. stress σ_{max}	2.1±0.3 Pa	1.8±0.1 Pa

Table 5.1: Rheological comparison of skeletal- and non-muscle actin.
The linear shear moduli are extracted from oscillatory rheology at the end of sample polymerization (Figure 5.3), while the yield strain and stress are extracted from strain ramps after polymerization (Figure 5.1). Networks are either RS or HP actin at 0.5 mg/mL with 1:100 biotin-actin.

Finally, we note that there is a significant variability between samples when comparing their non-linear strain stiffening behavior, even when these are run using the same batch of protein and consecutively on the same rheometer (Figure 5.6). We suspect these differences arise from differences in surface attachments and most significantly from variations in the exact network polymerization and microscopic structure between samples. However, despite this variability, the samples exhibit a high degree of self-similarity in the sense that normalizing to the maximal stress and strain collapse the curves onto a single curve. This suggests a useful approach for analyzing differences induced

by calponin while eliminating variability between samples of identical conditions.

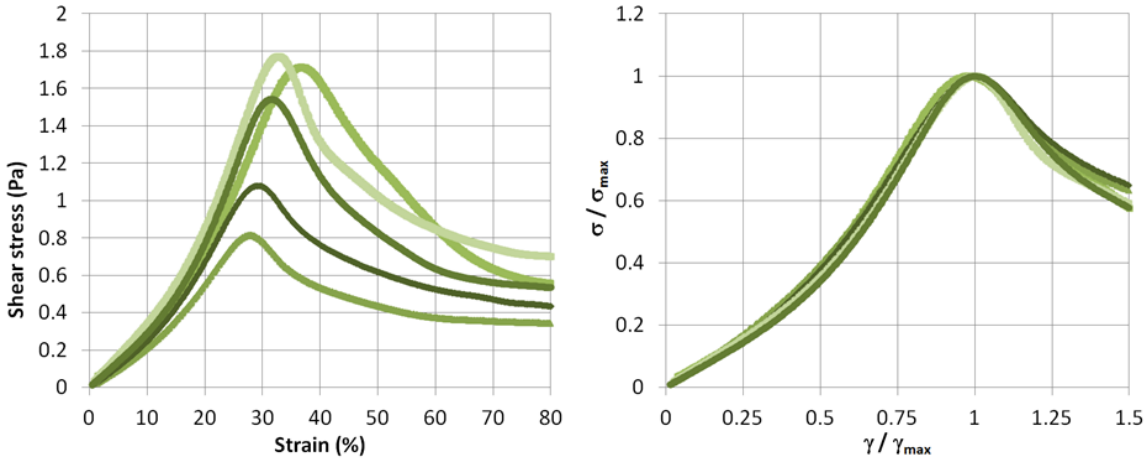

Figure 5.6: Self-similarity of actin network stress-strain behavior.
Shown are five strain ramps, all smoothed in Matlab, of HP actin networks at 0.5 mg/mL with 1:100 biotin-actin. When normalized to their yield strain and yield stress (Figure 5.1), the curves collapse onto one, suggesting a high degree of self-similarity between similar samples, despite the high degree of variability in absolute values.

5.3.2 Calponin strengthens actin and actin-tropomyosin networks

To investigate the effects of calponin on actin network mechanics, we use a model system of 0.5 mg/ mL actin networks crosslinked with 1:100 biotin-actin and neutravidin. In this system, basic calponin increases both the maximal strain and the maximal stress the networks can withstand, but the linear elastic modulus is largely unchanged (3.2 ± 0.3 Pa for plain actin networks vs. 2.8 ± 0.4 Pa for calponin-decorated actin networks, p=0.46). We also investigate tropomyosin-decorated actin networks and see a further increase in tensile

strength when calponin is added to these networks. Four such representative strain ramps are shown in Figure 5.7.

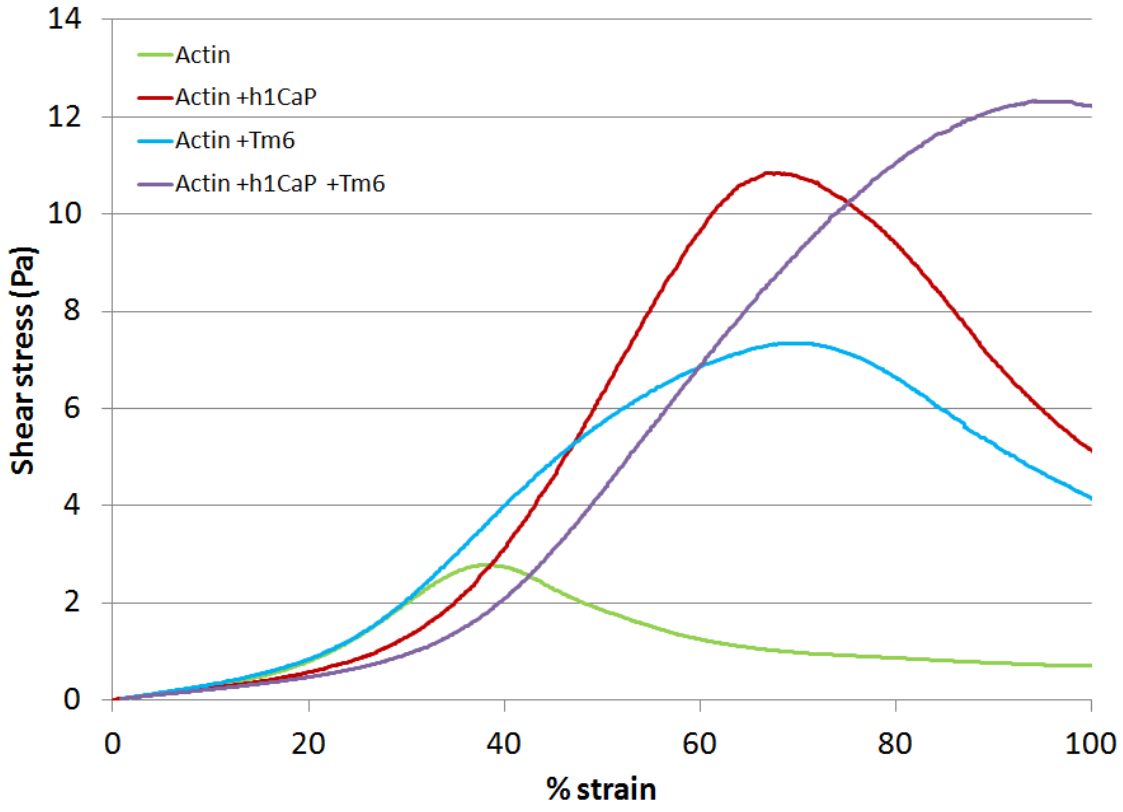

Figure 5.7: Representative stress-strain curves of actin networks.
Actin networks are 0.5 mg/mL HP actin with 1:100 biotin-actin. The green curve is plain actin, the red curve is actin with 2:1 h1CaP, the blue curve is actin with 0.2 Tm6, and the purple curve is actin with both actin and calponin present.

These data show that calponin increases the tensile strength of actin networks purely through mechanical interactions without other binding partners present, and that calponin can affect both plain actin and actin decorated with tropomyosin (Figure 5.8).

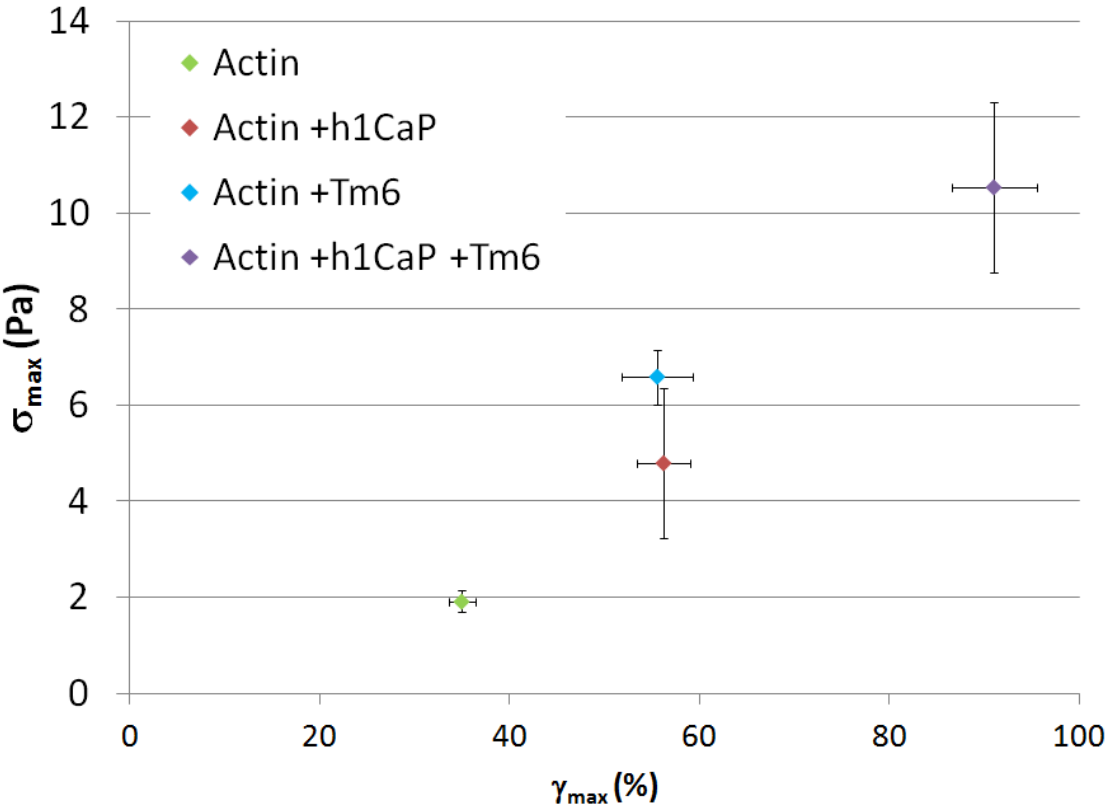

Figure 5.8: Yield stress and strain of actin networks.
Networks are 0.5 mg/mL HP actin with 1:100 biotin-actin. Concentrations of actin-binding proteins are as in Figure 5.7 and as described in Chapter 5.2.1. Error bars are standard errors, based on the number of samples for each data point (2-10 for each condition). Calponin increases the yield stress and strain of plain actin. Adding calponin to tropomyosin-decorated actin increases the yield stress and strain further, suggesting that calponin can have an effect on both plain actin and tropomyosin-decorated actin.

5.3.3 Changes in network strain stiffening behavior

To investigate the physical mechanism by which calponin increases the tensile strength of actin networks, we compare strain ramps of plain crosslinked actin to those of calponin-decorated actin networks.

The differences, most easily visualized by normalizing the stress-strain curves to γ_{max} and σ_{max}, show that calponin delays the onset of strain stiffening and prolongs the relative time spent in the linear regime (Figure 5.9). In contrast, the failure regime looks very similar between the two samples, suggesting that network failure occurs in a similar fashion in the two samples.

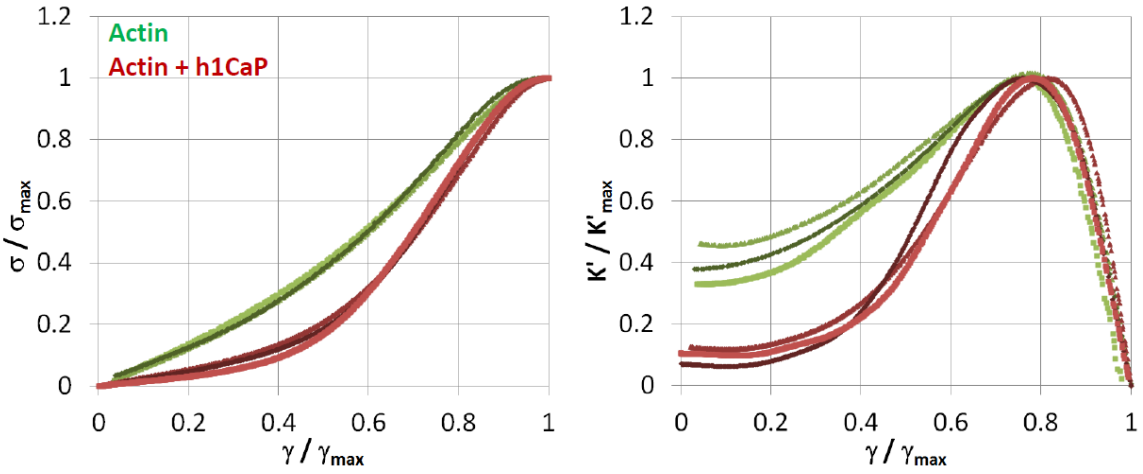

Figure 5.9: Calponin prolongs the linear regime under strain.
Shown are three strain ramps, all smoothed in Matlab, of 0.5 mg/mL HP actin with 1:100 biotin-actin either with (red) or without (green) 2:1 h1CaP. Note that the self-similarity previously observed for actin samples (Figure 5.6) is apparent for calponin-actin as well. While the failure regimes are very similar between plain actin and calponin-actin, calponin-actin spends more time in the linear regime, signifying a delay in the onset of strain stiffening.

The delay in strain stiffening can also be quantified in terms of absolute strain. One way of doing so is illustrated in Figure 5.10 and is similar to analysis previously employed [Tharmann et al., 2007]. Since the onset of strain stiffening occurs gradually, the differential modulus K' and strain are represented on a log-log plot and the onset defined by the intersection between the line

representing the unstrained K' (i.e., G'; red line on Figure 5.10) and the line representing the greatest growth in K' (green line on Figure 5.10). With this analysis, actin networks are seen to strain stiffen at 10 ± 0.6 % strain, while calponin-actin networks strain stiffen at 14.9 ± 1.0 % strain (error bars: standard error), consistent with the delayed strain stiffening inferred from Figure 5.9. While this definition is somewhat arbitrary, we try quantifying the strain stiffening onset from our data in different ways and find that it yields the same relative differences between samples as do other definitions, e.g., defining the strain stiffening as occurring when K' exceeds a certain fraction of G'.

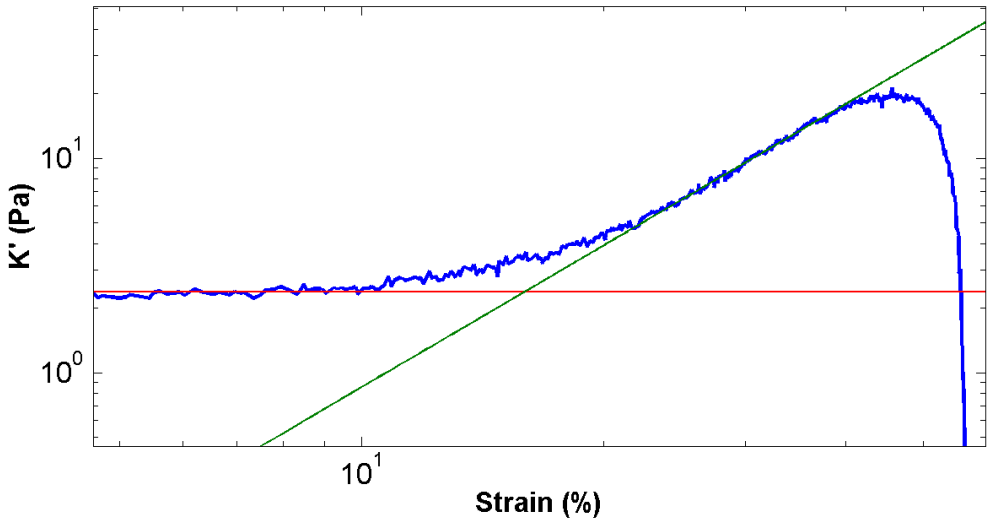

Figure 5.10: Quantifying the onset of actin network strain stiffening.
The curve shown here (blue) is a strain ramp of a 0.5 mg/mL HP actin network with 1:100 biotin-actin and 2:1 h1CaP. The sample gradually strain stiffens, increasing K' above the initial value (red line) and climbs in a polynomial fashion (green line; fit) until entering the failure regime, in which $\frac{\partial K\prime}{\partial \gamma} < 0$. The onset of strain stiffening is quantified as the intersection between the red and green lines.

5.4 Discussion and conclusions

We study the rheological properties of actin networks either with or without tropomyosin, and find that calponin delays the onset of strain stiffening in these networks and delays the onset of strain stiffening. Here, we argue that these mechanical effects can be explained solely in terms of the calponin-induced changes in actin persistence length discussed in Chapter 4 and propose a physical model for calponin mechanical stabilization of actin networks *in vivo*.

We note from our data that since entangled actin strain weakens under high strains, only the crosslinked actin networks experience network failure, evident as a regime of $K' < 0$ (Figure 5.4). These networks also exhibit very little elasticity under oscillatory linear rheology (Figure 5.3). To understand the effects of basic calponin on network tensile strength and failure, we therefore choose the crosslinked actin network as our model system. We also note that while different crosslinker densities result in quantitatively different stress-strain behavior (Figure 5.5), the qualitative strain stiffening and subsequent network failure behavior is similar; we therefore choose to hold the crosslinking density constant using 1:100 biotinylated actin (corresponding to a crosslinker density of 1:200). The resulting delayed strain failure and lower elasticity when lowering the crosslinking density are both expected within an affine model of a crosslinked network (see (2-69) and (2-70)) and are consistent with previous studies on actin networks with varying crosslinking ratios [Tharmann et al., 2007]. The strain

stiffening behavior is consistent with the behavior of a fully percolated network, and is expected until the concentration becomes so low that the network deformation is no longer affine [Gardel et al., 2004a]. The chosen biotin-neutravidin crosslinker, while not biologically occurring, mimics permanent biological crosslinkers well, such as the actin-binding protein scruin [Gardel et al., 2004a] and myosin in the absence of ATP [Tharmann et al., 2007]. Using a constant crosslinking density within the strain stiffening concentration regime allows us to search for relative changes in network behavior upon the addition of basic calponin.

Although the actin networks are not chemically adhered to the rheometer geometries, we interpret the eventual transition from $K' > 0$ to $K' < 0$ as network failure rather than a detachment of the network from the surface. First of all, the transition to failure is gradual even at very low strain rates, which is uncharacteristic of catastrophic and abrupt surface detachments. Secondly, actin networks have been strained to carry shear loads an order of magnitude or more beyond what is applied here without surface detachments [Gardel et al., 2006]; the geometries and rheometer used in this study are identical to the ones used in this previous work. Third, it has been shown previously (again, with the exact same rheometer and geometries as used in this work) that the maximal stress scales roughly linearly with the actin concentration present suggesting that the failure is due to individual actin filaments in the network, rather than bulk

surface detachments [Gardel et al., 2004b; Gardel et al., 2008]. Finally, it is unlikely that the addition of actin-binding proteins would greatly affect non-specific surface attachments of actin networks, resulting in such large changes in maximal stress and strain as seen here and in other published works, suggesting that these changes instead reflect a change in the tensile strength of the networks themselves.

While we see some moderate differences between actin isoforms in this study (Table 5.1), they are much less pronounced than previous studies, which found 10-fold or larger differences in linear moduli between the striated muscle and non-muscle actin isoforms [Allen et al., 1996]. Considering that the previously published study reported the use of entangled actin, rather than fully crosslinked networks as are used here, it is surprising that any significant elasticity is observed, and the reported values of $G' = 10\,\mathrm{Pa}$ or higher likely originate from impurities in the purified actin. As such, the reported differences between actin isoforms cannot be trusted. To avoid any potential complications arising from differences in actin isoforms, however, we choose to only use non-muscle actin from human platelets when investigating actin networks with tropomyosin and basic calponin. Non-muscle actin is chosen over rabbit skeletal actin, as all three calponin isoforms are abundant in smooth- and non-muscle cells. We also note from our investigations of single filament mechanics that

basic calponin binds both skeletal muscle and non-muscle actin and is able to affect the two in a similar fashion (Figure 4.3).

The major effect of adding calponin to crosslinked actin networks is that both the yield strain γ_{max} and the yield stress σ_{max} of the network are increased (Figure 5.8). This shows that calponin can have a direct mechanical effect on actin networks without other binding partners, and suggests that mechanical calponin stabilization of cytoskeletal actin is a purely mechanical effect not relying on other cellular components. This calponin-induced increase in tensile strength occurs even when the actin networks are decorated with tropomyosin, an actin-binding stabilizer prevalent in both muscle and non-muscle cells (Figure 5.8). The fact that calponin can affect both plain actin networks and actin networks decorated with tropomyosin in a similar fashion suggests that calponin can affect not only regions of tropomyosin-free actin in the cell [Geiger et al., 1981; Lin et al., 1988; DesMarais et al., 2002], but also tropomyosin-decorated actin as well.

To understand how calponin strengthens actin networks in this way, we compare our data to an affine network model (Chapter 2.7.3). Within this model, it is expected that a more flexible polymer results in a network with delayed strain stiffening onset and subsequently a higher yield strain γ_{max} (2-70), consistent with our observations. This suggests that our data can be explained within an affine network model simply in terms of a single parameter, the actin

persistence length. We can obtain an estimate of the persistence length change from our bulk rheology data by comparing the strain stiffening onset and G' for networks with and without calponin. From (2-68),

$$G' \sim \frac{{L_p}^2}{{l_c}^3} \tag{5-1}$$

and therefore, using (2-70),

$$\frac{(G')^3}{{\sigma_{\text{crit}}}^3} = \frac{1}{{\gamma_{\text{crit}}}^3} \sim \frac{{L_p}^3}{{l_c}^3} \sim G' L_p \tag{5-2}$$

Thus,

$$L_p \sim \frac{(G')^2}{{\sigma_{\text{crit}}}^3} \sim \frac{1}{G' \gamma_{\text{crit}}} \tag{5-3}$$

This result has previously been used to estimate the persistence length of neurofilaments and intermediate filaments [Lin et al., 2010]. Here, we simply compare the ratios of persistence lengths from our bulk rheological data. Using the measured values for G' (3.2 ± 0.3 Pa for plain actin networks vs. 2.8 ± 0.4 Pa for calponin-decorated actin networks) and γ_{crit} (10 ± 0.6 % for plain actin networks vs. 14.9 ± 1.0 % for calponin-decorated actin networks), we estimate the persistence length with calponin to be 35% of that of plain actin in the bulk rheology. This is in good agreement with the persistence length changes measured directly by fluorescence microscopy of single non-muscle actin

filaments (Figure 4.3) and further demonstrates that within an affine network model, our results are well described by changes of this single parameter.

Although the linear network shear elasticity for networks with calponin is slightly lower, the yield stress σ_{max} is substantially increased (Figure 5.8). In an affine network model, this should follow from the delay in strain stiffening and subsequent increase in yield strain; since it takes filaments longer to strain to their breaking point, more filaments will be engaged at any given bulk strain once the network has been strained past its linear region, resulting in a higher yield stress. To illustrate this point, we use a simple Matlab simulation in which different ensembles of filaments are subjected to an affine strain. It should be emphasized that this does not fully represent an actin network, as no non-linearities or connectivity between elements has been incorporated into the computations. Nonetheless, the outcome agrees well with our experimental data and shows that just changing the filament rigidity results in stress-strain curves very similar to what is seen for calponin-actin networks (Figure 5.11). This suggests that the increase in both γ_{max} and σ_{max} can be explained within an affine network model in terms of just the actin persistence length decrease brought about by calponin.

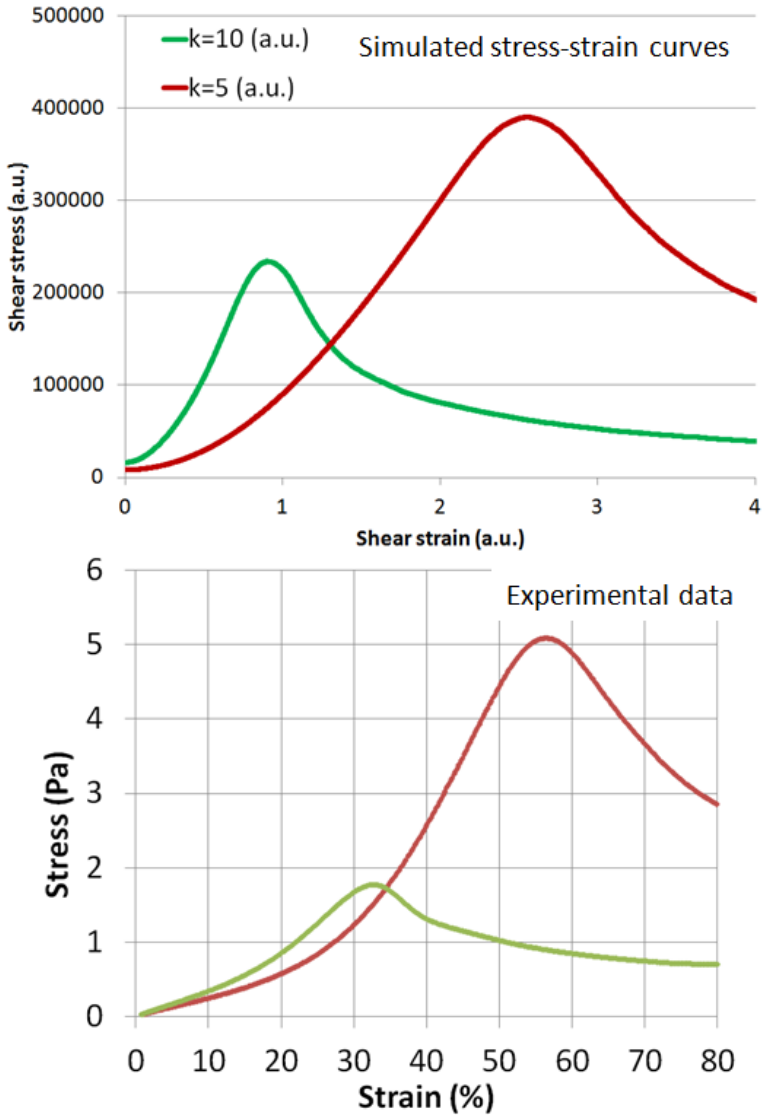

Figure 5.11: Simulated stress-strain curves for a network of linear springs. *Simulated strain ramps of an ensemble of linear springs (top panel) demonstrate that a softer spring network under affine strain results in a higher yield strain as well as a higher yield stress. For comparison, shown are experimental strain ramps (bottom panel) of 0.5 mg/mL HP actin with 1:100 biotin-actin with (red curve) or without (green curve) 2:1 h1CaP.*

In summary, we have shown that calponin, without any additional components or cellular machinery, can induce changes in actin networks

qualitatively identical to those seen in cells and tissues, suggesting that calponin stabilization of actin *in vivo* involves mechanical interactions with calponin alone, rather than multiple binding partners. While the linear stiffness of the networks is decreased, the tensile strength of the networks is increased, exactly as has been seen in smooth muscle tissue when calponin expression is upregulated [Arrigoni et al., 2006]. We propose a model of calponin stabilization of actin network structures *in vivo* in which calponin reduces the flexural rigidity of individual actin filaments [Jensen et al., 2012b], which in turn delays the onset on strain stiffening and increases the yield strain and stress of the network. This model captures all the qualitative behavior seen in cells and tissue and relies on only a single physical parameter, the filament persistence length, in explaining the network properties within an affine network model.

6 Summary and Future Directions

While much of biology can be studied and understood from the vantage point of cell systems and organisms of higher levels of complexity, gaining a detailed understanding of the physical mechanisms through which proteins and other cellular components function is often difficult in such complicated systems. In this work, we utilize an *in vitro* approach to characterize the mechanistic properties of two actin-binding proteins, caldesmon and calponin. Both these proteins are thought to be involved in regulation of cytoskeletal actin in the cell, but their exact function and mechanism remains unknown. This work helps elucidate both aspects of these proteins.

In Chapter 3, we demonstrate that the C-terminal fragment of caldesmon, H32K, stabilizes a transient state of F-actin, termed the nascent state. We show by TIRF microscopy that this nascent state has the same polymerization properties as caldesmon-free actin, and show by confocal fluorescence microscopy that caldesmon regulation of the actin state can function as a novel mechanism for tuning the affinity for actin of the branching and nucleating complex Arp2/3. Because of caldesmon's proximity to Arp2/3 complex at the leading edge of motile cells, this suggests a previously unknown mechanism for transiently targeting Arp2/3 complex to certain actin filaments during cell motility, and is the first direct observation of a functional effect of the nascent actin state. However, the nascent state remains largely unexplored; naturally,

actual structural information would be hugely illuminating, but may be difficult to obtain due to the highly transient nature of nascent actin. While H32K stabilizes the nascent state, it is very unlikely that the negative stain electron micrographs of nascent actin (Figure 3.2) actually represents direct structural information that can be extracted from a reconstruction algorithm. However, it is worth noting that other electron microscopy reconstructions have suggested the coexistence of several actin states within plain F-actin (e.g., [Galkin et al., 2010]); whether these relate directly to the nascent actin state remains to be seen. Furthermore, due to the fact that the notion of nascent actin is relatively new in the field, many potential effects on other actin-binding complexes and proteins are yet to be explored. As caldesmon stabilizes the transient nascent state, it could help facilitate studies on other interactions, similar to the studies presented here on Arp2/3 complex. Finally, this study suggests a different way of understanding actin-binding protein regulation; rather than actin-binding partners competing sterically for binding sites and thereby regulating which proteins bind to the filament, H32K regulates Arp2/3 affinity indirectly by altering the structural state of actin itself. The possibility that other actin-binding proteins could affect the lifetime of the actin nascent state and thereby regulate the accessibility of actin to other binding partners is as yet unexplored as well.

In Chapter 4, we characterize the mechanical effects of calponin on single actin filaments as a first step towards explaining the growing body of work pointing to calponin as an actin stabilizing protein in the cell. We find that calponin reduces the flexural rigidity of F-actin, likely through interactions with actin subdomain 2, a malleable part of F-actin previously proposed to be involved in tuning actin rigidity. To explore how this mechanical change affects a system a bit more like the cellular actin cytoskeleton, we use bulk rheology to characterize crosslinked actin networks with calponin and tropomyosin in Chapter 5. We find that calponin increases the tensile strength of the networks, increasing both the maximal strain and stress that the networks can withstand, and that this effect is present even when actin is decorated with tropomyosin. This behavior is highly similar to the effects of calponin seen in cells and tissues. Examination of the stress-strain behavior shows a behavior consistent with an affine network of more flexible polymers. Using simple physical arguments and previously published theoretical work, we argue that the increased tensile strength can be explained purely by calponin reducing the actin persistence length, making the network more compliant. This offers a simple model for how calponin can stabilize cytoskeletal actin networks under external strain *in vivo* in terms of a single parameter, the actin persistence length. While a strength of this model is the simplicity with which it captures the qualitative behavior observed *in vito*, it is unclear whether other mechanical properties of calponin-actin, such

as the filament torsional rigidity might play a role in a more fine-grained model; fluorescence anisotropy decay measurements can provide direct measurements of this mechanical parameter and could help put the understanding of the effects of calponin on single filament mechanics in better context with other binding proteins, such as cofilin, which drastically changes both flexural and torsional rigidity [Prochniewicz et al., 2005].

The model system of crosslinked actin can undergo further refinement to more closely resemble the cellular cytoskeleton. The system allows for dissemination of each component to better understand its effects, before adding in more complexity in a piecemeal fashion. While the crosslinkers used in this work are non-biological, they mimic biological permanent crosslinkers in terms of network rheological properties; however, using transient crosslinkers which allow the network to relax through continued binding and unbinding, such as filamin [Stossel et al., 2001], could add further complexity and possibly reveal new emergent behavior of calponin in actin networks more relevant to cellular function [Gardel et al., 2006; Kasza et al., 2009]. Perhaps most interestingly could be the addition of ATP-consuming actin-binding proteins (i.e., myosin motors), which not only walk along the actin filaments in the case of processive myosins such as myosin V, but form transient crossbridges through rapid binding and unbinding and greatly affect the mechanics of the network by adding additional energy to the network and increasing the fluctuations of the actin filaments

beyond thermal fluctuations [Brangwynne et al., 2008a; Brangwynne et al., 2008b; Koenderink et al., 2009].

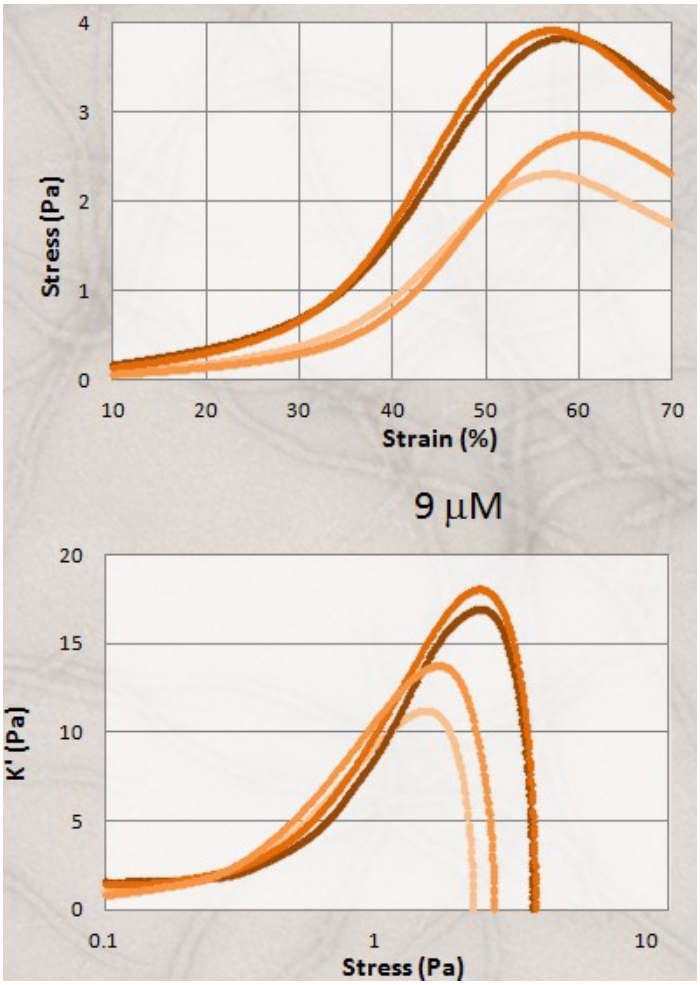

Figure 6.1: Strain ramps of actin-vimentin networks.
Actin concentration for the shown strain ramps is 9 μM with 1:100 biotin-actin. Vimentin concentrations are 0 μM (lightest color), 0.3 μM, 1.5 μM, and 3 μM (darkest color). The curves have been smoothed in Matlab.

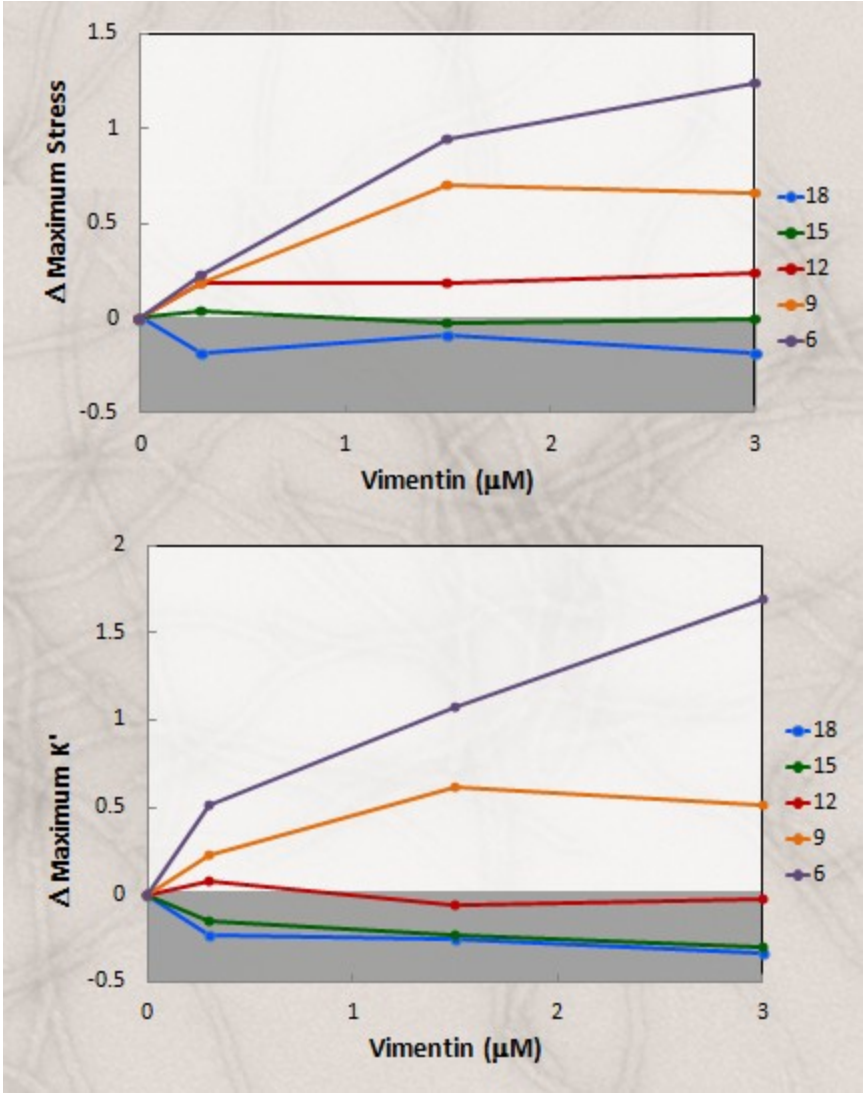

Figure 6.2: Differential effects of vimentin on crosslinked actin networks.
Actin concentrations range from 6 μM to 18 μM as indicated on the right of both panels. Yield stress and maximal differential modulus are determined from strain ramps as shown in Figure 6.1. The ordinate axes show the change relative to vimentin-free networks, with 0 representing no change and 1 representing a 100% increase. At low actin concentrations, vimentin increases both the maximal elasticity and the yield stress, while it has the reverse effect at high actin concentrations.

One such example of emergent behavior is seen by adding the intermediate filament vimentin to actin networks similar to those used in

Chapter 5. An example of the effect of vimentin on the stress-strain behavior of actin networks is shown in figure (Figure 6.1) for actin at 9 μM. Adding vimentin to such a dilute actin networks increases both the tensile strength and maximal stiffness of the network; in contrast, adding vimentin to an actin network of higher concentration reduces both the tensile strength and maximal stiffness of the composite network, as summarized in Figure 6.2. Thus, vimentin can have two very different effects on the mechanics of the network, depending solely on the actin concentration. The crossover between these two behaviors when varying the actin concentration occurs roughly when the actin mesh size becomes comparable to the distance between biotinylated actin monomers (see Table 6.1).

Actin concentration	*Mesh size*
6 μM	0.45 μm
9 μM	0.37 μm
12 μM	0.32 μm
15 μM	0.28 μm
18 μM	0.26 μm

Table 6.1: Mesh sizes of actin networks of various concentrations.
All mesh sizes are calculated from (2-63). For comparison, the average distance between biotinylated actin monomers is 0.27 μm. The crossover in mechanical behavior when vimentin is added to the networks (Figure 6.2) occurs when $\xi \sim l_c$.

Since these biotins are fixed in place along the actin filament on average 0.27 μm apart for a 1:100 biotin-actin:actin ratio [Huxley & Brown, 1967], the filaments need to explore space in order to find a crosslinking partner. At 6 μM actin there

is an excess of crosslinkers available; however, as the available crosslinkers become saturated, adding vimentin to the network sterically disrupts the thermal fluctuations of actin and effectively lowers the crosslinking density, thus lowering the tensile strength of the network. This hypothesis is currently being explored experimentally in collaboration with the laboratory of David A. Weitz at Harvard University by producing networks with fully formed biotin-neutravidin crosslinkers before letting the vimentin polymerize. It is a further example of how *in vitro* model systems such as those discussed in this work can yield physical insight into the emergent behavior of complex biological systems.

Appendices

A. Flexural rigidity Matlab code

```
% FlexRig
% Mikkel Herholdt Jensen, July 2010
%
% OVERVIEW:
% Program for determining the flexural rigidity of a polymer from a time
% sequence of polymer skeletons using the cosine correlation function.
% The program first takes the input from ImageJ and sorts all pixels in
% each frame sequentially.
% The skeletons are then parameterized in terms of an angle and its
% corresponding arc length.
% Finally, the temporal mean of the cosine of the difference in angle is
% computed as a function of arc length.
%
% INSTRUCTIONS:
% Place the program in the same folder as a .txt file containing the x-y
% coordinates of pixels in the following tab-delimited format:
% Column 1 - x coordinates
% Column 2 - y coordinates
% Column 3 - frame number
% (This is the standard output of ImageJ saving x-y coordinates.)
% Make sure each frame has exactly one object in it, and that each pixel
% has only one neighbor (no spurs in the skeleton)
% Set the user parameters and run the program.
%
% OUTPUT:
% The array "Meancos" contains the arc length (column 1) and the mean of
% the cosine of the angle change (column 2) or its logarithm (column 3),
% from which the persistence length can be determined.



% USER PARAMETERS
filename = '0;1 mov1-skel.txt'; %file containing x-y coordinates
zoomfactor = 5; %post-acquisition magnification
pixelwidth = 640; %width of the image (pixels)
pixsize = (pixelwidth * zoomfactor) / 88.48; %width of the images (microns)
range = 10; %the number of pixels the parameterization algorithm will look forward when
creating line segments



% READING ORIGINAL DATA FILE FROM IMAGEJ
disp('Reading x-y coordinates...')
Data = dlmread(filename,'\t');
Data(:,4) = [];
datasize = size(Data);
frametotal = Data(datasize(1),3);



% COUNTING NEIGHBORING PIXELS FOR EACH PIXEL IN THE DATA SET
frame = 0;
datarow = 1;
frametrack = 1;
disp('Counting neighbors of each pixel...')
disp('(If I get stuck, there is probably a frame with no pixels in it.)')
while(frame <= frametotal)
    disp(frame)
    while(true) %finding the first row of the current frame in "Data" array
        if(Data(frametrack,3) < frame)
```

```
            frametrack = frametrack + 1;
        elseif(Data(frametrack,3) == frame)
            framestart = frametrack;
            break
        end
        if(frametrack > datasize(1))
            break
        end
    end

    n = frametrack;
    while(true) %finding the last row of the current frame in "Data" array
        if(n > datasize(1))
            frameend = n - 1;
            break
        elseif(Data(n,3) ~= frame)
            frameend = n - 1;
            break
        elseif(Data(n,3) == frame)
            n = n + 1;
        end
    end

    while(datarow <= datasize(1) && frame == Data(datarow,3)) %doing the actual counting
of neighboring pixels
        neighbors = 0;
        x = Data(datarow,1);
        y = Data(datarow,2);
        m = framestart;
        while(m <= frameend)
            if(Data(m,3)==frame && Data(m,1)==x-1 && Data(m,2)==y-1)
                neighbors = neighbors + 1;
            elseif(Data(m,3)==frame && Data(m,1)==x && Data(m,2)==y-1)
                neighbors = neighbors + 1;
            elseif(Data(m,3)==frame && Data(m,1)==x+1 && Data(m,2)==y-1)
                neighbors = neighbors + 1;
            elseif(Data(m,3)==frame && Data(m,1)==x-1 && Data(m,2)==y)
                neighbors = neighbors + 1;
            elseif(Data(m,3)==frame && Data(m,1)==x+1 && Data(m,2)==y)
                neighbors = neighbors + 1;
            elseif(Data(m,3)==frame && Data(m,1)==x-1 && Data(m,2)==y+1)
                neighbors = neighbors + 1;
            elseif(Data(m,3)==frame && Data(m,1)==x && Data(m,2)==y+1)
                neighbors = neighbors + 1;
            elseif(Data(m,3)==frame && Data(m,1)==x+1 && Data(m,2)==y+1)
                neighbors = neighbors + 1;
            else
            end
            if(neighbors >= 3)
                disp('WARNING!!!  A pixel with 3 or more neighbors was found!')
                disp(frame)
            else
            end
            m = m + 1;
        end
        Data(datarow,4) = neighbors;
        datarow = datarow + 1;
    end
    frame = frame + 1;
end


% SORTING PIXELS SEQUENTIALLY FOR EACH FRAME TO BUILD A FILAMENT
disp('Sorting pixels by connectivity...')
disp('(If I get stuck, there is probably a frame with two separate objects in it.)')
DataTemp = Data;
```

```
frame = DataTemp(1,3);
disp(frame)
datarow = 1;
endpixelfound = 0;
while(endpixelfound == 0) %seeding DataSort, the sorted data array, with the first end
pixel of frame 0
    if(frame == DataTemp(datarow,3))
        if(DataTemp(datarow,4) == 1)
            DataSort(1,1) = DataTemp(datarow,1);
            DataSort(1,2) = DataTemp(datarow,2);
            DataSort(1,3) = DataTemp(datarow,3);
            DataTemp(datarow,:) = [];
            endpixelfound = 1;
            ds = 1;
        else
            datarow = datarow + 1;
        end
    else
    end
end

while(frame <= frametotal) %populating the rest of DataSort
    while(frame == DataTemp(1,3)) %building a filament once an end pixel is found
        ds = size(DataSort);
        x = DataSort(ds(1),1);
        y = DataSort(ds(1),2);
        m = 1;
        datatempsize = size(DataTemp);
        foundpixel = 0;
        while(foundpixel == 0 && m <= datatempsize(1))
            if(DataTemp(m,3)==frame && DataTemp(m,1)==x-1 && DataTemp(m,2)==y-1)
                DataSort(ds(1)+1,1) = DataTemp(m,1);
                DataSort(ds(1)+1,2) = DataTemp(m,2);
                DataSort(ds(1)+1,3) = DataTemp(m,3);
                DataTemp(m,:) = [];
                foundpixel = 1;
            elseif(DataTemp(m,3)==frame && DataTemp(m,1)==x && DataTemp(m,2)==y-1)
                DataSort(ds(1)+1,1) = DataTemp(m,1);
                DataSort(ds(1)+1,2) = DataTemp(m,2);
                DataSort(ds(1)+1,3) = DataTemp(m,3);
                DataTemp(m,:) = [];
                foundpixel = 1;
            elseif(DataTemp(m,3)==frame && DataTemp(m,1)==x+1 && DataTemp(m,2)==y-1)
                DataSort(ds(1)+1,1) = DataTemp(m,1);
                DataSort(ds(1)+1,2) = DataTemp(m,2);
                DataSort(ds(1)+1,3) = DataTemp(m,3);
                DataTemp(m,:) = [];
                foundpixel = 1;
            elseif(DataTemp(m,3)==frame && DataTemp(m,1)==x-1 && DataTemp(m,2)==y)
                DataSort(ds(1)+1,1) = DataTemp(m,1);
                DataSort(ds(1)+1,2) = DataTemp(m,2);
                DataSort(ds(1)+1,3) = DataTemp(m,3);
                DataTemp(m,:) = [];
                foundpixel = 1;
            elseif(DataTemp(m,3)==frame && DataTemp(m,1)==x+1 && DataTemp(m,2)==y)
                DataSort(ds(1)+1,1) = DataTemp(m,1);
                DataSort(ds(1)+1,2) = DataTemp(m,2);
                DataSort(ds(1)+1,3) = DataTemp(m,3);
                DataTemp(m,:) = [];
                foundpixel = 1;
            elseif(DataTemp(m,3)==frame && DataTemp(m,1)==x-1 && DataTemp(m,2)==y+1)
                DataSort(ds(1)+1,1) = DataTemp(m,1);
                DataSort(ds(1)+1,2) = DataTemp(m,2);
                DataSort(ds(1)+1,3) = DataTemp(m,3);
                DataTemp(m,:) = [];
                foundpixel = 1;
            elseif(DataTemp(m,3)==frame && DataTemp(m,1)==x && DataTemp(m,2)==y+1)
```

```
                DataSort(ds(1)+1,1) = DataTemp(m,1);
                DataSort(ds(1)+1,2) = DataTemp(m,2);
                DataSort(ds(1)+1,3) = DataTemp(m,3);
                DataTemp(m,:) = [];
                foundpixel = 1;
            elseif(DataTemp(m,3)==frame && DataTemp(m,1)==x+1 && DataTemp(m,2)==y+1)
                DataSort(ds(1)+1,1) = DataTemp(m,1);
                DataSort(ds(1)+1,2) = DataTemp(m,2);
                DataSort(ds(1)+1,3) = DataTemp(m,3);
                DataTemp(m,:) = [];
                foundpixel = 1;
            else
            end
            m = m + 1;
            datatempsize = size(DataTemp);
        end
        if(datatempsize(1)==0)
            break;
        end
    end
    if(datatempsize(1)==0)
        break;
    end

    frame = frame + 1; %finding an end pixel of the filament in the next frame
    disp(frame)
    if(frame <= frametotal)
        ds = size(DataSort);
        datarow = 1;
        endpixelfound = 0;
        while(endpixelfound == 0)
            if(frame ~= DataTemp(datarow,3))
                frame = frame + 1;
            elseif(DataTemp(datarow,4) == 1)
                DataSort(ds(1)+1,1) = DataTemp(datarow,1);
                DataSort(ds(1)+1,2) = DataTemp(datarow,2);
                DataSort(ds(1)+1,3) = DataTemp(datarow,3);
                DataTemp(datarow,:) = [];
                endpixelfound = 1;
            else
                datarow = datarow + 1;
            end
        end
    else
    end
end



% DETERMINING THE LENGTH OF EACH FILAMENT IN A FRAME (1-PIXEL ADDITION)
dimcheck = (pixelwidth * zoomfactor) / pixsize;
disp('Image dimension check!')
disp('Your original image has a width of (pixels):')
disp(pixelwidth)
disp('Your original picture x-dimension is (microns):')
disp(dimcheck)
disp('Your original image is magnified by a factor of:')
disp(zoomfactor)
frame = 0;
datarow = 1;
ds = size(DataSort);
frametotal = DataSort(ds(1),3);
L = 0;
while(frame <= frametotal)
    while(frame == DataSort(datarow,3) && datarow+1 <= ds(1))
        if(frame == DataSort(datarow+1,3))
```

```
            L = L + sqrt(((DataSort(datarow+1,1)-DataSort(datarow,1))/pixsize)^2 +
((DataSort(datarow+1,2)-DataSort(datarow,2))/pixsize)^2);
            datarow = datarow + 1;
        else
            datarow = datarow + 1;
        end
    end
    Lengths(frame+1,1) = frame;
    Lengths(frame+1,2) = L;
    frame = frame + 1;
    L = 0;
end



% PARAMETRIZING CURVE SHAPE IN TERMS OF ANGLE AND ARC LENGTH
disp('Parametrization segment length:')
disp(range)
disp('Parameterizing the skeletons in terms of angle and arc length...')
DataTemp = DataSort;
m = 1;
frame = 0;
while(frame <= frametotal)
    datatempsize = size(DataTemp);
    while(datatempsize(1) > range && frame == DataTemp(1,3))
        if(frame == DataTemp(1+range,3))
            dx = DataTemp(1+range,1) - DataTemp(1,1);
            dy = DataTemp(1+range,2) - DataTemp(1,2);
            %finding the angle theta
            if(dx > 0)
                theta = atan(dy/dx);
            elseif(dx == 0 && dy >0)
                theta = pi/2;
            elseif(dx == 0 && dy <0)
                theta = -pi/2;
            elseif(dx < 0 && dy > 0)
                theta = atan(dy/dx) + pi;
            elseif(dx < 0 && dy < 0)
                theta = atan(dy/dx) - pi;
            elseif(dy == 0 && dx < 0)
                theta = pi;
            else
                disp('WARNING!!!  A theta is undefined!')
            end
            %finding the segment length and writing it and theta to the array Param
            deltaS = sqrt((dx/pixsize)^2 + (dy/pixsize)^2);
            Param(m,1) = frame;
            Param(m,2) = theta;
            Param(m,3) = deltaS;
            n = 1;
            while(n <= range) %removing the procesed segment from DataTemp
                DataTemp(1,:) = [];
                n = n + 1;
            end
            m = m + 1;
        else
            n = 1;
            while(n <= range && frame == DataTemp(1,3))
                DataTemp(1,:) = [];
                n = n + 1;
            end
        end
        datatempsize = size(DataTemp);
    end
    frame = frame + 1;
end
```

```
% REARRANGING THE ARRAY "PARAM" TO GET THETA(S) IN NEW ARRAY
disp('Calculating <Cos(theta)>...')
ds = 0.05; %data point separation in microns
paramsize = size(Param);
frametotal = Param(paramsize(1),1);
currentframe = 0;
n = 1;
while(currentframe <= frametotal) %adding arc length to the fourth column of the Param
array
    arclength = 0;
    while(currentframe == Param(n,1))
        arclength = arclength + Param(n,3);
        Param(n,4) = arclength;
        n = n + 1;
        if(n > paramsize(1))
            break
        end
    end
    currentframe = currentframe + 1;
end



% BUILDING NEW ARRAY "ARCPARAM" OF COS(DELTA THETA) VS ARC LENGTH
m = 1;
currentframe = 0;
n = 1;
while(currentframe == Param(n,1))
    s = 0;
    theta0 = Param(n,2);
    while(currentframe == Param(n,1))
        if(s < Param(n,4) - Param(n,3)/2)
            Arcparam(m,1) = currentframe;
            Arcparam(m,2) = s;
            Arcparam(m,3) = cos(abs(theta0 - Param(n,2)));
            s = s + ds;
            m = m + 1;
        else
            n = n + 1;
        end
        if(n > paramsize(1))
            break
        end
    end
    if(n > paramsize(1))
        break
    else
        currentframe = currentframe + 1;
    end
end



% CALCULATING <COS(THETA)> AND WRITING TO "MEANCOS"
arcparamsize = size(Arcparam);
p = 1;
s = 0;

while(true)
    counter = 0;
    m = 1;
    n = 1;
    while(true)
        if(Arcparam(n,2) == s)
            Temp(m,1) = Arcparam(n,3);
```

```
            counter = counter + 1;
            m = m + 1;
        end
        n = n + 1;
        if(n > arcparamsize(1))
            break
        end
    end
    if(counter == 0)
        break
    else
        Meancos(p,1) = s;
        Meancos(p,2) = mean(Temp(:,1));
        Meancos(p,3) = log(mean(Temp(:,1)));
        Meancos(p,4) = counter;
        p = p + 1;
        s = s + ds;
        Temp = [];
    end
end

disp('Done!  The array "Meancos" contains
[s,<cosDeltaTheta>,ln<cosDeltaTheta>,framecount]')
```

B. Arp2/3 branch simulation Matlab code

```
% BranchingMonteCarlo
% Mikkel Herholdt Jensen, May 2012
%
% OVERVIEW:
% Program for simulating Arp2/3-induced branch locations on actin
% filaments in the absence of branching cooperativity
%
% INSTRUCTIONS:
% Indicate the lengths of individual actin filaments on which branches
% can occur in a .txt file (one filament per line).  Run the code after
% setting the user parameters, making sure it is in the same library as
% the .txt file containing the actin filament lengths.
%
% OUTPUT:
% 1. 'branches per filament.txt' contains the percentage of filaments with
%    0 (row 1), 1 (row 2), etc. branches, indicated in column 1.
%    Column 2 contains the standard deviation between runs.
% 2. 'distance between branches.txt' contains the percentage of neighboring
%    branches (column 2) binned by distance between branches (column 1).
% 3. 'distance from barbed.txt' contains the percentage of branches
%    (column 2) binned by their distance to the mother filament barbed end
%    (column 1).



% USER PARAMETERS
lengthfile = 'LengthsNascent.txt'; %text file containing filament lengths
branches = 280; %number of branches to be simulated
runs = 100000; %number of times the simulation will be run
binsize = 1; %bin size of histogram of distance between branches



% READING DATA FILE OF ACTIN LENGTHS
Filaments = dlmread(lengthfile,'\t');
datasize = size(Filaments);
totallength = sum(Filaments(:,1));
n = 1;
length = 0;
while(n <= datasize(1))
    Filaments(n,2) = length;
    Filaments(n,3) = length + Filaments(n,1);
    length = length + Filaments(n,1);
    n = n+1;
end



% SIMULATING BRANCH LOCATIONS ON THE ACTIN FILAMENTS
Branchcount = zeros(datasize(1),runs);
currentrun = 1;
neighborcount = 1;
barbedcount = 1;
disp('Now running Monte Carlo Simulation.  Iteration:')
while(currentrun <= runs)
    % Generating branch locations
    Locations = rand(branches,1)*totallength;
    Locations = sort(Locations);

    % Counting number of branches per filament
    n = 1;
    m = 1;
    while(n <= branches)
        if(Locations(n,1) <= Filaments(m,3))
```

```
            Branchcount(m,currentrun) = Branchcount(m,currentrun) +1;
            n = n+1;
        else
            m = m+1;
        end
    end

    % Measuring distance between neighboring branches
    n = 1;
    m = 1;
    while(n <= datasize(1))
        if(Branchcount(n,currentrun) >= 2)
            filamentends = [Filaments(n,2),Filaments(n,3)];
            while(Locations(m,1) < filamentends(1))
                m = m+1;
            end
            while(m+1 <= branches && Locations(m+1,1) < filamentends(2))
                Neighbors(neighborcount,1) = Locations(m+1,1)-Locations(m,1);
                neighborcount = neighborcount+1;
                m = m+1;
            end
        end
        n = n+1;
    end

    % Measuring distance to barbed ends
    n = 1;
    m = 1;
    while(n <= datasize(1))
        if(Branchcount(n,currentrun) >= 1)
            filamentends = [Filaments(n,2),Filaments(n,3)];
            while(Locations(m,1) < filamentends(1))
                m = m+1;
            end
            while(m <= branches && Locations(m,1) < filamentends(2))
                Barbedenddistance(barbedcount,1) = filamentends(2) - Locations(m,1);
                barbedcount = barbedcount+1;
                m = m+1;
            end
        end
        n = n+1;
    end

    % Incrementing run number and outputting the current run
    currentrun = currentrun + 1;
    disp(currentrun)
end



% ANALYZING THE SIMULATED BRANCHES PER FILAMENT
% Counting filaments with n branches for each simulation run
disp('Now analyzing the simulated branches per filament...')
maxbranch = max(max(Branchcount));
Branchesperfilament = zeros(maxbranch+1,runs);
n = 0;
while(n <= maxbranch)
    Branchesperfilament(n+1,:) = sum(Branchcount == n);
    n = n+1;
end
% Calculating mean and st. dev. of branches per filament in percent
Statsbpf = zeros(maxbranch+1,2);
Statsbpf(:,1) = mean(Branchesperfilament,2)/datasize(1)*100;
Statsbpf(:,2) = std(Branchesperfilament,1,2)/datasize(1)*100;
```

```
% ANALYZING THE SIMULATED DISTANCE BETWEEN BRANCHES
disp('Now analyzing the distance between simulated neighboring branches...')
% Analyzing distance between neighbor branches
totalneighbors = size(Neighbors,1);
Neighbors = sort(Neighbors);
n = 1;
bincount = 0;
currentbin = binsize;
binnumber = 1;
while(n <= totalneighbors)
    if(Neighbors(n,1) < currentbin)
        bincount = bincount + 1;
        n = n+1;
    else
        Statsdbb(binnumber,2) = bincount/totalneighbors*100;
        Statsdbb(binnumber,1) = currentbin;
        currentbin = currentbin + binsize;
        binnumber = binnumber + 1;
        bincount = 0;
    end
end
Statsdbb(binnumber,2) = bincount/totalneighbors*100;
Statsdbb(binnumber,1) = currentbin;

%Analyzing distance to mother filament barbed end
totalbarbed = size(Barbedenddistance,1);
Barbedenddistance = sort(Barbedenddistance);
n = 1;
bincount = 0;
currentbin = binsize;
binnumber = 1;
while(n <= totalbarbed)
    if(Barbedenddistance(n,1) < currentbin)
        bincount = bincount + 1;
        n = n+1;
    else
        Statsbarbed(binnumber,2) = bincount/totalbarbed*100;
        Statsbarbed(binnumber,1) = currentbin;
        currentbin = currentbin + binsize;
        binnumber = binnumber + 1;
        bincount = 0;
    end
end
Statsbarbed(binnumber,2) = bincount/totalbarbed*100;
Statsbarbed(binnumber,1) = currentbin;



% WRITING RESULTS TO FILES
disp('Now writing data to files...')
dlmwrite('branches per filament.txt',Statsbpf,'\t');
dlmwrite('distance between branches.txt',Statsdbb,'\t');
dlmwrite('distance from barbed.txt',Statsbarbed,'\t');
       disp('Done!')
```

C. Network strain simulation Matlab code

```
% NetworkStrain
% Mikkel Herholdt Jensen, December 2012
%
% OVERVIEW:
% Program for simulating an affine strain of an isotropic network of
% linear springs, each with a delayed stiffening onset.
%
% INSTRUCTIONS:
% Indicate the length at which the springs engage, the maximal length of
% each spring before it breaks, the stiffness of each spring, and the
% total number of springs to be simulated.  Also, indicate the starting
% end-to-end length of each spring.  The program will strain the network
% in the selected increments until the indicated maximal strain.
%
% OUTPUT:
% The array 'StressStrain' contains the shear strain (row 1) and
% shear stress (row 2) of the network.



% USER PARAMETERS
Li = 1; %mean initial end-to-end length of springs
Lsigma = 0 %standard deviation of Li distributions
Lk = 1; %between 0 and Lk, the springs have elasticity 0
Lf = 3 %between Lk and Lf, the springs have elasticity k
k = 5; %spring constant
N = 100000; %number of springs in the network
dx = 0.0010; %incremental strain applied between each iteration
maxstrain = 8; %the maximal strain for which shear stress is calculated



% BUILDING A SET OF ISOTROPICALLY DISTRIBUTED SPRINGS
disp('Now generating randomly orienting springs...')
n = 1;
% Generating spring angles
Theta = rand(N,1)*2*pi-pi;
Phi = rand(N,1)*pi;
disp('Now calculating cartesian coordinates of each spring:')
while(n <= N)
    R = normrnd(Li,Lsigma);
    SpringCoords(n,1) = R * cos(Phi(n,1)) * cos(Theta(n,1));
    SpringCoords(n,2) = R * cos(Phi(n,1)) * sin(Theta(n,1));
    SpringCoords(n,3) = R * sin(Phi(n,1));
    SpringCoords(n,4) = sqrt(SpringCoords(n,1)^2 + SpringCoords(n,2)^2 +
SpringCoords(n,3)^2);
    n = n + 1;
    disp(n)
end



% AFFINELY STRAINING THE NETWORK
disp('Now straining the network.  Current shear strain:')
strain = 0;
straincount = 1;
n = 1;
while(strain <= maxstrain)
    % Straining every spring x-component in the network by dx*z
    disp(strain)
    n = 1;
    while(n <= N)
        SpringCoords(n,1) = SpringCoords(n,1) + (dx * SpringCoords(n,3));
```

```
        SpringCoords(n,4) = sqrt(SpringCoords(n,1)^2 + SpringCoords(n,2)^2 +
SpringCoords(n,3)^2);
        n = n+1;
    end
    strain = strain + dx;
    StrainStress(straincount,1) = strain;

    % Calculating the corresponding shear stress
    stress = 0;
    n = 1;
    while(n <= N)
        if(SpringCoords(n,4) <= Lf && SpringCoords(n,4) >= Lk)
            F = k * (SpringCoords(n,4) - Lk);
            stress = stress + F * cos(atan(SpringCoords(n,2)/SpringCoords(n,1))) *
cos(asin(SpringCoords(n,3)/SpringCoords(n,4)));
        end
        n = n + 1;
    end
    StrainStress(straincount,2) = stress;
    straincount = straincount + 1;
end
disp('Done!')
```

REFERENCES

Allen PG, Shuster CB, Käs J, Chaponnier C, Janmey PA, Herman IM. (1996) *Phalloidin Binding and Rheological Differences Among Actin Isoforms*. Biochemistry **35**(45): 14062-14069.

Amann KJ, Pollard TD. (2001) *Direct Real-Time Observation of Actin Filament Branching Mediated by Arp2/3 Complex Using Total Internal Reflection Fluorescence Microscopy*. Proceedings of the National Academy of Sciences **98**(26): 15009-15013.

Andrianantoandro E, Pollard TD. (2006) *Mechanism of Actin Filament Turnover by Severing and Nucleation at Different Concentrations of ADF/Cofilin*. Molecular Cell **24**(1): 13-23.

Appel S, Allen PG, Vetterkind S, Jin J-P, Morgan KG. (2010) *h3/Acidic Calponin: an Actin-Binding Protein that Controls Extracellular Signal-Regulated Kinase 1/2 Activity in Nonmuscle Cells*. Molecular Biology of the Cell **21**(8): 1409-1422.

Arias, M-P, Pacaud M. (2001) *Macrophage Caldesmon is an Actin Bundling Protein*. Biochemistry **40**(43): 12974-12982.

Arrigoni C, Camozzi D, Imberti B, Mantero S, Remuzzi A. (2006) *The Effect of Sodium Ascorbate on the Mechanical Properties of Hyaluronan-Based Vascular Constructs*. Biomaterials **27**(4): 623-630.

Ayscough KR. (1998) *In Vivo Functions of Actin-Binding Proteins*. Current Opinion in Cell Biology **10**(1): 102-111.

Bednar Jan, Furrer P, Katritch V, Stasiak A, Dubochet J, Stasiak A. (1995) *Determination of DNA Persistence Length by Cryo-Electron Microscopy. Separation of the Static and Dynamic Contributions to the Apparent Persistence Length of DNA*. Journal of Molecular Biology **254**(4): 579-594.

Boczkowska M, Rebowski G, Petoukhov MV, Hayes DB, Svergun DI, Dominguez R. (2008) *X-Ray Scattering Study of Activated Arp2/3 Complex with Bound Actin-WCA*. Structure **16**(5): 695-704.

Brangwynne CP, Koenderink GH, Barry E, Dogic Z, MacKintosh FC, Weitz DA. (2007) *Bending Dynamics of Fluctuating Biopolymers Probed by Automated High-Resolution Filament Tracking*. Biophysical Journal **93**(1): 346-359.

Brangwynne CP, Koenderink GH, MacKintosh FC, Weitz DA. (2008a) *Cytoplasmic Diffusion: Molecular Motors Mix it Up*. The Journal of Cell Biology **183**(4): 583-587.

Brangwynne CP, Koenderink GH, MacKintosh FC, Weitz DA. (2008b) *Nonequilibrium Microtubule Fluctuations in a Model Cytoskeleton*. Physical Review Letters **100**(11): 118104.

Breitsprecher D, Kiesewetter AK, Linkner J, Faix J. *Analysis of Actin Assembly by In Vitro TIRF Microscopy*. (2009) Methods in Molecular Biology **571**: 401-415.

Bremer A, Aebi U. (1992) *The Structure of the F-Actin Filament and the Actin Molecule*. Current Opinion in Cell Biology **4**(1): 20-26.

Bremer A, Henn C, Goldie KN, Engel A, Smith PR, Aebi U. (1994) *Towards Atomic Interpretation of F-Actin Filament Three-Dimensional Reconstructions*. Journal of Molecular Biology **242**(5): 683-700.

Bretscher A, Lynch W. (1985) *Identification and Localization of Immunoreactive Forms of Caldesmon in Smooth and Nonmuscle Cells: a Comparison with the Distributions of Tropomyosin and α-Actinin*. Journal of Cell Biology **100**: 1656–1663.

Bretscher A. (1984) *Smooth Muscle Caldesmon. Rapid Purification and F-Actin Cross-Linking Properties*. Journal of Biological Chemistry **259**(20): 12873-12880.

Bryan KE, Rubenstein PA. (2005) *An Intermediate Form of ADP-F-Actin*. Journal of Biological Chemistry **280**(2): 1696-1703.

Carlier M-F, Pantaloni D. (1988) *Binding of Phosphate to F-ADP-Actin and Role of F-ADP-Pi-Actin in ATP-Actin Polymerization*. Journal of Biological Chemistry **263**(2): 817-825.

Carlier M-F. (1987) *Measurement of P_i Dissociation from Actin Filaments Following ATP Hydrolysis Using a Linked Enzyme Assay*. Biochemical and Biophysical Research Communications **143**(3): 1069-1075.

Chalovich JM, Cornelius P, Benson CE. (1987) *Caldesmon Inhibits Skeletal Actomyosin Subfragment-1 ATPase Activity and the Binding of Myosin Subfragment-1 to Actin*. Journal of Biological Chemistry **262**(12): 5711-5716.

Chalovich JM. (1988) *Caldesmon and Thin-Filament Regulation of Muscle Contraction*. Cell Biochemistry and Biophysics **12**(1): 73-85.

Chaponnier C, Goethals M, Janmey PA, Gabbiani F, Gabbiani G, Vandekerckhove J. (1995) *The Specific NH2-Terminal Sequence Ac-EEED of Alpha-Smooth Muscle Actin Plays a Role in Polymerization In Vitro and In Vivo.* Journal of Cell Biology **130**(4): 887-895.

Collins A, Huang R, Jensen MH, Moore JR, Lehman W, Wang C-LA. (2011) *Structural Studies on Maturing Actin Filaments*. BioArchitecture **1**(3): 127-133.

Cooper JA. (1991) *The Role of Actin Polymerization in Cell Motility*. Annual Review of Physiology **53**(1): 585-605.

De Gennes P-G. Pincus DP, Velasco RM, Brochard F. (1976) *Remarks on Polyelectrolyte Conformation*. Journal de Physique **37**(12): 1461-1473.

De La Cruz EM. (2009) *How Cofilin Severs an Actin Filament*. Biophysical Reviews **1**(2): 51-59.

DesMarais V, Ichetovkin I, Condeelis J, Hitchcock-DeGregori SE. (2002) *Spatial Regulation of Actin Dynamics: a Tropomyosin-Free, Actin-Rich Compartment at the Leading Edge*. Journal of Cell Science **115**(23): 4649-4660.

Dominguez R. (2004) *Actin-Binding Proteins – A Unifying Hypothesis*. Trends in Biochemical Sciences **29**(11): 572-578.

Drabikowski W, Gergely J. (1962) *The Effect of the Temperature of Extraction on the Tropomyosin Content in Actin*. Journal of Biological Chemistry **237**(11): 3412-3417.

Egelman EH, Orlova A. (1995) *Allostery, Cooperativity, and Different Structural States in F-Actin*. Journal of Structural Biology **115**(2): 159-162.

Egelman EH. (1985) *The Structure of F-Actin*. Journal of Muscle Research and Cell Motility **6**(2): 129-151.

Elzinga M, Collins JH, Kuehl WM, Adelstein RS. (1973) *Complete Amino-Acid Sequence of Actin of Rabbit Skeletal Muscle*. Proceedings of the National Academy of Sciences **70**(9): 2687-2691.

Eves R, Webb BA, Zhou S, Mak AS. (2006) *Caldesmon is an Integral Component of Podosomes in Smooth Muscle Cells*. Journal of Cell Science **119**(9): 1691-1702.

Galińska-Rakoczy A, Wawro B, Strzelecka-Gołaszewska H. (2009) *New Aspects of the Spontaneous Polymerization of Actin in the Presence of Salts*. Journal of Molecular Biology **387**(4): 869-882.

Galkin VE, Orlova A, Fattoum A, Walsh MP, Egelman EH. (2006) *The CH-Domain of Calponin Does Not Determine the Modes of Calponin Binding to F-Actin*. Journal of Molecular Biology **359**(2): 478-485.

Galkin VE, Orlova A, Schröder GF, Egelman EH. (2010) *Structural Polymorphism in F-Actin*. Nature Structural and Molecular Biology **17**(11): 1318-1323.

Gallant C, Appel S, Graceffa P, Leavis P, Lin JJ-C, Gunning PW, Schevzov G, Chaponnier C, DeGnore J, Lehman W, Morgan KG. (2011) *Tropomyosin Variants Describe Distinct Functional Subcellular Domains in Differentiated Vascular Smooth Muscle Cells*. American Journal of Physiology and Cell Physiology **300**(6): C1356-C1365.

Gardel ML, Kasza KE, Brangwynne CP, Liu J, Weitz DA. (2008) *Mechanical Response of Cytoskeletal Networks*. Methods in Cell Biology **89**: 487-519.

Gardel ML, Nakamura F, Hartwig JH, Crocker JC, Stossel TP, Weitz DA. (2006) *Prestressed F-Actin Networks Cross-Linked by Hinged Filamins Replicate Mechanical Properties of Cells*. Proceedings of the National Academy of Sciences of the United States of America **103**(6): 1762-1767.

Gardel ML, Shin JH, MacKintosh FC, Mahadevan L, Matsudaira P, Weitz DA. (2004a) *Elastic Behavior of Cross-Linked and Bundled Actin Networks*. Science **304**(5675): 1301-1305.

Gardel ML, Shin JH, MacKintosh FC, Mahadevan L, Matsudaira PA, Weitz DA. (2004b) *Scaling of F-Actin Network Rheology to Probe Single Filament Elasticity and Dynamics*. Physical Review Letters **93**(18): 188102.

Geeves MA, Holmes KC. (2005) *The Molecular Mechanism of Muscle Contraction*. Advances in Protein Chemistry **71**: 161-193.

Geiger B, Dutton AH, Tokuyasu KT, Singer SJ. (1981) *Immunoelectron Microscope Studies of Membrane-Microfilament Interactions: Distributions of Alpha-Actinin, Tropomyosin, and Vinculin in Intestinal Epithelial Brush Border and Chicken Gizzard Smooth Muscle Cells*. Journal of Cell Biology **91**(3): 614-628.

Gimona M, Kaverina I, Resch GP, Vignal E, Burgstaller G. (2003) *Calponin Repeats Regulate Actin Filament Stability and Formation of Podosomes in Smooth Muscle Cells*. Molecular Biology of the Cell **14**(6): 2482-2491.

Gittes F, Mickey B, Nettleton J, Howard J. (1993) *Flexural Rigidity of Microtubules and Actin Filaments Measured from Thermal Fluctuations in Shape*. Journal of Cell Biology 120(4): 923-934.

Goff LL, Hallatschek O, Frey E, Amblard F. (2002) *Tracer Studies on F-Actin Fluctuations*. Physical Review Letters **89**(25): 258101.

Goley ED, Welch MD. (2006) *The ARP2/3 Complex: an Actin Nucleator Comes of Age*. Nature Reviews Molecular Cell Biology **7**(10): 713-726.

Gordon AM, Homsher E, Regnier M. (2000) *Regulation of Contraction in Striated Muscle*. Physiological Reviews **80**(2): 853-924.

Gordon DJ, Boyer JL, Korn ED. (1977) *Comparative Biochemistry of Non-Muscle Actins*. Journal of Biological Chemistry **252**(22): 8300-8309.

Graceffa P, Wang C-LA, Stafford WF. (1988) *Caldesmon. Molecular Weight and Subunit Composition by Analytical Ultracentrifugation*. Journal of Biological Chemistry **263**(28): 14196-14202.

Greenberg, MJ, Wang C-LA, Lehman W, Moore JR. (2008) *Modulation of Actin Mechanics by Caldesmon and Tropomyosin*. Cell Motility and the Cytoskeleton 65(2): 156-164.

Griffiths DJ. (1999) *Introduction to Electrodynamics, 3rd Edition*. Prentice Hall: Upper Saddle River, NJ.

Hahn C, Schwartz MA. (2009) *Mechanotransduction in Vascular Physiology and Atherogenesis*. Nature Reviews Molecular Cell Biology **10**(1): 53-62.

Hawkins M, Pope B, Maciver SK, Weeds AG. (1993) *Human Actin Depolymerizing Factor Mediates a pH-Sensitive Destruction of Actin Filaments*. Biochemistry **32**(38): 9985-9993.

Hayden SM, Miller PS, Brauweiler A, Bamburg JR. (1993) *Analysis of the Interactions of Actin Depolymerizing Factor with G- and F-Actin*. Biochemistry **32**(38): 9994-10004.

Helfman DM, Levy ET, Berthier C, Shtutman M, Riveline D, Grosheva I, Lachish-Zalait A, Elbaum M, Bershadsky AD. (1999) *Caldesmon Inhibits Nonmuscle Cell Contractility and Interferes with the Formation of Focal Adhesions*. Molecular Biology of the Cell **10**(10): 3097-3112.

Herman IM. *Actin Isoforms*. (1993) Current Opinion in Cell Biology **5**(1): 48-55.

Hodgkinson JL, El-Mezgueldi M, Craig R, Vibert P, Marston SB, Lehman W. (1997) *3-D Image Reconstruction of Reconstituted Smooth Muscle Thin Filaments Containing Calponin: Visualization of Interactions Between F-Actin and Calponin*. Journal of Molecular Biology **273**(1): 150-159.

Holmes KC, Popp D, Gebhard W, Kabsch W. (1990) *Atomic Model of the Actin Filament*. Nature **347**(6288): 44-49.

Hossain MM, Crish JF, Eckert RL, Lin JJ-C, Jin J-P. (2005) *h2-Calponin is Regulated by Mechanical Tension and Modifies the Function of Actin Cytoskeleton*. Journal of Biological Chemistry **280**(51): 42442-42453.

Howard J. (2001) *Mechanics of Motor Proteins and the Cytoskeleton*. Sinauer Associates Inc. Publishers: Sunderland, MA.

Huang R, Grabarek Z, Wang C-LA. (2010) *Differential Effects of Caldesmon on the Intermediate Conformational States of Polymerizing Actin*. Journal of Biological Chemistry **285**: 71-79.

Huxley HE. (1969) *The Mechanism of Muscular Contraction*. Science **164**(3886): 1356.

Huxley, HE, Brown W. (1967) *The Low-Angle X-Ray Diagram of Vertebrate Striated Muscle and its Behaviour During Contraction and Rigor*. Journal of molecular biology **30**(2): 383.

Ichetovkin I, Grant W, Condeelis J. (2002) *Cofilin Produces Newly Polymerized Actin Filaments that are Preferred for Dendritic Nucleation by the Arp2/3 Complex*. Current Biology **12** (1): 79-84.

Isambert H, Maggs AC. (1996) *Dynamics and Rheology of Actin Solutions*. Macromolecules **29**(3): 1036-1040.

Isambert H, Venier P, Maggs AC, Fattoum A, Kassab R, Pantaloni D, Carlier M-F. (1995) *Flexibility of Actin Filaments Derived from Thermal Fluctuations. Effect of Bound Nucleotide, Phalloidin, and Muscle Regulatory Proteins*. Journal of Biological Chemistry **270**(19): 11437-11444.

Janmey PA. (1998) *The Cytoskeleton and Cell Signaling: Component Localization and Mechanical Coupling*. Physiological Reviews **78**(3): 763-781.

Jégou A, Niedermayer T, Orbán J, Didry D, Lipowsky R, Carlier M-F, Romet-Lemonne G. (2011) *Individual Actin Filaments in a Microfluidic Flow Reveal the Mechanism of ATP Hydrolysis and Give Insight Into the Properties of Profilin*. PLoS Biology **9**(9): e1001161.

Jensen MH, Morris EJ, Huang R, Rebowski G, Dominguez R, Weitz DA, Moore JR, Wang C-LA. (2012a) *The Conformational State of Actin Filaments Regulates Branching by Actin-Related Protein 2/3 (Arp2/3) Complex*. Journal of Biological Chemistry **287**(37): 31447-31453.

Jensen MH, Watt J, Hodgkinson JL, Gallant C, Appel S, El-Mezgueldi M, Angelini TE, Morgan KG, Lehman W, Moore JR. (2012b) *Effects of Basic Calponin on the Flexural Mechanics and Stability of F-Actin*. Cytoskeleton **69**(1): 49-58.

Jiang Q, Huang R, Cai S, Wang C-LA. (2010). *Caldesmon Regulates the Motility of Vascular Smooth Muscle Cells by Modulating the Actin Cytoskeleton Stability*. Journal of Biomedical Science **17**(1): 6.

Kabsch W, Mannherz HG, Suck D, Pai EF, Holmes KC. (1990) *Atomic Structure of the Actin: DNase I Complex*. Nature **347**: 37-44.

Kake T, Kimura S, Takahashi K, Maruyama K. (1995) *Calponin Induces Actin Polymerization at Low Ionic Strength and Inhibits Depolymerization of Actin Filaments*. Biochemical Journal **312(**2): 587.

Käs J, Strey H, Bärmann M, Sackmann E. (1993) *Direct Measurement of the Wave-Vector-Dependent Bending Stiffness of Freely Flickering Actin Filaments*. Europhysics Letters **21**(8): 865.

Käs J, Strey H, Tang JX, Finger D, Ezzell R, Sackmann E, Janmey PA. (1996) *F-Actin, a Model Polymer for Semiflexible Chains in Dilute, Semidilute, and Liquid Crystalline Solutions*. Biophysical Journal **70**(2): 609-625.

Kasza KE, Koenderink GH, Lin YC, Broedersz CP, Messner W, Nakamura F, Stossel TP, MacKintosh FC, Weitz DA. (2009) *Nonlinear Elasticity of Stiff Biopolymers Connected by Flexible Linkers*. Physical Review **E79**(4): 041928.

Katsumi A, Orr AW, Tzima E, Schwartz MA. (2004) *Integrins in Mechanotransduction*. Journal of Biological Chemistry **279**(13): 12001-12004.

Khaitlina SY. (2001) *Functional Specificity of Actin Isoforms*. International Review of Cytology **202**: 35-98.

Kim HR, Gallant C, Leavis PC, Gunst CJ, Morgan KG. (2008) *Cytoskeletal Remodeling in Differentiated Vascular Smooth Muscle is Actin Isoform Dependent and Stimulus Dependent*. American Journal of Physiology and Cell Physiology **295**(3): C768-C778.

Koenderink GH, Dogic Z, Nakamura F, Bendix PM, MacKintosh FC, Hartwig JH, Stossel TP, Weitz DA. (2009) *An Active Biopolymer Network Controlled by Molecular Motors*. Proceedings of the National Academy of Sciences **106**(36): 15192-15197.

Kordowska J, Hetrick T, Adam LP, Wang C-LA. (2006) *Phosphorylated l-Caldesmon is Involved in Disassembly of Actin Stress Fibers and Postmitotic Spreading*. Experimental Cell Research **312**: 95–110.

Köster S, Steinhauser D, Pfohl T. (2005) *Brownian Motion of Actin Filaments in Confining Microchannels*. Journal of Physics: Condensed Matter **17**(49): S4091.

Kozuka J, Yokota H, Arai Y, Ishii Y, Yanagida T. (2006) *Dynamic Polymorphism of Single Actin Molecules in the Actin Filament*. Nature Chemical Biology **2**(2): 83-86.

Kueh HY, Brieher WM, Mitchison TJ. (2008) *Dynamic Stabilization of Actin Filaments*. Proceedings of the National Academy of Sciences **105**(43): 16531-16536.

Kuhn JR, Pollard TD. (2005) *Real-Time Measurements of Actin Filament Polymerization by Total Internal Reflection Fluorescence Microscopy*. Biophysical Journal **88**(2): 1387-1402.

Kumar A, Crawford K, Close L, Madison M, Lorenz J, Doetschman T, Pawlowski S, Duffy J, Neumann J, Robbins J, Boivin GP, OToole BA, Lessard JL. (1997) *Rescue of Cardiac Alpha-Actin-Deficient Mice by Enteric Smooth Muscle Gamma-Actin*. Proceedings of the National Academy of Sciences **94**:4406-4411.

Lai FPL, Szczodrak M, Block J, Faix J, Breitsprecher D, Mannherz HG, Stradal TEB, Dunn GA, Small JV, Rottner K. (2008) *Arp2/3 Complex Interactions and Actin Network Turnover in Lamellipodia*. EMBO Journal **27**(7): 982-992.

Landau LD, Lifshitz E M. (1980) *Statistical Physics*. Pergamon Press: Oxford, U.K.

Landau LD, Lifshitz E M. (1986) *Theory of Elasticity*. Pergamon Press: Oxford, U.K.

Lehman W, Craig R, Lui J, Moody C. (1989) *Caldesmon and the Structure of Smooth Muscle Thin Filaments: Immunolocalization of Caldesmon on Thin Filaments*. Journal of Muscle Research and Cell Motility **10**(2): 101-112.

Lehman W, Kaminer B. (1984) *Identification of a Thin Filament Linked-35,000 Dalton Protein in Vertebrate Smooth Muscle*. Biophysical Journal **45**: 104a.

Lehman W, Vibert P, Craig R. (1997) *Visualization of Caldesmon on Smooth Muscle Thin Filaments*. Journal of Molecular Biology **274**(3): 310-317.

Li XE, Tobacman LS, Mun JY, Craig R, Fischer S, Lehman W. (2011) *Tropomyosin Position on F-Actin Revealed by EM Reconstruction and Computational Chemistry*. Biophysical Journal **100**(4): 1005-1013.

Lin JJ, Hegmann TE, Lin JL. (1988) *Differential Localization of Tropomyosin Isoforms in Cultured Nonmuscle Cells*. Journal of Cell Biology **107**(2): 563-572.

Lin JJC, Li Y, Eppinga RD, Wang Q, Jin JP. (2009) *Roles of Caldesmon in Cell Motility and Actin Cytoskeleton Remodeling*. International Review of Cell and Molecular Biology **274**: 1-68.

Lin Y-C, Yao NY, Broedersz CP, Herrmann H, MacKintosh FC, Weitz DA. (2010) *Origins of Elasticity in Intermediate Filament Networks*. Physical Review Letters **104**(5): 58101.

Lu FWM, Freedman MV, Chalovich JM. (1995) *Characterization of Calponin Binding to Actin*. Biochemistry **34**(37): 11864-11871.

Mabuchi K, Wang C-LA. (1991) *Electron Microscopic Studies of Chicken Gizzard Caldesmon and its Complex with Calmodulin*. Journal of Muscle Research and Cell Motility **12**(2): 145-151.

MacKintosh FC, Käs J, Janmey PA. (1995) *Elasticity of Semiflexible Biopolymer Networks*. Physical Review Letters **75**(24): 4425-4428.

MacKintosh FC. (2006) *Elasticity and Dynamics of Cytoskeletal Filaments and Their Networks*. Soft Condensed Matter Physics in Molecular and Cell Biology: 139-155.

Marston, S. (1990) *Stoichiometry and Stability of Caldesmon in Native Thin Filaments from Sheep Aorta Smooth Muscle*. Biochemical Journal **272**(2): 305.

McCullough BR, Blanchoin L, Martiel J-L, De La Cruz EM. (2008) *Cofilin Increases the Bending Flexibility of Actin Filaments: Implications for Severing and Cell Mechanics*. Journal of Molecular Biology 381(3): 550-558.

McGough A. (1998) *F-Actin-Binding Proteins*. Current Opinion in Structural Biology **8**(2): 166-176.

Murakami K, Yasunaga T, Noguchi TQP, Gomibuchi Y, Ngo KX, Uyeda TQP, and Wakabayashi T. (2010) *Structural Basis for Actin Assembly, Activation of ATP Hydrolysis, and Delayed Phosphate Release*. Cell **143**(2): 275-287.

Niedermayer T, Jégou A, Chièze L, Guichard B, Helfer E, Romet-Lemonne G, Carlier M-F, Lipowsky R. (2012) *Intermittent Depolymerization of Actin Filaments is Caused by Photo-Induced Dimerization of Actin Protomers*. Proceedings of the National Academy of Sciences **109**(27): 10769-10774.

Nigam R, Jin J-P, Triggle CR. (1998) *h1- and h2-Calponins are not Essential for Norepinephrine- or Sodium Fluoride-Induced Contraction of Rat Aortic Smooth Muscle*. Journal of Muscle Research and Cell Motility **19**(6): 695-703.

North AJ, Gimona M, Lando Z, Small JV. (1994) *Actin Isoform Compartments in Chicken Gizzard Smooth Muscle Cells*. Journal of Cell Science **107**(3): 445-455.

Oda T, Iwasa M, Aihara T, Maéda Y, Narita A. (2009) *The Nature of the Globular- to Fibrous-Actin Transition*. Nature **457**(7228): 441-445.

Oda T, Maéda Y. (2010) *Multiple Conformations of F-Actin*. Structure **18**(7): 761-767.

Odijk T. (1983) *The Statistics and Dynamics of Confined or Entangled Stiff Polymers*. Macromolecules **16**(8): 1340-1344.

Onck PR, Koeman T, Van Dillen T, Van der Giessen E. (2005) *Alternative Explanation of Stiffening in Cross-Linked Semiflexible Networks*. Physical Review Letters **95**(17): 178102.

Oosawa F, Kasai M. (1962) *A Theory of Linear and Helical Aggregations of Macromolecules*. Journal of Molecular Biology **4**(1): 10-21.

Orlova A, Egelman EH. (1993) *A Conformational Change in the Actin Subunit can Change the Flexibility of the Actin Filament*. Journal of Molecular Biology **232**(2): 334-341.

Orlova A, Egelman EH. (1997) *Cooperative Rigor Binding of Myosin to Actin is a Function of F-Actin Structure*. Journal of Molecular Biology **265**(5): 469-474.

Otey CA, Kalnoski MH, Lessard JL, Bulinski JC. (1986) *Immunolocalization of the Gamma Isoform of Nonmuscle Actin in Cultured Cells*. The Journal of Cell Biology **102**(5): 1726-1737.

Ott A, Magnasco M, Simon A, Libchaber A. (1993) *Measurement of the Persistence Length of Polymerized Actin Using Fluorescence Microscopy*. Physical Review E **48**(3): 1642-1645.

Paavilainen VO, Bertling E, Falck S, Lappalainen P. (2004) *Regulation of Cytoskeletal Dynamics by Actin-Monomer-Binding Proteins*. Trends in Cell Biology **14**(7): 386-394.

Pardee JD, Spudich JA. (1982) *Purification of Muscle Actin*. Methods in Cell Biology **24**(Pt A): 271-289.

Pardo JV, Pittenger MF, Craig SW. (1983) *Subcellular Sorting of Isoactins: Selective Association of γ Actin with Skeletal Muscle Mitochondria*. Cell **32**(4): 1093-1103.

Parker CA, Takahashi K, Tao T, Morgan KG. (1994) *Agonist-Induced Redistribution of Calponin in Contractile Vascular Smooth Muscle Cells*. American Journal of Physiology and Cell Physiology **267**(5): C1262-C1270.

Pollard TD, Borisy GG. (2003) *Cellular Motility Driven by Assembly and Disassembly of Actin Filaments*. Cell **112**(4): 453-465.

Prochniewicz E, Janson N, Thomas DD, De La Cruz EM. (2005) *Cofilin Increases the Torsional Flexibility and Dynamics of Actin Filaments*. Journal of Molecular Biology **353**(5): 990-1000.

Prochniewicz E, Zhang Q, Janmey PA, Thomas DD. (1996) *Cooperativity in F-Actin: Binding of Gelsolin at the Barbed End Affects Structure and Dynamics of the Whole Filament*. Journal of Molecular Biology **260**(5): 756-766.

Rozenblum GT, Gimona M. (2008) *Calponins: Adaptable Modular Regulators of the Actin Cytoskeleton*. The International Journal of Biochemistry & Cell Biology **40**(10): 1990-1995.

Rubenstein PA. (1990) *The Functional Importance of Multiple Actin Isoforms*. Bioessays **12**(7): 309-315.

Schmidt CF, Baermann M, Isenberg G, Sackmann E. (1989) *Chain Dynamics, Mesh Size, and Diffusive Transport in Networks of Polymerized Actin: a Quasielastic Light Scattering and Microfluorescence Study*. Macromolecules **22**(9): 3638-3649.

Sheterline P, Sparrow JC. (1994) *Actin*. Protein Profile **1**(1): 1.

Shibukawa Y, Yamazaki N, Kumasawa K, Daimon E, Tajiri M, Okada Y, Ikawa M, Wada Y. (2010) *Calponin 3 Regulates Actin Cytoskeleton Rearrangement in Trophoblastic Cell Fusion*. Molecular Biology of the Cell **21**(22): 3973-3984.

Shirinsky VP, Biryukov KG, Hettasch JM, Sellers JR. (1992) *Inhibition of the relative movement of* actin and myosin by caldesmon and calponin. Journal of Biological Chemistry 267(22): 15886-15892.

Small VJ, Resch GP. (2005) *The Comings and Goings of Actin: Coupling Protrusion and Retraction in Cell Motility*. Current Opinion in Cell Biology **17**(5): 517-523.

Sousa D, Cammarato A, Jang K, Graceffa P, Tobacman LS, Li X, Lehman W. (2010) *Electron Microscopy and Persistence Length Analysis of Semi-Rigid Smooth Muscle Tropomyosin Strands*. Biophysical Journal **99**(3): 862-868.

Spudich JA, Watt S. (1971) *The Regulation of Rabbit Skeletal Muscle Contraction*. Journal of Biological Chemistry **246**(15): 4866-4871.

Stafford WF, Jancso A, Graceffa P. (1990) *Caldesmon from Rabbit Liver: Molecular Weight and Length by Analytical Ultracentrifugation*. Archives of Biochemistry and Biophysics **281**(1): 66-69.

Steinmetz MO, Goldie KN, Aebi U. (1997) *A Correlative Analysis of Actin Filament Assembly, Structure, and Dynamics*. Journal of Cell Biology **138** (3) 559-574.

Stossel TP, Condeelis J, Cooley L, Hartwig JH, Noegel A, Schleicher M, Shapiro SS. (2001) *Filamins as Integrators of Cell Mechanics and Signalling*. Nature Reviews Molecular Cell Biology **2**(2): 138-145.

Straub FB. (1942) *Actin*. Studies from the Institute of Medical Chemistry University Szeged **2**:3-4.

Suarez C, Roland J, Boujemaa-Paterski R, Kang H, McCullough BR, Reymann A-C, Guérin C, Martiel J-L, De La Cruz EM, Blanchoin L. (2011) *Cofilin Tunes the Nucleotide State of Actin Filaments and Severs at Bare and Decorated Segment Boundaries*. Current Biology **21**(10): 862-868.

Suck D, Kabsch W, Mannherz HG. (1981) *Three-Dimensional Structure of the Complex of Skeletal Muscle Actin and Bovine Pancreatic DNAse I at 6-Å Resolution*. Proceedings of the National Academy of Sciences **78**(7): 4319-4323.

Takahashi K, Abe M, Hiwada K, Kokubu T. (1988a) *A Novel Troponin T-Like Protein (Calponin) in Vascular Smooth Muscle: Interaction with Tropomyosin Paracrystals*. Journal of Hypertension Supplement **6**(4): S40.

Takahashi K, Hiwada K, Kokubu T. (1986) *Isolation and Characterization of a 34000-Dalton Calmodulin- and F-Actin-Binding Protein from Chicken Gizzard Smooth Muscle*. Biochemical and Biophysical Research Communications **141**(1): 20-26.

Takahashi K, Hiwada K, Kokubu T. (1988b) *Vascular Smooth Muscle Calponin. A Novel Troponin T-Like Protein*. Hypertension **11**(6) Pt 2: 620-626.

Takebayashi T, Morita Y, Oosawa F. (1977) *Electronmicroscopic Investigation of the Flexibility of F-Actin*. Biochimica et Biophysica Acta – Protein Structure **492**(2): 357-363.

Tang J, Hu G, Hanai J-I, Yadlapalli G, Lin Y, Zhang B, Galloway J, Bahary N, Sinha S, Thisse B, Thisse C, Jin J-P, Zon LI, Sukhatme VP. (2006) *A Critical Role for Calponin 2 in Vascular Development*. Journal of Biological Chemistry **281**(10): 6664-6672.

Tang JX, Szymanski PT, Janmey PA, Tao T. *Electrostatic Effects of Smooth Muscle Calponin on Actin Assembly*. (1997) European Journal of Biochemistry **247**(1): 432-440.

Tharmann RM, Claessens MAE, Bausch AR. (2007) *Viscoelasticity of Isotropically Cross-Linked Actin Networks*. Physical Review Letters **98**(8): 88103.

Tirado MM, García de La Torre J. (1979) *Translational Friction Coefficients of Rigid, Symmetric Top Macromolecules. Application to Circular Cylinders*. Journal of Chemical Physics **71**: 2581.

Tobacman LS, Korn ED. (1983) *The Kinetics of Actin Nucleation and Polymerization*. Journal of Biological Chemistry **258**(5): 3207-3214.

Trybus KM. (1991) Regulation of Smooth Muscle Myosin. Cell Motility and the Cytoskeleton 18: 81-85.

Vandekerckhove J, Weber K. (1978a) *Actin Amino-Acid Sequences*. European Journal of Biochemistry **90**(3): 451-462.

Vandekerckhove J, Weber K. (1978b) *At Least Six Different Actins are Expressed in a Higher Mammal: an Analysis Based on the Amino Acid Sequence of the Amino-Terminal Tryptic Peptide*. Journal of Molecular Biology **126**(4): 783.

Vandekerckhove J, Weber K. (1979) *The Amino Acid Sequence of Actin From Chicken Skeletal Muscle Actin and Chicken Gizzard Smooth Muscle Actin*. FEBS Letters **102**(2): 219.

Volkmann N, Amann KJ, Stoilova-McPhie S, Egile C, Winter DC, Hazelwood L, Heuser JE, Li R, Pollard TD, Hanein D. (2001) *Structure of Arp2/3 Complex in its Activated State and in Actin Filament Branch Junctions*. Science **293**(5539): 2456-2459.

Wang C-LA. (2008) *Caldesmon and the regulation of cytoskeletal functions*. Advances in Experimental Medicine and Biology **644**: 250-272.

Wegner A, Engel J. (1975) *Kinetics of the Cooperative Association of Actin to Actin Filament*. Biophysical Chemistry **3**(3): 215-225.

Winder SJ, Walsh MP. (1990) *Smooth Muscle Calponin. Inhibition of Actomyosin MgATPase and Regulation by Phosphorylation*. Journal of Biological Chemistry **265**(17): 10148-10155.

Yanagida T, Nakase M, Nishiyama K, Oosawa F. (1984) *Direct Observation of Motion of Single F-Actin Filaments in the Presence of Myosin*. Nature **307**: 58-60.

Yang, YZ, Korn ED, Eisenberg E. (1979) *Cooperative Binding of Tropomyosin to Muscle and Acanthamoeba Actin*. Journal of Biological Chemistry **254**(15): 7137-7140.

Yeoh S, Pope B, Mannherz HG, Weeds A. (2002) *Determining the Differences in Actin Binding by Human ADF and Cofilin*. Journal of Molecular Biology **315**(4): 911-925.

CURRICULUM VITAE